ISSN: 2227-6912
E-ISSN: 2790-0479

Azerbaijan Technical University

# MACHINE SCIENCE

1
2022

International scientific-technical journal

# MACHINE SCIENCE

## MAŞINŞÜNASLIQ МАШИНОВЕДЕНИЕ

International scientific-technical journal
*Beynəlxalq elmi-texniki jurnal*
*Международный научно-технический журнал*

**Volume 11**
**Number 1**
**2022**

**Founder:** The Ministry of Education of Azerbaijan Republic
***Təsisçi:*** *Azərbaycan Respublikası Təhsil Nazirliyi*
***Учредитель:*** *Министерство образования Азербайджанской Республики*

***The journal is included into the list confirmed by Higher Attestation Commission of the Azerbaijan Republic of editions for the publication of works of competitors for scientific degrees***

*Jurnal Azərbaycan Respublikası Ali Atestasiya Komissiyasının təsdiq etdiyi elmi dərəcə iddiaçılarının əsərlərinin çap edildiyi dövri elmi nəşrlərin siyahısına daxil edilmişdir.*

*Журнал входит в перечень, утвержденных ВАК Азербайджанской Республики, изданий для публикации трудов соискателей ученых степеней*

Journal was founded according the order No1861 Ministry of Education of Azerbaijan Republic on the date 25.11.2011. Registration No 3521. Journal is published at least twice a year.

*Jurnal Azərbaycan Respublikası Təhsil Nazirliyinin 25.11.2011-ci il tarixli 1861 saylı əmri əsasında təsis edilmişdir. Qeydiyyat No 3521. İldə ən azı iki nömrə nəşr edilir.*

*Учреждено приказом за №1861 от 25.11.2011 года Министерства образования Азербайджанской Республики. Регистрация № 3521. Ежегодно публикуется два номера.*

It has been published since 2001. Published in 2001 - 2011 with a name "Mechanics-machine building"
*2001-ci ildən nəşr edilir. 2001 – 2011-ci illərdə "Mexanika-maşınqayırma" adı ilə çap edilmişdir.*
*Издается с 2001 года. В 2001 – 2011 годах издано под названием «Механика-машиностроение»*

***The journal has been included in international citation and indexation system INSPEC since 2011.***
*Jurnal 2011-ci ildən* ***INSPEC*** *beynəlxalq xülasələndirmə və indeksləndirmə sisteminə daxil edilmişdir.*
*Журнал включен в международную систему цитируемости и индексации* ***INSPEC*** *с 2011 года*

***The "MACHINE SCIENCE" journal is supported by Azerbaijan Technical University, which means there are no publication fees for authors.***
*"MAŞINŞÜNASLIQ" jurnalı Azərbaycan Texniki universiteti tərəfindən dəstəklənir və məqalələrin nəşri üçün müəlliflərdən hər hansı ödəniş tələb olunmur.*
*Журнал «МАШИНОВЕДЕНИЕ» поддерживается Азербайджанским Техническим Университетом, что означает, что с авторов не взимается плата за публикацию статей.*



| | | |
|---|---|---|
| ***Editorial address*:**<br>***Redaksiyanın ünvanı:***<br>***Адрес редакции:*** | Baku, AZ1073, H.Javid ave., 25. AzTU<br>Tel: (+994 12) 539 12 25<br>E-mail: msj@aztu.edu.az | © Machine Science, 2022<br>**ISSN:** 2227-6912<br>**E-ISSN:** 2790-0479 |

MACHINE SCIENCE

ISSN: 2227-6912
E-ISSN: 2790-0479

2022, Volume 11, № 1. Pages 4 – 9

# DETERMINATION OF THE DYNAMIC STATE OF SHIFT-DEFORMABLE SANDWICH NANOCOMPOSITE CYLINDRICAL PANELS

**Mahmure AVEY [1*], Elçin YUSUFOGLU [2], Yusif HASANOV [3], Eckart SCHNACK [4], Kemal ERTUNÇ[5]**

[1*]Division of Mathematics in Graduate School of Natural and Applied Sciences of Usak University, Usak, Türkiye
[2]Department of Mathematics Faculty of art and Science of Usak University, Usak, Türkiye
[3]Department of Applied Mechanics Azerbaijan State Marine Academy, Baku, Azerbaijan
[4]Department of Solids mechanics, Karlsruhe Institute of Technology, Karlsruhe, Germany
[5]Student of Department of Civil Engineering, Engineering Faculty, Suleyman Demirel Universiy, Isparta, Türkiye

*E-mail:* mahmureavet@gmail.com[1], elçin.yusufoglu@usak.edu.tr[2], yusif_nadiroglu@mail.ru[3], eckart.schnack@kit.edu[4], ertkml15@gmail.com[5]

**Abstract:** In this study, the dynamic behavior of shear deformable heterogeneous nanocomposite sandwich cylindrical panels containing carbon nanotube (CNT) patterned layers is investigated. The basic differential equations of the sandwich cylindrical panel composed of CNT patterned layers based on the Donnell type shell theory are derived. Then basic equations are solved by applying Galerkin method and obtained expression for the nondimensional free vibration frequency of three-layer nanocomposite cylindrical panels within the first order shear deformation shell theory (FOSDST). Finally, the influences of transverse shear strains, volume fractions, arrangement of sandwich nanocomposite layers on the nondimensional free vibration frequency are studied.

***Keywords:*** *Carbon nanotube, nanocomposite, sandwich panel, free vibration, frequency, shear deformation theory*

**Introduction.** The typical sandwich structure consists of two surface layers containing a core layer [1]. The sandwich panels are one of the most used elements in structural applications and are frequently used especially in space vehicles, machinery, ship and automotive industries. In most aerospace applications, panels are used as coating elements in rocket systems as well as a part of pressurized fuel tank. The sandwich panels are one of structural elements that lead to optimum conditions in dynamic behavior. Investigation of vibration behavior of sandwich panels of any geometry plays an important role in successful applications of such structural elements.

The carbon nanotubes have recently attracted increased interest of researchers due to their unique properties in terms of strength, thermal stability, and electrical conductivity. CNTs were discovered experimentally by Japanese materials scientist Iijima in 1991 during the production of fullerenes by evaporation of arc discharge [2]. It has been experimentally proven that CNTs have outstanding mechanical properties compared to continuous carbon fibers [3, 4]. CNT reinforced composite materials are generally used in structural components of complex structural systems. Therefore, the dynamic behavior of structural components composed of CNT reinforced composites is extremely important for the efficient design process. Nanocomposites reinforced with CNTs, especially polymer-based nanocomposites are one of the most interesting research areas among nanocomposites. Many studies have shown that carbon nanotubes can be an effective tool for modifying the strength properties of polymer composite materials [5-7].

The first studies on the static and dynamic behavior of monolayer heterogeneous nanocomposite cylindrical panels belong to Liew et al. [8,9]. After this study, Kiani [10] investigated the dy-

namic behavior of functionally graded (FG)-CNT reinforced composite cylindrical panel under a moving load. Wang et al. [11] presented a semi-analytical method for vibration analysis of FG sandwich double-curved panels and rotary shells. In the research paper, Setoodeh and co-authors [12] examined the vibrational behavior of FG-CNT reinforced surface sheets and double-curved smart sandwich shells with FG porous cores. Di Sciuva and Sorrenti [13] analyzed the free vibration and buckling of functionally graded carbon nanotube reinforced sandwich plates using the Extended Refined Zigzag Theory. Avey et al. [14] carried out nonlinear vibration analysis of multilayer shell type structural elements with double curvature consisting of CNT patterned layers in different theories. The literature study reveals that the vibration problem of multi-layered structural elements consisting of CNT reinforced layers has not been sufficiently studied yet. In this study, the free vibration of sandwich cylindrical panels composed of CNT patterned layers is investigated within FOSDT.

**Formulation of problem.** The sandwich cylindrical panel composed of CNT patterned layers with side lengths $a$, radius $R$, and total thickness $h$ is shown in Fig. 1. It is assumed that the sandwich cylindrical panel is composed of CNT patterned lamina of equal thickness. The lamina are perfectly bonded to each other, they do not slip, and all layers remain elastic during deformation. The main axes of elasticity of each lamina are assumed to be parallel to the coordinate axes on the reference surface. The curvilinear coordinate system $Oxyz$ is located on the reference surface and left corner of the cylindrical panel; where $x$ and $y$ axes are on the reference surface $z=0$ and the $z$ axis is in the normal direction to the reference surface and is directed inward.

The effective material properties of each layer of sandwich panels with CNT patterns, based on the expanded rule of the mixture are expressed as follows [15]:

$$Y_{11}^{(k)}=\eta_1^{(k)}V_{cn}^{(k)}Y_{11cn}^{(k)}+V_m^{(k)}Y_m^{(k)},\ Y_{22}^{(k)}=\frac{\eta_2^{(k)}Y_m^{(k)}Y_{22cn}^{(k)}}{Y_{22cn}^{(k)}V_m^{(k)}+Y_m^{(k)}V_m^{(k)}},\ S_{12}^{(k)}=\frac{\eta_3^{(k)}S_m^{(k)}S_{12cn}^{(k)}}{S_{12cn}^{(k)}V_m^{(k)}+S_m^{(k)}V_{cn}^{(k)}}$$
$$S_{12}^{(k)}=S_{13}^{(k)}=1.2S_{23}^{(k)},\ p_{12}^{(k)}=V_{cn}^{*(k)}p_{12cn}^{(k)}+V_m^{(k)}p_m^{(k)},\ D_t^{(k)}=V_{cn}^{(k)}D_{cn}^{(k)}+V_m^{(k)}D_m^{(k)},(k=1,2,3) \quad (1)$$

where $Y_m^{(k)},S_m^{(k)},D_m^{(k)},p_m^{(k)}$ are the elasticity modulus, density and Poisson's ratio in the layers of sandwich panels, and $Y_{ijcn}^{(k)}$, $S_{ijcn}^{(k)}$, $D_{cn}^{(k)}$, $p_{12cn}^{(k)}(i,j=1,2,3)$ are the corresponding mechanical properties for the pattering CNT phase, respectively, $\eta_i^{(k)}(i=1,2,3)$ are the efficiency parameters in the layers of sandwich panels. Here $V_{cn}^{(k)}$ and $V_m^{(k)}$ are the volume fraction of CNTs in the layers of sandwich panels that obey the rule of $V_{cn}^{(k)}+V_m^{(k)}=1$.

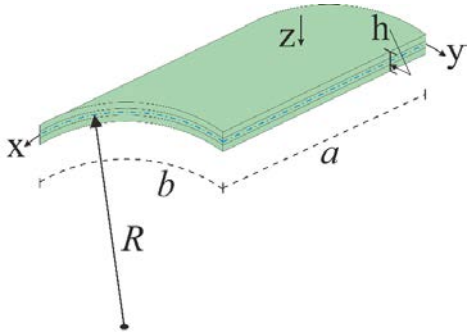


*Fig. 1. Sandwich cylindrical panel with CNT reinforced sheets, and coordinate system*

The cross-section of sandwich nanocomposite cylindrical panel is presented in Fig. 2, in which **(a)** 0-monolayer panel, **(b)** (0/90/0)-array sandwich panel, and **(c)** (90/0/90)-array sandwich panel.

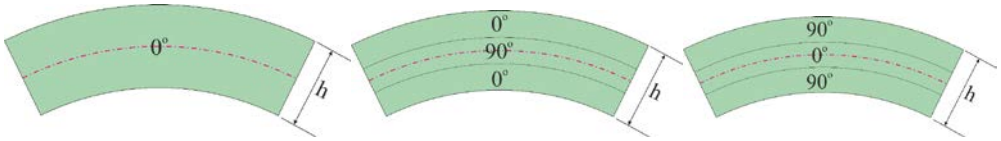


*a)* *b)* *c)*

*Fig 2. The cross-section of sandwich nanocomposite cylindrical panel*

The pattern of the volume fraction for CNTs over the thickness of the layers of sandwich panels as uniform pattern (U-pattern) and V-pattern is shown in Fig. 3.

$$V_{cn}^{(k)} = \begin{cases} \text{U} & at \;\; V_{cn}^{*(k)} \\ \text{V} & at \;\; 2\left(0.5-\overline{z}\right)V_{cn}^{*(k)}, \;\; \overline{z} = z/h \end{cases} \tag{2}$$

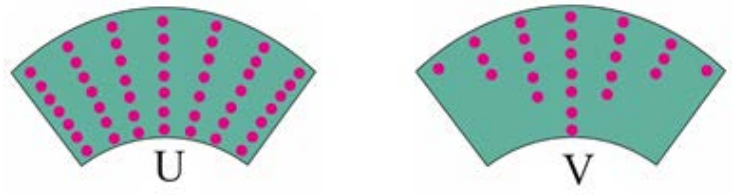


*a)* *b)*

*Fig. 3. The cross-section of CNT patterned sheets (a) U-patterned, (b) B-patterned*

The basic relations for the layers of sandwich panels patterned by CNTs within FOSDST can be defined as [14]:

$$\begin{bmatrix} \tau_{11}^{(k)} \\ \tau_{22}^{(k)} \\ \tau_{12}^{(k)} \\ \tau_{13}^{(k)} \\ \tau_{23}^{(k)} \end{bmatrix} = \begin{bmatrix} q_{11\overline{z}}^{(k)} & q_{12\overline{z}}^{(k)} & 0 & 0 & 0 \\ q_{21\overline{z}}^{(k)} & q_{22\overline{z}}^{(k)} & 0 & 0 & 0 \\ 0 & 0 & q_{66\overline{z}}^{(k)} & 0 & 0 \\ 0 & 0 & 0 & q_{55\overline{z}}^{(k)} & 0 \\ 0 & 0 & 0 & 0 & q_{44\overline{z}}^{(k)} \end{bmatrix} \begin{bmatrix} \varepsilon_{11} \\ \varepsilon_{22} \\ \varepsilon_{12} \\ \varepsilon_{13} \\ \varepsilon_{23} \end{bmatrix} (k = 1,2,3) \tag{3}$$

where $\tau_{ij}^{(k)} (i = 1,2;\; j = 1,2,3, k = 1,2,3)$ are the stresses in the layers of sandwich panels, $\varepsilon_{ij} (i,\; j = 1,2,3)$ are the strains and $q_{ij\overline{x}_3}^{(k)}, (i,\; j = 1,2,6)$, denote material properties of CNT originating in the layers of sandwich panels.

The force and moments of sandwich panels composed of CNT originating layers are obtained as [16]:

$$\left(N_{ij},\; S_j\right) = \int_{-h/2}^{-h/6} \left(\tau_{ij}^{(1)}, \tau_{1j_1}^{(1)}\right) \mathrm{dz} + \int_{-h/6}^{h/6} \left(\tau_{ij}^{(2)}, \tau_{1j_1}^{(2)}\right) \mathrm{dz} + \int_{h/6}^{h/2} \left(\tau_{ij}^{(3)}, \tau_{1j_1}^{(3)}\right) \mathrm{dz}, \tag{4}$$

$$M_{ij} = \int_{-h/2}^{-h/6} \tau_{ij}^{(1)} \mathrm{zdz} + \int_{-h/6}^{h/6} \tau_{ij}^{(2)} \mathrm{zdz} + \int_{h/6}^{h/2} \tau_{ij}^{(3)} \mathrm{zdz}, \; (i,\; j = 1,2,\; j_1 = 2,3) \tag{5}$$

With the Airy stress function $\Phi$, the in-plane forces are defined as [16]:

$$T_{11} = h\frac{\partial^2 \Phi}{\partial y^2}, T_{22} = h\frac{\partial^2 \Phi}{\partial x^2}, T_{12} = -h\frac{\partial^2 \Phi}{\partial x \partial y} \tag{6}$$

Substituting (4) into (5) and then substituting the resulting expressions and the relation (6) in the basic equations [14], the governing equations of sandwich panels with CNT origin can be obtained as:

$$\begin{aligned} &L_{11}(\Phi)+L_{12}(w)+L_{13}(\psi_1)+L_{14}(\psi_2)=0\\ &L_{21}(\Phi)+L_{22}(w)+L_{23}(\psi_1)+L_{24}(\psi_2)=0\\ &L_{31}(\Phi)+L_{32}(w)+L_{33}(\psi_1)+L_{34}(\psi_2)=0\\ &L_{41}(\Phi)+L_{42}(w)+L_{43}(\psi_1)+L_{44}(\psi_2)=0 \end{aligned} \tag{7}$$

where $L_{ij}(i=1,2,...,4,\ j=1,2,..,4)$ are differential operators and defined in ref. [14].

The following approximation functions is sought for sandwich panels containing CNT reinforced layers:

$$\begin{aligned} &w=f(t)\sin(m_1x)\sin(n_1y),\ \Phi=f_0(t)\sin(m_1x)\sin(n_1y),\\ &\psi_1=f_1(t)\cos(m_1x)\sin(n_1y),\ \psi_2=f_2(t)\sin(m_1x)\cos(n_1y) \end{aligned} \tag{8}$$

where $f(t)$ and $f_i(t)$ $(i=0,1,2)$ are the functions of a time, $m_1=\dfrac{m\pi}{a}$, $n_1=\dfrac{n\pi}{b}$, in which $(m,n)$ are the wave numbers.

After substituting the functions of (8) into the system of Eqs. (7), the Galerkin method is applied and the unknowns $f_i(t)$ $(i=0,1,2)$ are eliminated from the resulting system of equations, the following expression is obtained for the free vibration frequency sandwich panels containing CNT reinforced layers in the framework of FOSDST:

$$\Omega_{sdt}=\sqrt{\frac{u_4u_1-u_2u_3}{\bar{D}_tu_1}} \tag{9}$$

where $\bar{D}_t=\int\limits_{-h/2}^{-h/6}D_t^{(1)}\mathrm{d}z+\int\limits_{-h/6}^{h/6}D_t^{(2)}\mathrm{d}z+\int\limits_{h/6}^{h/2}D_t^{(3)}\mathrm{d}z$, $u_i(i=1,2,..,4)$ are parameters depending on the properties of the sandwich panels containing the CNT reinforced layers, and the following expression is used for the nondimensional frequency parameter:

$$\Omega_{1sdt}=\Omega_{sdt}h\sqrt{\frac{D_m^{(1)}}{E_m^{(1)}}} \tag{10}$$

The expressions (9) and (10) transform into expressions of dimensional and nondimensional frequencies within the framework of classical shell theory (CST), when the transverse shear stresses $\tau_{13}^{(k)}$ and $\tau_{23}^{(k)}$ in the layers of the sandwich panel are not taken into account in the basic relations.

**Analysis of the obtained results.** In the numerical analysis, A poly (methyl methacrylate) called PMMA reinforced with (10,10) single-walled CNTs is used. The elastic properties of the PMMA matrix are as follows: $Y_m^{(k)}=2.5\,\mathrm{GPa}$, $p_m^{(k)}=0.34$ and $D_m^{(k)}=1150\,\mathrm{kg/m^3}$ ($k$=1 and 3). The geometry and elastic properties of CNT are defined as: $r=9.26\,\mathrm{nm}$, $a_1=0.68\,\mathrm{nm}$, $h_1=0.067\,\mathrm{nm}$ and $Y_{11}^{cn(k)}=5.6466\,\mathrm{TPa}$, $Y_{22}^{cn(k)}=7.08\,\mathrm{TPa}$, $S_{12}^{cn(k)}=1.9445\,\mathrm{TPa}$, $p_{12}^{cn(k)}=0.175$, $D_{cn}^{(k)}=1400\,\mathrm{kg/m^3}$. The total volume fractions and productivity parameters of CNTs in the layers are defined as follows: $\eta_1^{(k)}=0.137$, $\eta_2^{(k)}=1.022$, $\eta_3^{(k)}=0.715$ at $V_{cn}^{*(k)}=0.12$, $\eta_1^{(k)}=0.142$, $\eta_2^{(k)}=1.626$, $\eta_3^{(k)}=1.138$ at $V_{cn}^{*(k)}=0.17$ and $\eta_1^{(k)}=0.141$, $\eta_2^{(k)}=1.585$, $\eta_3^{(k)}=1.109$ at $V_{cn}^{*(k)}=0.28$

[15]. The shear stresses of sandwich panels containing CNT patterned layers are used as, $\varphi_j^{(k)}(z) = z(1-4z^2/3h^2)$, $(j=1,2)$ [16].

The variation of nondimensional free frequency parameters of nanocomposite sandwich panels for three types of sequences of layers with U-and V-patterns depending on the $R/a$ ratio is tabulated in Table 1. The following data are used in the computations: $a/b=1$, $a/h=20$, $V_{cn}^{*(k)}=0.12$ and $(m,n)=(1,1)$. The sandwich panel consists of (0/90/0) and (90/0/90)-arranged layers, and calculations are also made for the (0)-monolayer panel for the comparison. As can be seen from Table 1, the nondimensional free vibration frequency values decrease due to the increase of $R/a$ in all the heterogeneous nanocomposite panels containing CNT layers with (0), (0/90/0) and (90/0/90)-arrays. The free frequency values in sandwich panels containing U-patterned layer are higher than the frequency values for V-patterned sandwich panels. Depending on the increase in the $R/a$ ratio, the shear deformation effect on the frequency values increases. The highest shear deformation effect (90/0/90)-arrayed U-patterned sandwich panel is 14.22 % for $R/a$ =3, the least effect is (0)-arrayed occurs in the monolayer panel at $R/a$ =1 (9.40%). Despite the decrease the effect of shear deformations on frequency values for V-patterned layers, it maintains its importance. For example, the highest shear deformations effect in (90/0/90)-arrayed U-patterned sandwich panel is 9.53% at $R/a$ =3 and the least effect is at $R/a$ =1 in (0)-array monolayer panel occurs (5.94%). Also, in (0/90/0)-patterned sandwich panels, the highest effect is 11.99% at R/a=3 in the U-pattern, while the least effect occurs at $R/a$ =1 in V-pattern sandwich panels (7.41%).

*Table 1. The variation of nondimensional free frequency parameters of sandwich panels for three types of sequences of layers with U-and V-patterns depending on the* $R/a$

| | | U-pattern | | V-pattern | |
|---|---|---|---|---|---|
| Sequences | $R/a$ | $10\Omega_{1sdt}$ | | | |
| 0/0/0 | 1.0 | 0.464 | 0.512 | 0.430 | 0.457 |
| | 1.5 | 0.428 | 0.480 | 0.388 | 0.418 |
| | 2.0 | 0.414 | 0.468 | 0.372 | 0.403 |
| | 2.5 | 0.408 | 0.462 | 0.364 | 0.396 |
| | 3 | 0.404 | 0.459 | 0.360 | 0.391 |
| 0/90/0 | 1.0 | 0.465 | 0.514 | 0.433 | 0.462 |
| | 1.5 | 0.429 | 0.481 | 0.392 | 0.424 |
| | 2.0 | 0.415 | 0.469 | 0.376 | 0.409 |
| | 2.5 | 0.409 | 0.464 | 0.369 | 0.402 |
| | 3 | 0.405 | 0.461 | 0.364 | 0.398 |
| 90/0/90 | 1.0 | 0.490 | 0.554 | 0.449 | 0.484 |
| | 1.5 | 0.455 | 0.524 | 0.409 | 0.447 |
| | 2.0 | 0.443 | 0.513 | 0.394 | 0.433 |
| | 2.5 | 0.437 | 0.508 | 0.387 | 0.427 |
| | 3 | 0.434 | 0.505 | 0.382 | 0.423 |

In the (0)-monolayer panel, when the $R/a$ ratio increases, the V-pattern effect on the frequency values increases from (-7.38%) to (-11.01%) within SDT, while this effect increases from (-10.79%) to (-14.67%) under the CST. When the $R/a$ ratio increases in (0/90/0) layered sandwich panel, the V-pattern effect on the frequency values increases from (-6.81%) to (-10.11%) in the framework of the SDT, while this effect increases from (-10.07%) to (-13.63%) within the CST. In the (90/0/90)-layered sandwich panel, when the $R/a$ increases, the V-pattern effect on the frequency values increases from (-8.29%) to (-11.78%) in the framework of SDT, while this effect increases from (-12.64%) to (16.35%) within CST.

**Conclusion.** In this study, the free vibration of sandwich cylindrical panels composed of CNT patterned layers is investigated within FOSDST. The governing equations of sandwich cylindrical

panels composed of CNT patterned layers based on the Donnell type shell theory are derived. Then solved by applying the Galerkin method and obtained expression for the frequency based on the FOSDST. The effects of transverse shear strains, volume fraction, sequence of nanocomposite layers on the frequency are discussed. The analyzes and interpretations carried out revealed that the effects of above-mentioned factors on the nondimensional vibration frequency are very important and it is necessary to consider these factors during the design of sandwich nanocomposite panels.

## REFERENCES

[1]. Vinson JR. Sandwich structures. Applied Mechanics Reviews 2001;54:201–14.
[2]. Iijima S. Helical microtubules of graphitic carbon. Nature 1991;354:56–58.
[3]. Sun CH, Li F, Cheng HM, Lu GQ. Axial Young's modulus prediction of single-walled carbon nanotube arrays with diameters from nanometer to meter scales. Applied Physics Letters 2005;87: 193101.
[4]. Jia J, Zhao J, Xu G, Di J, Yong Z, Tao Y, Fang C, Zhang Z, Zhang X, Zhang L, Li Q. A comparison of the mechanical properties of fibers spun from different carbon nanotubes. Carbon 2011;49:1333–1339.
[5]. Thostenson ET, Ren Z, Chou TW. Advances in the science and technology of carbon nanotubes and their composites: a review. Composites Science Technology 2001;61:1899–912.
[6]. Eswai AMK, Farag MM. Carbon nanotube reinforced composites: potential and current challenges. Material Design 2007;28:2394–2401.
[7]. Martone A, Formicola C, Giordano M, Zarrelli M. Reinforcement efficiency of multi-walled carbon nanotube/epoxy nano composites. Composites Science Technology 2010;70(7): 154–160.
[8]. Zhang LW, Lei ZX, Liew KM, Yu JL. Static and dynamic of carbon nanotube reinforced functionally graded cylindrical panels. Composite Structures 2014;111:205–212.
[9]. Lei ZX, Zhang LW, Liew KM. Vibration analysis of CNT-reinforced functionally graded rotating cylindrical panels using the element-free Kp-Ritz Method. Composites Part B Engineering 2015;77:291-303.
[10]. Kiani Y. Dynamics of FG-CNT reinforced composite cylindrical panel subjected to moving load. Thin-Walled Structures 2017;111:48-57.
[11]. Wang Q, Cui X, Qin B, Liang Q, Tang J. A semi-analytical method for vibration analysis of functionally graded (FG) sandwich doubly-curved panels and shells of revolution. International Journal of Mechanical Sciences 2017;134:479–499.
[12]. Setoodeh AR, Shojaee M, Malekzadeh P. Vibrational behavior of doubly curved smart sandwich shells with FGCNTRC face sheets and FG porous core. Composites Part B Engineering 2019;165:798–822.
[13]. Di Sciuva M, Sorrenti M. Bending, free vibration and buckling of functionally graded carbon nanotube-reinforced sandwich plates, using the extended Refined Zigzag Theory. Composite Structures 2019;227:111324.
[14]. Avey M, Fantuzzı N, Sofıyev AH, Kuruoglu N. Nonlinear vibration of multilayer shell-type structural elements with double curvature consisting of CNT patterned layers within different theories. Composite Structures 2021; 2751:114401.
[15]. Shen HS, He XQ. Large amplitude free vibration of nanotube-reinforced composite doubly curved panels resting on elastic foundations in thermal environments. Journal of Vibration and Control 2017;23(16): 2672–2689.
[16]. Reddy JN. Mechanics of laminated composite plates and shells. Theory and Analysis, Boca Raton, CRC Press, 2004.

**Received:** 14.01.2022
**Accepted:** 03.02.2022

MACHINE SCIENCE

ISSN: 2227-6912
E-ISSN: 2790-0479

2022, Volume 11, № 1. Pages 10 – 13

# ENGINEERING DESIGN AS KEY AREA OF TECHNICAL BACKGROUND FOR ENGINEERS

**Rasim ALIZADE[1], Arkadiy TEMIROV[2], Allahverdi ALAKBAROV[3*]**

[1,3]Department of "Mechatronic and machine design", Azerbaijan Technical University, Baku, Azerbaijan,
[2]ENCOTEC
*E-mail:* rasima@aztu.edu.az[1], encotec@encotec.az[2], allahverdi.elekberov@aztu.edu.az[3*]

**Abstract:** The article identifies some areas of engineer's background, which are not sufficiently covered in curriculums of national universities. These gaps mainly relate to issues of clear understanding of real engineering and design processes, capability to apply system thinking approach to realization of engineering tasks, which is basis of systems engineering. Properly configured curriculums will allow students smoothly move forward from basics of engineering processes and disciplines up to Engineering Project Management.

***Keywords:*** *Engineering Design, Curriculum, System Approach, System Engineering, Engineering Design Process, Syllabus*

**Introduction.** Up-to-date level of technical progress and intensive character of innovative processes in different areas of science and industry require from the specialists with engineering background capability for quick involving into complicated processes of engineering tasks realization, ability to switch over from one technical orientation to another one. These requirements can be achievable only in the case if engineer besides fundamental knowledge has clear understanding that engineering design is a process of system realization.

The basis for understanding of engineering design process shall be set up during study in university and be further improved in course of professional activity.

Lot of universities worldwide today propose to high school students innovative engineering curriculums, which are based on system approach to the engineering defining [1-5]. These curriculums provide flexible engineering foundation, do not prescribe specific modules but offer integration with wide range of other disciplines

Long-term experience of working in engineering company involved into real engineering and design projects of different size and complexity, allows the author to consider the process how just graduated engineers and specialists are entering into practice of routine engineering operation and are involved into execution of real engineering projects.

As a result of conducted analysis the areas of engineering qualification, where deficient attitude and imperfection of syllabuses in national universities are displayed in a maximum extent, are identified. These gaps in engineer's background could have serious consequences for professionals and need to be further compensated by experience gathered during practical work. So, it is essential for engineering syllabuses to ensure that by the time of professional activity commencement the engineer is in possession of main principles of systems engineering.

Systems engineering is an interdisciplinary field of engineering that focuses on how to design and manage complex engineering systems over their life cycles.

The main ideas of systems engineering approach relevant to engineers who supposed to work in engineering and design companies are mainly considered within the frame of this article.

**Engineering design as system realization process.** Engineering and design is a process with final goal to define architecture, components, interfaces and other characteristics of system or its parts. This process results in final design – integrated package of models, properties or characteristics presented in the form, which allows to carry out system realization. Engineering and design process along with analysis of requirements is a part of system overall life cycle, which is

called “system definition”. Outcome of this stage is input data which will be used during system realization stage.

System design is focused on presentation of system, which will correspond to established target, principles and intention. This process includes assessment and decision making regarding selection of system components, which meet the system architecture and confine themselves within prescribed limits.

At its core systems engineering utilizes systems thinking principles to organize this body knowledge. Issues such as requirements engineering, reliability, coordination of different teams, testing and evaluation, maintainability and many other disciplines necessary for successful system development, design, and implementation, become more difficult when dealing with large or complex projects. Systems engineering deals with work-processes, optimization methods, and risk management tools in such projects. It overlaps technical and human-centered disciplines such as industrial engineering, manufacturing engineering, control engineering, software engineering, electrical engineering, cybernetics, organizational studies, and project management. Systems engineering ensures that all likely aspects of a project or system are considered, and integrated into a whole.

As defined by International Council of Systems Engineering’s (INCOSE), systems engineering is based on following main principles [6-8]:

- Systems engineering is a discipline that concentrates on the design and application of the whole (system) as distinct from the parts and involves looking at a problem in its entirety;
- Systems engineering is an iterative process of top-down synthesis, development, and operation of a real-world system that satisfies, in a near optimal manner, the full range of requirements for the system;
- Systems engineering is an interdisciplinary approach and means to enable the realization of successful systems.

Systems engineering signifies only an approach and, more recently, a discipline in engineering. The aim of education in systems engineering is to formalize various approaches simply and in doing so, identify new methods and research opportunities similar to that which occurs in other fields of engineering. As an approach, systems engineering is holistic and interdisciplinary in flavor.

**Engineering design process as a subject for syllabus.** Syllabus is considered as constituent part of mechanism for customization of engineering education in high school as well as a support structure to sustain and continuously improve engineering education in high school.

One of main concern to syllabuses for engineers in national universities is luck of clear understanding the principal distinctions between qualifications of engineer and designer [9-11].

Traditionally in practice of national high school the engineer’s syllabuses include lot of topics (descriptive geometry, technical drawing, etc.) which actually relate to qualification of designer, while many issues essential for engineering background (system thinking, problem definition, brain storming, backward design, systems engineering, engineering design process, etc.) are missed. Clear understanding and perception of engineering and design process is departing point in professional training for all engineers.

The engineering design process is a series of steps that engineers should follow to come up with a solution to a problem. Many times the solution involves designing a product (like a machine or computer code) that meets certain criteria and/or accomplishes a certain task.

Defining the problem is most important and difficult step, because only when a problem has been clearly and accurately identified, a process can be conducted properly.

*“If you define problem correctly you almost have the solution”* (Steve Jobs).

Engineering design process is different from the steps and approaches used in the Scientific Method. If your project involves making observations and doing experiments, you should probably follow the Scientific Method.

But if your project involves such tasks as designing, building, and testing of something, you need to follow the Engineering Design Process.

The steps of the engineering design process are to:

- Define the Problem;
- Do Background Research;
- Specify Requirements;
- Collect Input Data;
- Identify Concept Solutions;
- Brainstorm Solutions;
- Conduct Technical and Other Risks Assessment;
- Conduct Economic/Financial Assessment;
- Choose the Best Solution;
- Do Development Work;
- Validate Design;
- Build a Prototype;
- Test and Redesign.

Engineers do not always follow the engineering design process steps in order, one after another. It is very common to design something, test it, find a problem, and then go back to an earlier step to make a modification or change to your design. This way of working is called **iteration**, and it is likely that your process will do the same.

All steps of design process above are essential as theoretical knowledge as well as practical skill all engineers shall be in possession. Actually, these items could be considered as self-independent topics of technical curriculum.

Technical curriculums shall be originated and structured so that to ensure the future engineer clearly understands as principles of overall engineering and designing process as well as details of its separate constituent parts, like:

- Final goal of design;
- Input Data (Design input);
- Main and additional design requirements;
- Design methodology;
- Quality assurance and quality control for design process;
- Final product (Design output);
- Tools and criteria for design verification and validation

**Understanding of engineering and its core disciplines.** Students of high school will come to understanding of increasingly complex content and concepts of modern engineering scinces through the learning, practicing and applying main principles of engineering design, thinking and skills for solutions of complex technical tasks up to concepts of Engineering Project Management, which consolidates project management skills incorporating multidisciplinary contributions.

Modern engineers should realize that any engineering task should be considered and analyzed from the point of close interrelation and interdependence of all engineering disciplines. So, irrespective of selected area for future specialization all engineering syllabuses should include introduction into main engineering disciplines, such Mechanical Engineering, Civil Engineering, Electrical Engineering, Computer use in Engineering, Bioengineering, Industrial & Manufacturing Engineering. Only through the clear understanding of main concepts and principles of these areas of human expertise high school students can come to well-grounded and deliberate decision about direction for their further engineering specialization.

**Conclusions.** Modern curriculums proposed by national universities for engineering background besides fundamental knowledge in areas of science should ensure that engineers are in possession of methods and approaches of Engineering and Design process based on system thinking principles.

## REFERENCES

[1]. Dr. Shamsnaz Virani, Iris B. Burnham, *"Innovative Curriculum for Engineering in High School (ICE-HS) - Status Update"*, American Society for Engineering Education, 2012
[2]. National Science Board. (2007). Moving forward to improve engineering education. http://www.nsf.gov/pubs/2007/nsb07122/index.jsp
[3]. Rebrin O. I. *New models of engineering education* [Text] / O. I. Rebrin. - Yekaterinburg: LLC "Publishing House" Azhur ", 2015. - 77 p.
[4]. *Reproduction of engineering personnel: challenges of the new time* / Ed. ed. L.N. Bannikova. - Yekaterinburg: Publishing House of Ural.un-ta, 2015. - 364 p.
[5]. A Tuning-AHELO Conceptual Framework of Expected Desired/Learning Outcomes in Engineer. Available at: http://www.unideusto.org/tuningeu/images/stories/Summary_of_outcomes_TN/AHELO_Engineering.pdf
[6]. Sheregi F. E. *Partnership interaction of companies, universities and research organizations for the implementation of scientific programs and innovative production* [Text] / F. E. Sheregi, E. V. Klyuchev. M.: CSFaM, 2013. - 211 p.
[7]. Crawley E. F., Malmqvist J., Lucas W. A. *The CDIO Syllabus v2. 0. An Updated Statement of Goals for Engineering Education*. Proceedings of the 7th International CDIO Conference, Technical University of Denmark, Copenhagen. 2011. Available at: http://publications.lib.chalmers.se/records/fulltext/local_143186.pdf
[8]. EUR-ACE Framework Standards and Guidelines document Edition 31st March 2015. Available at: http://www.cti-commission.fr/IMG/pdf/eur-ace-framework-standards-and guidelines-mar-2015.Pdf
[9]. OECD Science, Technology and Industry Scoreboard 2015. Innovation for growth and society. DOI: 10. 1787/sti_scoreboard-2015-en. Available at: http://dx.doi.org/10.1787/sti_scoreboard-2015-en
[10]. Usoltsev A.P., Shamalo T.N. On the concept of "engineering thinking" // Formation of engineering thinking in the learning process [Text]: materials of the international. scientific-practical. Conf., April 7-8, 2015, Yekaterinburg, Russia: / Ural State Pedagogical University; resp. ed. T.N. Shamalo. - Yekaterinburg: 2015 – 284 p. ISBN 978-5-7186-0683-6

**Received:** 15.01.2022
**Accepted:** 29.03.2022

MACHINE SCIENCE

ISSN: 2227-6912
E-ISSN: 2790-0479

2022, Volume 11, № 1. Pages 14 – 22

# REAL TIME CONTROLLED TWO DoF FIVE BAR ROBOT MANIPULATOR

**Fatih Cemal CAN[1*], Hayrettin ŞEN[2]**

[1,2]Department of Mechatronics Engineering, Izmir Katip Çelebi University, Izmir, Türkiye

*E-mail: fatihcemal.can@ikc.edu.tr[1*]*

**Abstract:** In this research, computer controlled two DoF five bar robot manipulator is investigated. In order to control manipulator, a human machine interface program is developed in Visual C# after completing inverse kinematic analysis of robot manipulator. By the help of inverse kinematics, this program calculates two joint variables for given positions of end point. Then the program sends a data package containing these joint variables to Arduino microcontroller. Arduino microcontroller set the positions of two servos according to calculated joint angles. Also using standard geometries, robot can follow trajectory a line, a circle and a rectangle. Furthermore, a lot of patterns can be generated using function with variable radius and angle of rotation.

**Keywords:** *two DoF Robot, five bar, linkage mechanism, Arduino, Visual C#*

**Introduction.** The five-bar linkage mechanism applications have been used in different engineering fields. Researcher working in mechatronics, biomedical, mechanical and electrical and electronics engineering fields designed and implemented the five bar mechanism in their published investigations. Inverse kinematics, link design, medical application, dynamic simulation, calibration and performance were topics of research interest on the five-bar linkage mechanism. Some studies about these topics are presented as follows.

As a biomedical engineering application, a laparoscopic robotic camera system based on five-bar linkage was designed and tested by Kobayashi and et al. [1]. Thisrobotic system reduce the process time for different surgical operations if human assisted camera system is compared to robot assisted the camera system.

Hybrid five-bar mechanism was investigated by researchers [2, 3]. A dynamic simulation and control of these kinds of mechanism was carried out in Simmechanics of Matlab by Zi and et al. [3]. The five-bar was driven by a constant velocity motor and servo motor in this study. The aim of the study was to control tracking trajectory of the end point of the mechanism via Traditional PD control and closed loop PD-type iterative learning control.

Inverse kinematics analysis of six different five-bar planar parallel manipulators which were RRRRR, RRRRP, PRRRP, RPRPR, RRRPR and RPRRP was presented by Alıcı[4]. Sylvester elimination method was used to solve the set of nonlinear equations in his study.

Villarreal-Cervantesand et al. [5] optimized design parameters of a five-bar parallel robot by using a novel mechatronic design approach. They designed kinematic and dynamic parameters of the five-bar's links with respect to desired trajectories [5, 6].

A position accuracy calibration of a five-bar planar parallel robot (DexTAR) was established by Joubair and et al. [7]. Experimental validation setup was constructed and the position error reduced to 0.08 mm with in the entire robot workspace of 600x600 mm.

A real-time control of a five-bar parallel robot (DexTAR) was studied using dynamic model of the robot to implement minimum time trajectory planning by Bourbonnais and et al. [8]. They used working mode region to reach points of pick and place operations. Several working modes are considered to reach same pick and place points in their study.

In this study, a five-bar linkage was designed and two links of the mechanism were produced

by using 3D printer. In section 2, the inverse kinematics analysis of five-bar manipulator will be presented. In the next section human machine interface design and control algorithm will be explained. In section four electronic hardware and circuit are illustrated along with figures. Then, experimental test results will be presented in section five. Finally, a conclusion will be drawn at the end of the study.

**Inverse Kinematic Analysis of the Robot Manipulator.** Five bar mechanism has two degrees of freedom according to Grubler formulation. In inverse kinematics, endpoint location (P) is known in Fig. 1. Using this location, two input angles $\theta_1$ and $\theta_2$ must be calculated. This problem can be solved by dividing manipulator into two serial RR manipulators.

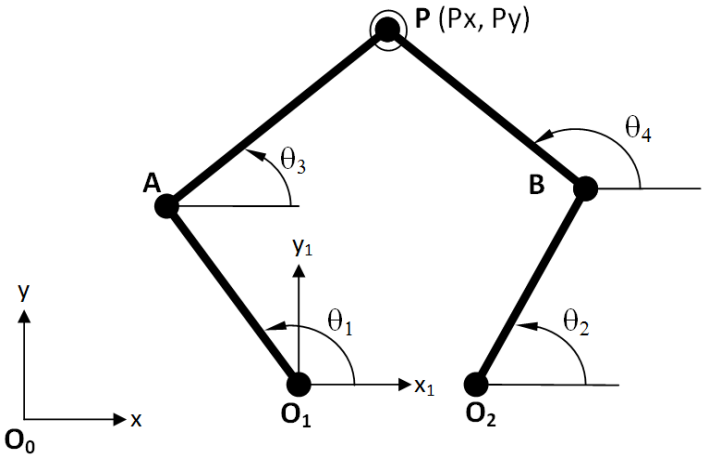


*Figure 1. Two DoF Five Bar Robot*

From the first serial kinematic chain, vector loop closure equation (1) is as follows,

$$O_0O_1 + O_1A + AP = O_0P \tag{1}$$

Second, the second serial kinematic chain, vector loop closure equation (2) is as follows,

$$O_0O_2 + O_2B + BP = O_0P \tag{2}$$

In this study, user of the robot manipulator changes $O_0P$ vector in human machine interface. However these equations are dependent on each joint angle related to kinematic chain. In order to compute input angles, other joint variables must be eliminated.

$$d_{x1} + i\, d_{y1} + L_1 e^{i\,\theta_1} + L_3 e^{i\,\theta_3} = P_x + i\, P_y \tag{3}$$

$$d_{x2} + i\, d_{y2} + L_2 e^{i\,\theta_2} + L_4 e^{i\,\theta_4} = P_x + i\, P_y \tag{4}$$

Rearranging equation (3), angle which is need to be eliminated is kept alone,

$$L_3 e^{i\,\theta_3} = P_x + i\, P_y - d_{x1} - i\, d_{y1} - L_1 e^{i\,\theta_1} \tag{5}$$

The offset distances in equation (5) can be combined with the end coordinates as follows,

$$L_3 e^{i\,\theta_3} = (P_x - d_{x1}) + i\big(P_y - d_{y1}\big) - L_1 e^{i\,\theta_1} \tag{6}$$

Conjugate of the equation (6) is written as follows,

$$L_3 e^{-i\,\theta_3} = (P_x - d_{x1}) - i\big(P_y - d_{y1}\big) - L_1 e^{-i\,\theta_1} \tag{7}$$

Multiplying equations (6) and (7), angle $-i\,\theta_3$ is able to be eliminated.

$$L_3^2 = (P_x - d_{x1})^2 + \left(P_y - d_{y1}\right)^2 + L_1^2 - (P_x - d_{x1})L_1\left(e^{i\,\theta_1} + e^{-i\,\theta_1}\right) + \\ +\left(P_y - d_{y1}\right)L_1\,i\left(e^{i\,\theta_1} - e^{-i\,\theta_1}\right) \quad (8)$$

Remember that $\left(e^{i\,\theta_1} + e^{-i\,\theta_1}\right)$equals to $2\cos(\theta_1)$ and $i\left(e^{i\,\theta_1} - e^{-i\,\theta_1}\right)$ equals to $2\sin(\theta_1)$ in equation (8). The equation can be simplified using these equalities as follows,

$$A\cos(\theta_1) + B\sin(\theta_1) + C = 0 \quad (9)$$

where $A = -2\,(P_x - d_{x1})L_1$, $B = -2\left(P_y - d_{y1}\right)L_1$ and$C = (P_x - d_{x1})^2 + \left(P_y - d_{y1}\right)^2 + L_1^2 - L_3^2$. Half-tangent rule can be used for this equation in order to solve one unknown ($\cos(\theta_1) = \frac{1-t_1^2}{1+t_1^2}$, $\sin(\theta_1) = \frac{2\,t_1}{1+t_1^2}$and$t_1 = \text{atan}(\frac{\theta_1}{2})$).

$$(C - A)t_1^2 + 2\,B\,t_1 + (C + A) = 0 \quad (10)$$

Two different roots are able to be obtained from the equation. Discriminant must be real for physically realizable result.

$$dis1 = \sqrt{4B^2 - 4(C^2 - A^2)} \quad (11)$$

One unknown $t_1$ is calculated using discriminant.

$$t_1 = \frac{(-4\,B \mp dis1)}{2(C-A)} \quad (12)$$

One can compute the angle using half tangent value.

$$\theta_1 = 2\tan(t_1) \quad (13)$$

Once $\theta_1$ is known, other angle of kinematic chain is calculated as follows,

$$\theta_3 = atan2(P_x - d_{x1} - L_1\cos(\theta_1)\,, P_y - d_{y1} - L_1\sin(\theta_1)\,) \quad (14)$$

Similarly, applying same process to the second kinematic chain, we can obtain the discriminant as follows,

$$dis2 = \sqrt{4E^2 - 4(F^2 - D^2)} \quad (15)$$

where $D = -2\,(P_x - d_{x2})L_2$, $E = -2\left(P_y - d_{y2}\right)L_2$ and $F = (P_x - d_{x2})^2 + \left(P_y - d_{y2}\right)^2 + L_2^2 - L_4^2$

Similar to pervious solution, unknown of the second kinematic chain is now known using equation as follows,

$$t_2 = \frac{(-4\,E \mp dis2)}{2(F-D)} \quad (15)$$

$$\theta_2 = 2\tan(t_2) \quad (16)$$

$$\theta_4 = atan2(P_x - d_{x2} - L_2\cos(\theta_2)\,, P_y - d_{y2} - L_2\sin(\theta_2)\,) \quad (17)$$

Two solutions are obtained for each angle. Totally four modes can be found for the robot. But, the robot is working on just one mode which is shown in Fig.1.

## 1. Visual C# Interface Design and Program for Human - Machine Interaction.

The program of the robot is constructed on kinematic analysis of the robot. Two coordinates of the end point location are inputs for this program. User is able to use mouse cursor in order to define end point location of the robot. User must click mouse left button on the Form then he must move cursor wherever he wants. Program solves angles according to end points and redraws lines of the robot.

Human machine interface consists of two parts. The first part is the interface design of the program. This part is related to graphical drawing of the robot, angles in text boxes and control buttons and output of the program. The design of the program is illustrated in Fig. 2.

The second part is algorithm or coding. Follow chart of the visual program is depicted in Fig. 3. This code is written using events of graphical objects such as buttons, lines, form and buttons. This kind of programming is named event based programming. We use load, mouse down, mouse move and mouse up events for our code.

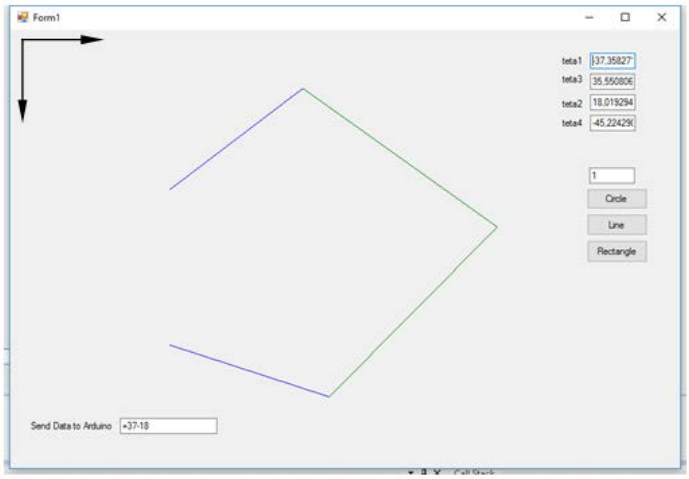


*Figure 2. Human Machine Interface in Visual C#*

***Start:*** Form1_Load event is working. In this event, link lengths and other constant parameters are defined.

***Input:*** Form1_Mousedown, Form1_MouseMove and Form1_MouseUp events are working.

***Calculate:*** dis1 and dis2 are calculated according to inverse kinematic analysis of the robot.

***Are roots of dis1 and dis2 real?*** Program must decide that the results are physically realizable or not. Non real results cannot be used in real environment. Therefore, they are unnecessary.

***Calculate:***If roots are real, angles are calculated using Equations (13, 14, 16 and 17).

***Prepare and send data packages to Arduino:*** When two angles are calculated, they are packaged in order for sending. The data package includes plus and minus symbols which show the direction of the rotation, and two digit numbers which indicate magnitude of the rotation.

One Data Package

| | | | | | |
|---|---|---|---|---|---|
| + | 9 | 0 | - | 4 | 5 |

***Is Arduino serial connection OK?:*** In order to send packages to Arduino, COM port number of Arduino must be valid and connected. Baud rate of the connection must be selected correctly.

***Is close of Form clicked?:*** The program runs until close of form is clicked. The program ends if it is clicked.

The flow chart of Arduino program is illustrated in Figure 4. This code waits for the input from interface program, separate according to data package format and sends these to servo motors.

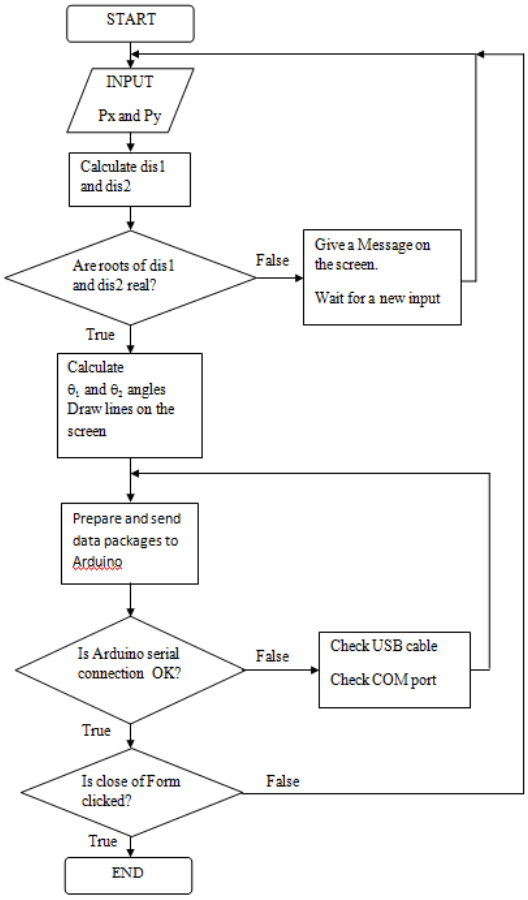


*Figure 3. Flow Chart of Visual C# Human Machine Interface (HMI) Program*

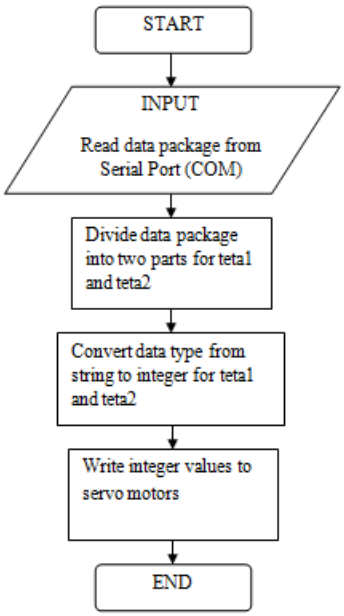


*Figure 4. Flow Chart of Arduino Program*

## 2. Electronic Hardware and Circuit

Arduino Mega 1280 Micro Controller is used to control the robot. The robot has two servos connected to digital pins 9 and 10 which are used as PWM (pulse width modulation) ports of Arduino. The electronic circuit of the robot is seen in Figure 5. This circuit is created in Autodesk Circuit Online Software. Arduino Uno is used in the circuit because Arduino mega is not available in this software. One 5V DC power source must be used to supply required power to servo motors. The Arduino code can be simulated in the program. Simulation can be seen in Figure 6.

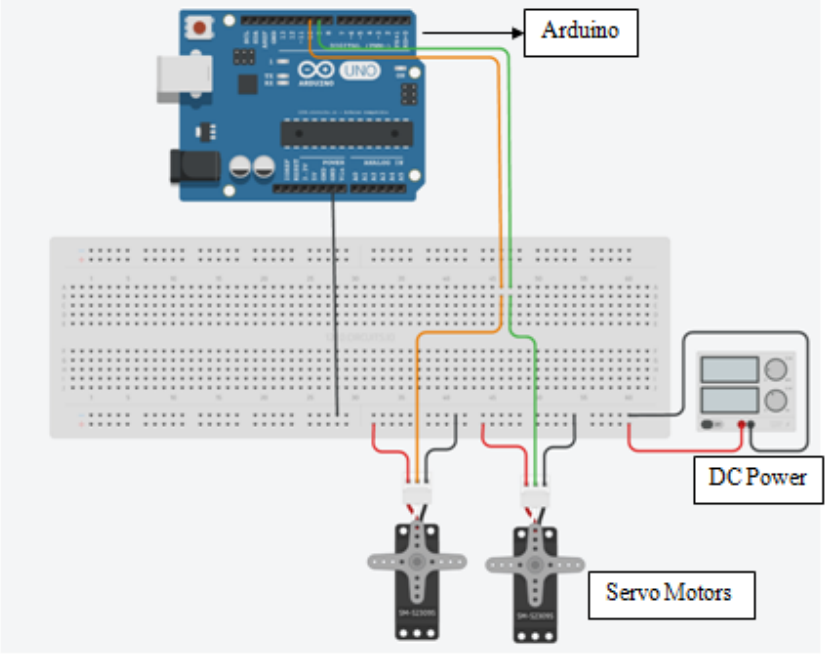


*Figure 5. Electronic Circuit in Autodesk Circuits*

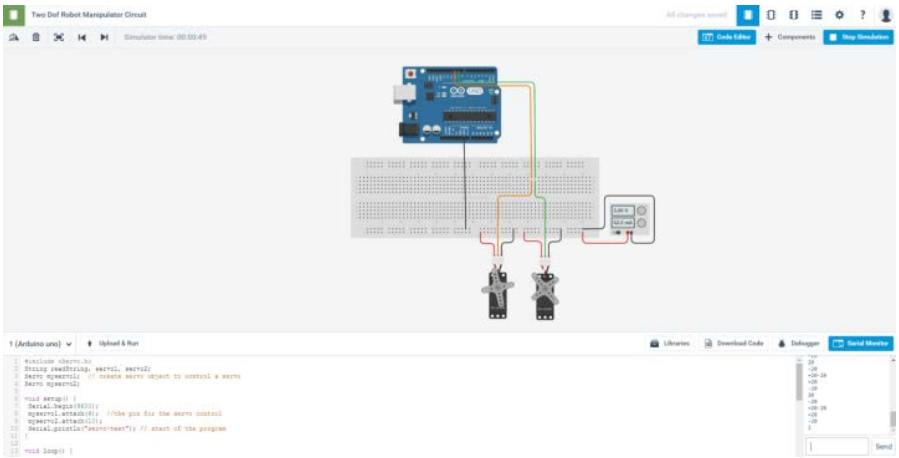

*Figure 6. Simulation in Autodesk Circuits*

## 3. The robot construction and test results

The robot is constructed using two Emax ES 3005 water proof servo motors and 3-D printed parts. Two link lengths $L_1$and $L_2$ are chosen same (20 mm) because they are servo links packaged in servo motor box. Other two link lengths $L_3$ and $L_4$ are selected to be same (30 mm). Distance between shafts of two servo motors is 19 mm.

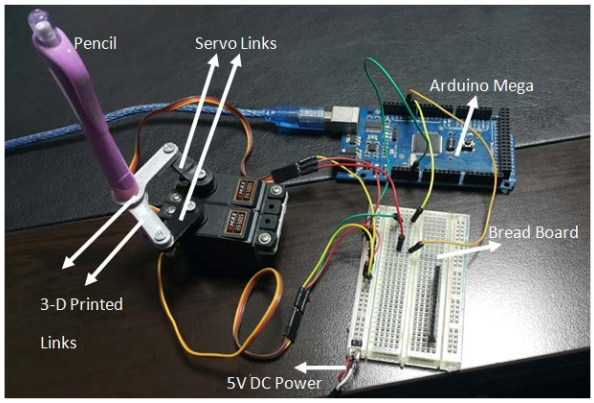


*Figure. 7. Electrical connection and whole setup*

### 3.1. Drawing a line and a rectangle

These two shapes are the most basic task to test our robot. Simply, pencil translates forward and backward between two points to draw a line and four lines are used to draw a rectangle (Fig. 8.). We defined the length of the line as 20 mm in the program. The straightness of the line was good but the length of the line was nearly 19.20 mm. This dimension error depends on joint clearances and friction at the joints. Next, the rectangle was drawn. Fillets are created by our robot at the corner. This rectangle was not perfect dimensioned similar to the line. But straightness and appearance of the rectangle is acceptable.

a) b)

*Figure 8. Drawing Test (a) Line Drawing (b) Rectangle drawing*

### 3.2. Computer Aided Free Hand Drawing

We tried to test our robot manipulator using human machine interface (HMI). User entered required points from HMI, points were sent to microcontroller and microcontroller set angles of two servo motors. Acceptable outputs were obtained as seen from Figures 9 and 10. We firstly tried to draw a letter and then a spiral. The letter and the shape are very close to original shape which is drawn on HMI.

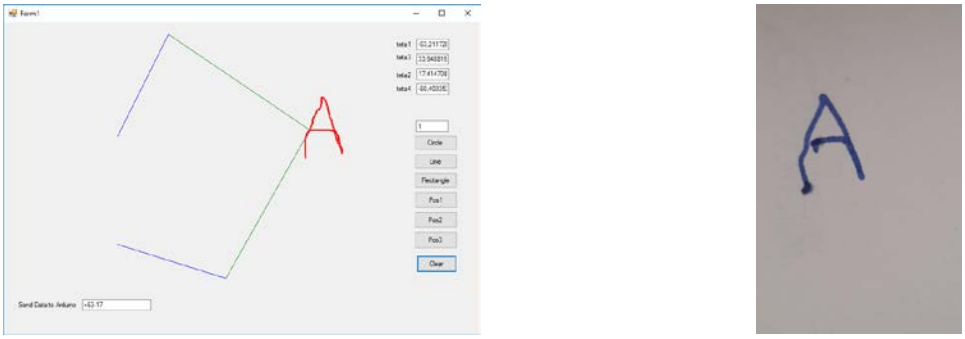

(a) (b)

*Figure 9. Free hand drawing of letter A (a) Input from Human-Machine Interface (b) Output on the paper*

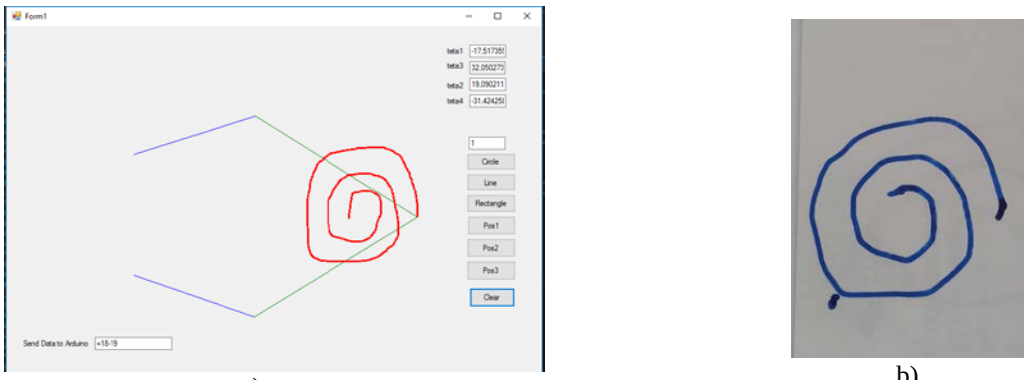


a) b)

*Figure 10. Free hand drawing of a spiral (a) Input from Human-Machine Interface (b) Output on the paper*

### 3.3. Drawing a pattern

In this section, a circular pattern drawing will be explained along with examples. We created the pattern by using Equations as follows,

$$P_x = 60 + rcos\left(\beta\frac{\pi}{180}\right) \quad (15)$$

$$P_y = 60 + rsin\left(\beta\frac{\pi}{180}\right) \quad (16)$$

Where Px and Py are coordinates of the end point of the robot, r is radius of circle, β is angle of the rotation of radius. If radius is constant and β angle is changing uniformly, we will get a circle. However, if radius is changed according to a linear function (r=r+a·k, if r>90 then k=-1, if r<1 then k=+1) and also changing rotation of angle (β =β+dt), the patterns can be drawn. According to this pattern configuration and formulation, the end-effector of five-bar robot drew the patterns shown in Fig. 11.

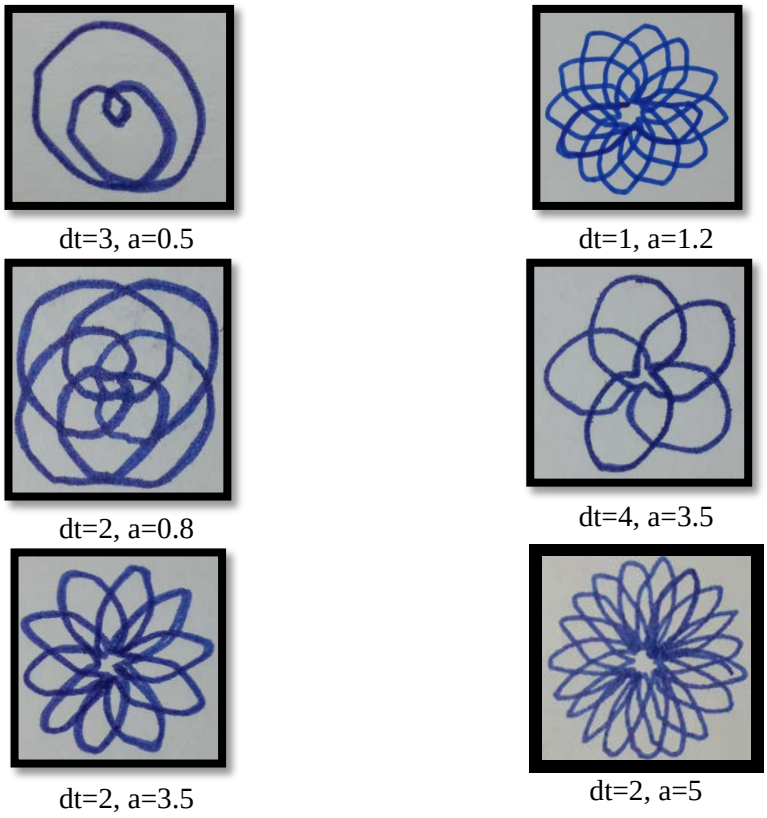

dt=3, a=0.5 dt=1, a=1.2

dt=2, a=0.8 dt=4, a=3.5

dt=2, a=3.5 dt=2, a=5

*Figure 11. Some pattern drawings for different dt and a values*

**Conclusion.** The five-bar robot manipulator was constructed and tested in this study. Two servo motors of the robot were controlled using HMI program through Arduino microcontroller. Test results were shown for a line, a rectangle, free hand drawing and patterns. Cost of our robot manipulator is very low (it is nearly 50$) compared to other robot manipulators. Readability and appearance of the test shapes are good. However, accuracy and repeatability are not very well. Therefore, they must be improved. Due to its cost, this robot manipulator will be useful to explain the working principle of the five-bar robot manipulator and application of the robot to engineering students.

## REFERENCES

[1]. Kobayashi, E., Masamune, K., Sakuma, I., Dohi, T., & Hashimoto, D. *A new safe laparoscopic manipulator system with a five-bar linkage mechanism and an optical zoom*. Computer Aided Surgery, 4(4), pages 182-192, 1999.

[2]. Cheng, L., Lin, Y., Hou, Z. G., Tan, M., Huang, J., & Zhang, W. J.. *Adaptive tracking control of hybrid machines: a closed-chain five-bar mechanism case*. IEEE/ASME Transactions on Mechatronics, 16(6), pages 1155-1163, 2011.

[3]. Zi, B., J. Cao, and Z. Zhu. *Dynamic simulation of hybrid-driven planar five-bar parallel mechanism based on simmechanics and tracking control.* International Journal of Advanced Robotic Systems, 8(4), pages 28-33, 2011.

[4]. Alici, G., *An inverse position analysis of five-bar planar parallel manipulators.* Robotica, 20(02), pages 195-201, 2002.

[5]. Villarreal-Cervantes, M.G., Cruz-Villar, C. A., Alvarez-Gallegos, J., & Portilla-Flores, E. A., *Differential evolution techniques for the structure-control design of a five-bar parallel robot.* Engineering Optimization, 42(6), pages 535-565, 2010.

[6]. Kim, J., *Task based kinematic design of a two DOF manipulator with a parallelogram five-bar link mechanism.* Mechatronics, 16(6), pages 323-329, 2006.

[7]. Joubair, A., M. Slamani, and I.A. Bonev. *Kinematic calibration of a five-bar planar parallel robot using all working modes, Robotics and Computer-Integrated Manufacturing.* 29(4), pages 15-25, 2013.

[8]. Bourbonnais, F., P. Bigras, and I.A. Bonev. *Minimum-time trajectory planning and control of a pick-and-place five-bar parallel robot.* IEEE/ASME Transactions on Mechatronics, 20(2), pages 740-749, 2015.

**Received:** 28.01.2022
**Accepted:** 18.03.2022

MACHINE SCIENCE

ISSN: 2227-6912
E-ISSN: 2790-0479

2022, Volume 11, № 1. Pages 23 – 40

# A NOVEL TWO-POLYNOMIALS CRITERIA FOR HIGHER-ORDER SYSTEMS STABILITY BOUNDARIES DETECTION AND CONTROL

**Nazim MIR-NASIRI**

Swinburne University of Technology, Melbourne, Australia

*E-mail: nazim.mir-nasiri@swinburne.edu.my*

**Abstract.** There are many methods of identifying general stability of complex dynamic systems. Routh and Hurwitz's criterion is one of the earliest and commonly used analytical tools analysing stability of a dynamic system. However, it requires redundant calculation of all the elements of the Routh array to identify stability, even the low-order system. Therefore, it is not a simple method to identify, especially analytically, the stability boundaries for the coefficients of the characteristic equation due to tedious and lengthy derivation of all the Routh array elements. The proposed brand-new criterion or algorithm is an effective alternative and a universal technique to identify analytically the stability of up to sixth-order linear time-invariant dynamic system based on the set of unique for all possible system equations (2) and (3) that relate coefficients of the system characteristic polynomial at the stability boundaries by means of a single additional constant *k*. The expressions derived on this basis for a higher-order dynamic system can be used effectively to identify the boundaries of its stable behaviour spans. It defines the necessary and sufficient conditions for absolute stability of higher-order dynamic systems. It also allows the analysing of the system's precise marginal stability condition (whether stable or not) and the nature of the system roots at the stability boundaries, i.e. when they are relocated on imaginary $j\omega$-axis of s-plane. The criterion proposed by the authors, in contrast to Routh criteria, simplifies significantly the identification of maximum and minimum stability limits for any coefficient of the higher-order characteristic equation. The paper also presents the numerical analysis of stability boundaries for systems with order higher than six based on criteria (2) or (3). The derived stability boundary formulas (2) and (3) for the polynomial coefficients are successfully used for PID controller gains selection in close-loop control systems and this achievement does not have analogy in control theory.

**Keywords:** *higher-order dynamics, characteristic polynomial, stability boundaries, absolute and marginal stability.*

**Introduction.** The research on stability of higher-order systems was initiated by Edward Routh and Adolf Hurwitz long ago, their theory is being used now by control experts while analysing stability of dynamic systems and added to many books on control engineering [1-4]. It provides an effective tool for identifying stability condition dynamic system and roots of its system polynomial on the $j\omega$-axis of *s*-plane. However, it does not provide an effective method for identifying precise stability limits of higher-order system operation in analytical or numerical way by mathematically analysing the coefficients of the system characteristic polynomial. Deriving analytical expressions based on the Routh array is a very tedious and lengthy process. It becomes formidable task for systems with order higher than four. Besides, for special cases of all zeros in an array raw, the use of standard Routh procedure does not provide solution to the problem.

Some researchers have managed to solve specific system stability problems by using the Routh-Hurwitz criterion. In paper [5], the authors use the Hermite-Biehler theorem to derive Routh-Hurwitz criterion and managed to capture the system's unstable root counting. While performing stability analysis the Routh array may suffer some singularities. One example is when the first element of a row turns out to be zero. The solution to this case was discussed in some papers [5, 6, and 7] and textbooks [1-4]. Some researchers have used the $\epsilon$-method to solve the stability problem for the special case when there are zero leftmost elements together with an all-zero row in the Routh

array [6]. A minor reconstruction of Routh's array is presented in [7] to solve a special case of leading array elements in the array becoming zero. In reconstructed array, locations of of a polynomial root are defined by means of considering first-column sign changes, similar to Routh's method, which eliminates the necessity of implementing the $\epsilon$-approach.

The singularity in Routh array may also occur in case where all elements of a row become zero. In [8], the authors have presented a solution for the roots of a polynomial in the right-half of *s*-plane and on the $j\omega$-axis for the case when a few elements of a row in the Routh array become zero. They have used the continued fraction approach to solve the problem. When a system parameter is of the $\epsilon$-order, the advantage of the $\epsilon$-method of the Routh-Hurwitz criterion for the zero row was elaborated in [9]. In [10], authors have replaced zero row coefficients with the derivative of the polynomial corresponding to the row next to the zero-row to fill the row as an additional procedure and doing that they have succeeded in identifying the location of the symmetric roots of the polynomial on the right and left and/or on the $j\omega$-axis. [7].

Importantly, the Routh-Hurwitz criterion unable to determine the case of instability for the case of multiple roots on the $j\omega$-axis of the *s*-plane [2, 4, and 11]. Routh array does not provide solution for the number of $j\omega$-axis roots with multiplicity greater than unless solving it with the auxiliary polynomial. Moreover, Routh's array does not show sign change in the first column of the array for *some unstable systems* with repeated multiple roots on $j\omega$-axis even by applying the auxiliary polynomial procedure, i.e. indicating that there are no roots of the system polynomials in the right half *s*-plane [11]. In [10], the authors are managed to count the number of roots on $j\omega$-axis that are complex polynomials. The authors in [12] have investigated possible relation between the multiplicity of $j\omega$-axis poles and the numbers of zero rows in the Routh array. The main outcome was a prove that existence of more than one zero row in the Routh array is a source of instability of the system regardless of any sign change in the first column. In paper [13], authors have aimed for modelling and analysis of cyclic physical phenomenon and investigated harmonic oscillations of higher-order systems at the borders of stability regions. Stability boundary oscillations are used in many science and engineering applications [13]. The authors in [14, 15] conducted boundary locus analysis to achieve a stable control system design. The authors identified stability regions of controller coefficients based on a solution of characteristic polynomial equation in *s* domain for $s=j\omega$. In the research paper [13], the authors have identified the harmonic oscillation boundary of systems by mapping the roots of the characteristic polynomial to amplitude-angle $(M-\theta)$ plane and presenting roots of polynomial in the form of $\lambda = Me^{j\theta}$.

Another common method of *n*-th order systems stability studies is related to analysing numerical eigenvalues of of *n* state equations [16, 17]. However, it does not simplify the solution of the problem for *n*-th order system, the dimensions of a matrix of eigenvalues and matrix **A**, i.e ($\lambda$**I**-**A**), are of the same *n*-th order. Therefore, the level of complexity of stability problem solution is similar to analysing roots of the original *n*-th order system characteristic polynomial. In other words, it requires calculation numerically the roots $\lambda$ of *n*-th order polynomial to verify stability of a given system and therefore analytical solution of the problem is not possible.

The literature review has shown that so far there is no any systematic and exact solution for stability problem of linear higher-order dynamic systems that is able to identify exact stability boundaries of system behaviour in terms of the coefficients of its characteristic polynomial and doing that is able thoroughly analyse and differentiate marginal stability or instability of systems at the boundary regions of stability. The importance of such theory could also contribute to closed-loop controllers design and selection of controller gains for real dynamic systems. The closed-loop controller gains are part of the system characteristic polynomial coefficients and, therefore, stability limits of the coefficients can be used, in turn, to identify stability limits for the gains. The method described in this paper aims to solve these problems. In addition, it can precisely define the number and types of conjugate roots on the $j\omega$-axis of the *s*-plane while dynamic system is at the stability

boundary region and their influence on marginal stability or instability for some special cases of zero coefficients.

The new theory of stability was initially introduced in [18]. However, current paper in section II introduces a completely modified systematic and more simple approach for identifying stability of higher-order linear time-invariant dynamic systems with only two polynomials as an alternative to the renowned Routh-Hurwitz criterion and any other method. The discovered criterion and algorithms for system stability has no analogy to other criteria published so far in the field of stability control. The algorithms in this paper have been developed intuitively based on certain systematic relations of the coefficients of characteristic polynomial at the boundaries of stability and they are undoubtedly and successfully worked with all higher-order dynamic systems either with randomly selected coefficients of characteristic polynomials or randomly selected engineering applications with closed-loop controllers. The presented method is a simple and the only available procedure to identify the stability boundaries of the coefficients of a higher-order system characteristic polynomial. The difficulty of achieving the same objective by using the Routh has been discussed in section III for a sixth-order system. The presented algorithms are essential tools to identify marginal stability or instability of the systems for the case of multiple roots of the polynomials on $j\omega$-axis of the $s$-plane. Section III discusses in details and set the rules to identify stability boundaries for third-order, fourth-order, fifth-order and sixth-order dynamic systems in analytical form. The paper presents separate rules for absolute and marginal stability of systems when the multiple roots occur on the $j\omega$ -axis of the $s$-plane. Section IV also presents the numerical technique to identify stability boundaries for the dynamic systems with orders higher than six when it was difficult to derive analytical solution for the problem. For all the systems analysed in this paper, the boundary limits of lowest order dependent coefficients of characteristic polynomial $a_0$ as a function of other coefficients were determined. Section V demonstrate the use of the developed theory for defining of stability limits for the gains of closed loop controllers for various engineering systems with higher-order dynamic models.

**Presentation of general stability criteria.** In general the characteristic polynomial for higher-order dynamic system can be presented as follows:

$$a_n s^n + a_{n-1} s^{n-1} + a_{n-2}\, s^{n-2} + \cdots + a_1 s + a_0 \;= 0 \tag{1}$$

One of the conditions of possible stability is that all the coefficients of the polynomial must be positive real numbers [2.3]. However, positive values of the coefficients alone do not provide stability of the system. The current paper presents stability criteria of the higher-order systems system with all positive values coefficients as well as when some coefficients having zero values which leads to special cases of marginal stability or instability.

The general necessary stability criteria for any $n$-order dynamic system (where $n \geq 3$) can be uniquely expressed by the set of two non-linear algebraic equations (2) or (3) with introduction of an additional unknown variable $k$ that couples both equations together. If the highest order of the system $n$ is an *odd* number then two equations are presented, as follows:

$$\begin{aligned} a_n &= (a_{n-2} - (a_{n-4} - \cdots - (a_3 - a_1 k)k) \ldots)k \\ a_{n-1} &= (a_{n-3} - (a_{n-5} - \cdots - (a_2 - a_0 k)k) \ldots)k \end{aligned} \tag{2}$$

If the highest order of the system $n$ is an *even* number then two equations are presented differently, as follows:

$$\begin{aligned} a_n &= (a_{n-2} - (a_{n-4} - \cdots - (a_2 - a_0 k)k) \ldots)k \\ a_{n-1} &= (a_{n-3} - (a_{n-5} - \cdots - (a_3 - a_1 k)k) \ldots)k \end{aligned} \tag{3}$$

It can be seen from (2) and (3) that unknown parameter *k* must be a real positive number to ensure that coefficients $a_n$ and $a_{n-1}$ are positive real numbers which is obvious stability condition for the system.

The *fundamental law of marginal or boundary stability* of any dynamic system with order $n \geq 3$ is stated as follows: "if equations (2) or (3) are satisfied and there exists solution of these equations with at least one common *k* as a positive real root, then all the coefficients in (1) are having stability boundary values and the system under consideration is in the state of marginal or boundary stability condition". At this state some of the roots of characteristic polynomial (1) form conjugate pairs and strictly located on the imaginary *jω*-axis of the *s*-plane. Therefore, (2) or (3) represent the *necessary and sufficient* criteria to define accurately stability boundary value for all the coefficient of dynamic system characteristic polynomial with order $n \geq 3$, provided algebraic equations (2) or (3) have at least one common positive real solutions for *k*. In other words, if conditions (2) or (3) satisfy, then the dynamic system is in the state of marginal stability or instability, i.e. it is exactly in between the stable and unstable zones of behaviour. The boundary values for the coefficients of *n*-th order system (1) can be obtained by mathematically excluding unknown *k* from both equations (2) or (3). The newly developed expressions (2) or (3) have no similarity to any stability criteria published so far in the literature. The relationship between the coefficients of the characteristic polynomial at the state of system stability boundary regions has been discovered intuitively but can be verified by any other method that describes stability boundary conditions for a dynamic system.

The lowest order of the system to be solved with (2) or (3) is *n*=3. For this 3rd order system (odd order), expression (2) can be expressed as follows:

$$a_3 = (a_1)k \quad \text{an} \quad a_2 = (a_0)k$$

Excluding *k* from both equations can lead to the stability boundary expression for the third order system, i.e. $a_2/a_0 = a_3/a_1$. This system is fully stable if the following inequality is satisfied:

$$\frac{a_2}{a_0} \geq \frac{a_3}{a_1} \tag{4}$$

The equal sign means a marginal stability of the system with *one pair of roots* symmetrically located on the *jω*-axis of the *s*-plane. The validity of (4) can be verified by using other methods such as Routh criteria and root-locus method.

**Analytical solution for the stability boundaries for up to sixth-order systems.**

*a. Stability criterion for the fourth-order dynamic system*

The system is presented by the following characteristic polynomial:

$$a_4 s^4 + a_3 s^3 + a_2 s^2 + a_1 s^1 + a_0 = 0 \tag{5}$$

Since the highest order of the system *n*=4, i.e. it is an even number, equations (3) were used to describe the boundary conditions for the polynomial (5).

$$a_4 = (a_2 - a_0 k)k \tag{6}$$
$$a_3 = (a_1)k \tag{7}$$

According to the newly developed fundamental law of boundary stability condition of any dynamic system with with order $n \geq 3$, values of *k* in (6) and (7) must be real positive numbers. Solving (6) and (7) for *k* leads to the following results:

$$k = \frac{\left(a_2 \pm \sqrt{a_2^2 - 4a_0 a_4}\right)}{2a_0}; \quad k = \frac{a_3}{a_1}$$

From these expressions part of the *necessary* boundary stability conditions for the system (5) can be derived. For *k* to be positive real number the following conditions must satisfy:

$$a_2^2 \geq 4a_0a_4;\ a_1 \neq 0;\ a_3 \neq 0 \tag{8}$$

Excluding *k* from both (6) and (7) and some algebra leads to the following single *necessary boundary or marginal stability* expression for the coefficients of (5):

$$a_0{a_3}^2 = (a_2a_3 - a_1a_4)a_1 \tag{9}$$

For $a_0$ to have positive non-zero value the following *necessary* boundary stability condition must be satisfied:

$$a_2a_3 > a_1a_4 \tag{10}$$

As a conclusion, it can be stated that (9) presents the *necessary and sufficient boundary or marginal stability* expression for the coefficients of (5) provided (8) and (9) are fully satisfied. The analysis shows that when the coefficients reach their stability boundary values, the system becomes *marginally stable* with *two (i.e. one pair of conjugate complex numbers) out of four roots located symmetrically on jω*-axis *of the s-plane*.

For comparison and *prove of validity* for (9), the expressions of the Routh array elements (two columns with five rows) for the fourth-order system were presented. The final equation in the first column of the Routh array can be presented as follows:

$$a_1 - \frac{a_3a_0}{A} = 0 \tag{11}$$

Substituting $A=(a_2a_3 - a_1a_4)/a_3$ into (11), the same expression (9) can be derived. Therefore, Routh method solution serves as an *'elementary' prove* of validity for the proposed stability criteria (3).

The expression (9) can be easily used to define the boundary values of any coefficient of the characteristic equation (5). For example, for this system to be *absolutely stable*, $a_0$ must be within the range in between its minimum and maximum boundary values, as it was defined from (9):

$$0 < a_0 < \frac{(a_2a_3 - a_1a_4)a_1}{{a_3}^2} \tag{12}$$

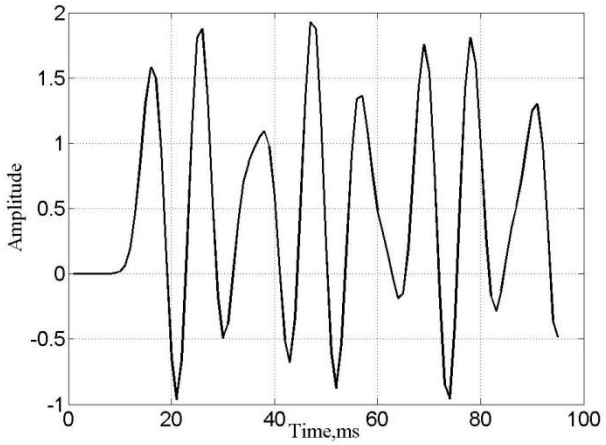


*Figure 1 Marginally stable system*

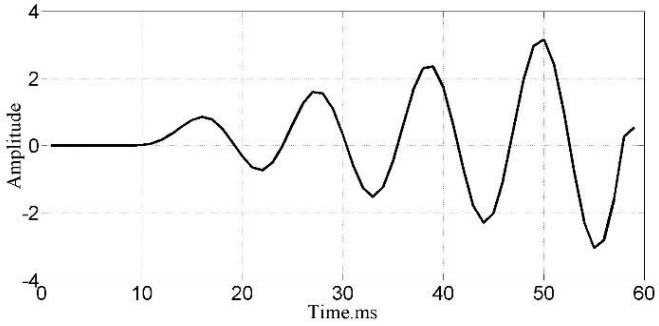


*Figure 2 Marginally unstable system*

In accordance to (9), in the case $a_1 = a_3 = 0$, i.e. when (9) yields 0=0, the following *special case* of marginal stability or marginal instability when *all four roots of polynomial are located on jω -axis* of the *s*-plane has been derived. If $a_1 = a_3 = 0$, the system becomes <u>*marginally stable*</u> and its characteristic polynomial will have *all four roots (in this case two different pairs of conjugate complex numbers) symmetrically located on jω-axis of the s-plane if* $a_2^2 > 4a_0a_4$, or if still $a_1 = a_3 = 0$, the system becomes <u>*marginally unstable*</u> and its characteristic polynomial will *have all four roots* (in *this case two repeated pairs of conjugate complex numbers) symmetrically located on jω-*axis *of the s-plane if* $a_2^2 = 4a_0a_4$. This special case marginal stability is a unique case when the same condition of coefficients $a_1 = a_3 = 0$ lead to two different behaviour of the 4th order system and different type of roots of the polynomial (5) depending of the values of its remaining coefficients.

The example of a system polynomial that has *marginal stability* is $s^4 + 3s^2 + 2 = 0$ and Fig. 1 shows response of this system to the unity input. The example of a system polynomial that has *marginal instability* is $s^4 + 4s^2 + 4 = 0$ and Fig. 2 shows response of this system to the unity input. The difference in both system responses with the same condition for the coefficients $a_1 = a_3 = 0$ can be seen clearly in Fig. 1 and Fig. 2. This unique condition of marginal stability or instability was not identified by using the Routh method of stability analysis.

*b. Stability criterion for the fifth-order dynamic system*

The system is presented by the following characteristic polynomial:

$$a_5s^5 + a_4s^4 + a_3\,s^3 + a_2\,s^2 + a_1s + a_0 = 0 \tag{13}$$

Solving the boundary problem for a system polynomial (10) coefficients can be done by taking *n*=5 (odd number) in (2). It leads to the following two non-linear equations:

$$a_5 = (a_3 - a_1k)k \tag{14}$$

$$a_4 = (a_2 - a_0k)k \tag{15}$$

According to the newly developed fundamental law of boundary stability condition of any dynamic system with with order $n \geq 3$, values of *k* in (14) and (15) must be real positive numbers. Solving (14) and (7) for *k* leads to the following results:

$$k = \frac{\left(a_3 \pm \sqrt{a_3^2 - 4a_1a_5}\right)}{2a_1};\;\; k = \frac{\left(a_2 \pm \sqrt{a_2^2 - 4a_0a_4}\right)}{2a_0}$$

From these expressions the *necessary and sufficient* boundary stability conditions for the system (13) can be derived. For *k* to be positive real number the following conditions for all six coefficients must satisfy:

$$a_3^2 \geq 4a_1a_5;\ a_2^2 \geq 4a_0a_4 \tag{16}$$

Excluding *k* from both (14) and (15) and some algebra leads to the following single *necessary boundary or marginal stability* expression for the coefficients of (13):

$$(a_1a_4 - a_0a_5\ )^2 = (a_1a_2 - a_0a_3\ )(a_3a_4 - a_2a_5) \tag{17}$$

Expression (17) requires the following additional conditions to be satisfied:

$$a_{\ 1}a_2 > a_0a_3\ and\ a_3a_4 > a_2a_5 \tag{18}$$

As a conclusion, it can be stated that (17) presents the *necessary and sufficient boundary or marginal stability* expression for the coefficients of (13) provided conditions (16) and (18) are fully satisfied. The analysis shows that when the coefficients reach their stability boundary values, the system becomes *marginally stable* with *two (i.e. one pair of conjugate complex numbers) out of five roots located symmetrically on jω*-axis *of the s-plane and with one of the roots (negative real number) located on the real axis of the s-plane.* In this case, the expressions (14) and (15) have only *one common* real positive root *k.*

The expression (17) can be easily used to define the boundary values of any coefficient of the characteristic equation (13). For example, for this system to be *absolutely stable*, $a_0$ must be within the range in between its minimum and maximum boundary values, as it was defined from (13):

$$a_0^{min} = \frac{(a_2a_5 - a_3a_{\ 4})\left(a_3 + \sqrt{a_3^2 - 4a_1a_5}\right) + 2a_1a_{\ 4}a_{\ 5}}{2a_5{}^2} \tag{19}$$

$$a_0^{max} = \frac{(a_2a_5 - a_3a_{\ 4})\left(a_3 - \sqrt{a_3^2 - 4a_1a_5}\right) + 2a_1a_{\ 4}a_{\ 5}}{2a_5{}^2} \tag{20}$$

If equation (19) yields a negative value, then $a_0^{min}$ should be assigned a zero-boundary value instead.

In accordance to (17), in the case of $a_0a_5 = a_1a_4,\ a_0a_3 = a_1a_2, and\ a_2a_5 = a_3a_4,$ i.e. when (17) yields 0=0, the following *special case* of marginal stability or marginal instability when *four roots of polynomial out of five are located on jω -axis* of the *s*-plane has been derived. If $a_0a_5 = a_1a_4,\ a_0a_3 = a_1a_2,\ a_2a_5 = a_3a_4$ and $a_3^2 > 4a_1a_5\ ,\ a_2^2 > 4a_0a_4$, the system becomes <u>*marginally stable*</u> and the systems characteristic polynomial will have *four roots (two pairs of different conjugate complex numbers) located symmetrically on jω-axis of the s-plane and one root (negative real number) located on the real axis of the s-plane*. Subsequently, if $a_0a_5 = a_1a_4,\ a_0a_3 = a_1a_2,\ a_2a_5 = a_3a_4$ and $a_3^2 = 4a_1a_5\ ,\ a_2^2 = 4a_0a_4,$ the system becomes <u>marginally *unstable*</u> *but with four repeated roots (two pairs of same conjugate complex numbers) located symmetrically on jω-axis of s-plane and one root (negative real number) located on the real axis of the s-plane*. Should be notes that if conditions $a_0a_5 = a_1a_4\ and\ a_0a_3 = a_1a_2$ are satisfied then condition $a_2a_5 = a_3a_4$ is satisfied by default as well. In both cases, the expressions (14) and (15) have *two common* real positive roots *k*.

The example of a system polynomial that has *marginal stability* is $4s^5 + s^4 + 8s^3 + 2s^2 + s + 0.25 = 0$ and Fig. 3 shows response of the system to the unity input. The example of a system polynomial that has *marginal instability* is $s^5 + s^4 + 8s^3 + 8s^2 + 16s + 16 = 0$ and Fig. 4 shows response of the system to the unity input. The difference in both system responses with the same

conditions for the coefficient values $a_0a_5 = a_1a_4,\ a_0a_3 = a_1a_2,\ a_2a_5 = a_3a_4$ can be seen clearly in Fig. 3 and Fig. 4. This unique condition of marginal stability or instability was not identified by using the Routh method of stability analysis.

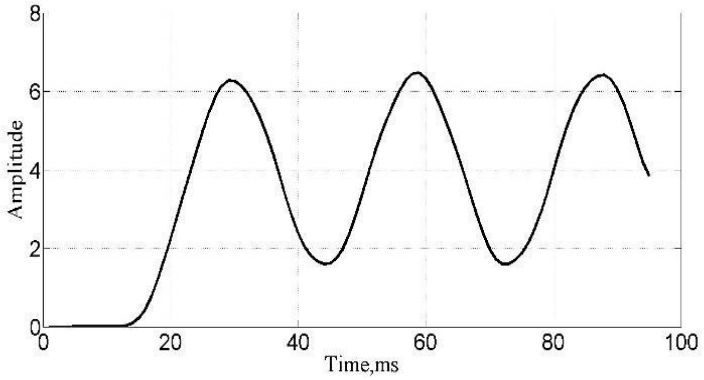


*Figure 3 Marginally stable system (Rule 6)*

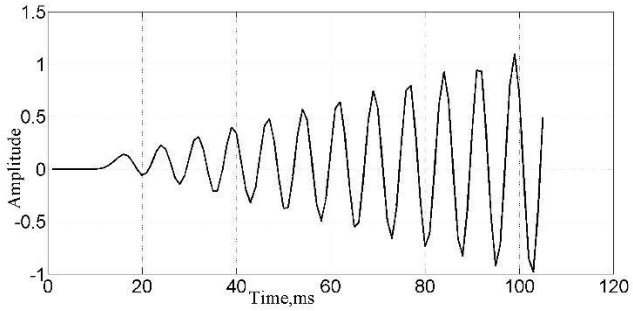


*Figure 4. Unstable system (Rule 6)*

*c. Stability criterion for the sixth-order dynamic system*

The sixth-order system is presented by the following characteristic polynomial:

$$a_6s^6 + a_5s^5 + a_4s^4 + a_3\,s^3 + a_2\,s^2 + a_1s + a_0\ = 0 \tag{21}$$

Solving the boundary problem for the system polynomial (21) coefficients can be done by taking *n*=6 (even number) in (3). It leads to the following set of two non-linear equations:

$$a_6 = (a_4 - (a_2 - a_0k)k)k \tag{22}$$
$$a_5 = (a_3 - a_1k)k \tag{23}$$

By excluding $k$ from the expressions (22) and (23) the necessary marginal stability criteria for the system (21) coefficients can be analytically derived. Th resulting equation is expressed as follows:

$$Aa_6^2 - Ba_6 + C = 0, \tag{24}$$

where:

$$A = a_1^3,$$
$$B = (a_1a_2 - a_0a_3)(3a_1a_5 - a_3^2) + a_1^2(a_3a_4 - a_2a_5),$$
$$C = -a_5[(a_3a_4 - a_2a_5)(a_1a_2 - a_0a_3) - (a_1a_4 - a_0a_5)^2].$$

The positive solution for $a_6$ in equation (24) exists, if the following condition satisfies:

$$B^2 - 4AC > 0 \tag{25}$$

As a conclusion, it can be stated that (24) presents the *necessary and sufficient boundary or marginal stability* expression for the coefficients of (21) provided conditions (16), (18), and (25) are fully satisfied. The analysis shows that when the coefficients reach their stability boundary values, the system becomes *marginally stable* with *two (i.e. one pair of conjugate complex numbers) out of five roots located symmetrically on jω*-axis *of the s-plane and with one of the roots (negative real number) located on the real axis of the s-plane.* In this case, the expressions (22) and (23) have only *one common* real positive root *k*. The expression (24) can be easily used to define the boundary values of any coefficient of the characteristic equation (21).

In special case of marginal stability, when $B^2 = 4AC$, $a_6$, has only one value and the sixth-order system (21) becomes marginally stable with four (*two pairs of different conjugate complex numbers**)** roots symmetrically located on jω-axis of the s-plane and two roots (one pair of conjugate complex numbers) located symmetrically on left half of the s-plane.* In this special case the expressions (22) and (23) have *two common* real positive roots *k*. The example of such system polynomial is shown below:

$$s^6 + 2s^5 + 4s^4 + 3s^3 + 4s^2 + 0.5s + 0.625 = 0$$

Fig. 5 shows the response of this system to the unity input. The validity of the Rules 7, 8, 9 have been verified by solving a numerical example of the systems with randomly selected polynomial coefficients.

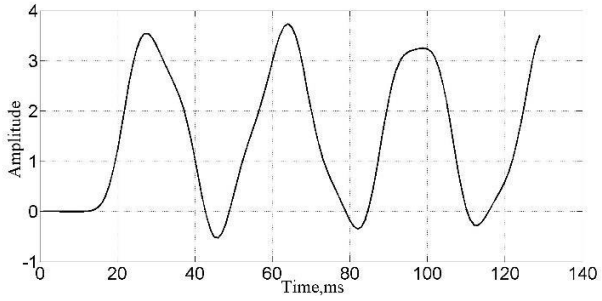


*Figure 5 Marginally stable system*

The attempt to derive stability boundary equation for the 6th order system by using Routh array (three columns and seven rows) leads to the following preliminary formulas:

$$ED - Ca_0 = 0$$
$$E = (BC - AD)/C$$
$$D = (Aa_1 - a_5a_0)/A$$
$$C = (Aa_3 - Ba_5)/A$$
$$B = (a_5a_2 - a_6a_1)/a_5$$
$$A = (a_5a_4 - a_6a_3)/a_5$$

Substituting these expressions one into another *does not* guarantee that the final expression for $a_6$ can be presented in the form of a quadratic equation and this demonstrates the deficiency and complexity of the Routh approach for the sixth and higher orders system stability analysis.

**Numerical analysis of stability boundaries for the systems with orders higher than six.** The analytical solution of the boundary problem (in form of radicals for *k*) for dynamic systems with any order is possible by systematically excluding *k* from equations (2) or (3) and finally reaching one polynomial equation with higher order for the coefficients of the characteristic

equation (1). However, it becomes a tedious process for the systems with orders $n \geq 7$. In general, the system of any order is marginally stable if equations (2) or (3) satisfy the *fundamental law of marginal or boundary stability*, that is if they have at least one *common positive* roots *k* and have a pair or pairs of conjugate roots on *jω-axis of the s-plane*.

This low has been applied numerically to an eleventh order ($n$=11) system to prove validity of the law. The system with order $n$=11 is presented by the following characteristic polynomial:

$$a_{11}s^{11} + a_{10}s^{10} + a_9s^9 + a_8s^8 + a_7s^7 + a_6s^6 + a_5s^5 + \\ + a_4s^4 + a_3s^3 + a_2s^2 + a_1s + a_0 = 0 \quad (29)$$

The stability boundary equations (2) for this system $n$=11 (odd number) can be presented in the following form:

$$a_{11} = (a_9 - (a_7 - (a_5 - (a_3 - a_1k)k)k)k)k \quad (30)$$
$$a_{10} = (a_8 - (a_6 - (a_4 - (a_2 - a_0k)k)k)k)k \quad (31)$$

Alternatively, (30) and (31) can be rewritten in the following forms with alternating signs for the terms:

$$a_{11} = a_9k - a_7k^2 + a_5k^3 - a_3k^4 + a_1k^5 \quad (32)$$
$$a_{10} = a_8k - a_6k^2 + a_4k^3 - a_2k^4 + a_0k^5 \quad (33)$$

In order to have a marginal stability condition, the roots of both fifth order polynomials (32) and (33) must have at least one real positive root in common. A randomly selected example of such equation (32) that has real positive roots is as follows:

$$0.3 = 2.7k - 7.2k^2 + 6.6k^3 - 2.4k^4 + 0.3k^5 \quad (34)$$

Five roots of this equation are, in fact, real positive numbers:

$$k = [3.247, \mathbf{2.618}, 1.555, 0.382, 0.1981] \quad (35)$$

In order for equation (33) to have at least one root to be the same with any root of equation (34), each of the *k* roots (35) is inserted into equation (33) with randomly selected coefficients except $a_0$. A random example of equation (33) can be presented as follows:

$$0.1 = 0.6k - 0.9k^2 + 0.5k^3 - 0.1k^4 + a_0k^5 \quad (36)$$

Calculation of $a_0$ for each *k* root from the list (35) yields the following result:

$$a_0 = [0.004544, 0.0034, 0.0053, -2.9034, 41.7902] \quad (37)$$

Then the polynomial (29) with all the preselected coefficients is presented as follows:

$$0.3s^{11} + 0.1s^{10} + 2.7s^9 + 0.6s^8 + 7.2s^7 + 0.9s^6 + \\ + 6.6s^5 + 0.5s^4 + 2.4s^3 + 0.1s^2 + 0.3s + a_0 = 0 \quad (38)$$

Solution of equation (38) for five possible $a_0$ from (37) shows that only two of them present actual stability boundaries for the polynomial (38), namely $a_0^{min}$ = 0.003444 and $a_0^{max}$ =0.004544. These two boundary values of $a_0$ in polynomial (38) lead to one pair of conjugate roots on the *jω-axis* of the s-plane, namely 0 ± 0.6180i and 0 ± 0.5550i. The system turns to be fully stable in between these two boundary values of $a_0$. The roots of boundary polynomial (36) at the boundary values of $a_0$ yield real positive values. For example, for $a_0$ = 0.004544 the roots of polynomial (36) yield $k = [3.267, 2.6180, 1.8658, 1.0425, 0.2451]$. Therefore, two boundary polynomials (32) and (33) have one common positive real root *k*=2.6180 as it was stated by the *fundamental law of marginal or boundary stability*.

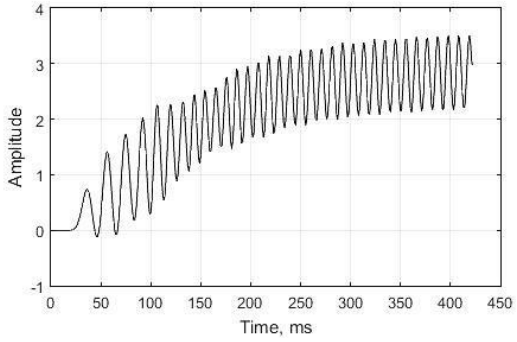


*Figure 6 Marginally stable system*

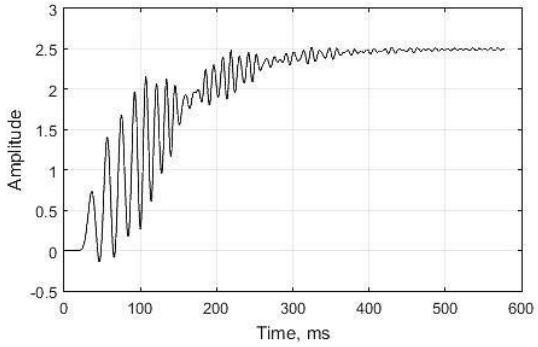


*Figure 7. System with absolute stability*

Fig. 6 shows the response of the system with characteristic polynomial (38) having value of $a_0$ =0.00344 to step input 0.01. From Fig. 6 it can be seen that the system is in the state of marginal stability. Fig. 7 shows the response of the system to step input 0.01 for $a_0$ selected in between its boundary values [0.003444, 0.004544]. From Fig. 7 it can be seen that the system is in the state of absolute stability.

**Stability range for the closed-loop control systems.** The *s*-domain transfer function for the closed-loop control system can be expressed as follows:

$$\frac{Y(s)}{R(s)} = \frac{G(s)K(s)}{1 + G(s)K(s)H(s)} \tag{39}$$

In (39), *R(s)* is the input signal, *Y(s)* is the output signal, *H(s)* is the feedback signal, *G(s)* is the plant model (system under observation), and *K(s)* is the controller model.

Expressions (2) or (3) can be successfully applied to identify stability ranges for the gains of closed-loop control system (39).

*a. Case of single gain controller design*

The stability analysis of a system with single gain controller can be demonstrated on the *model of hard disk drive* with the *lead compensator*. The plant model of the hard disk drive system can be expressed as follows [19]:

$$G(s) = A/B \text{ , where} \tag{40}$$

$$A = n_4 s^4 + n_3 s^3 + n_2 s^2 + n_1 s + n_0,$$
$$B = d_{10} s^{10} + d_9 s^9 + d_8 s^8 + \cdots + d_4 s^4 + d_3 s^3 + d_2 s^2,$$

where:

$$n_4 = 1.197 \cdot 10^{26},\ n_3 = 2.12 \cdot 10^{29}, n_2 = 5.826 \cdot 10^{34},$$
$$n_1 = 4.366 \cdot 10^{37},\ n_0 = 6.189 \cdot 10^{42},\ d_{10} = 1,\ d_9 = 5336,$$
$$d_8 = 4.124 \cdot 10^{9},\ d_7 = 1.302 \cdot 10^{13},\ d_6 = 4.216 \cdot 10^{18},$$
$$d_5 = 6.72 \cdot 10^{21},\ d_4 = 1.198 \cdot 10^{27},\ d_3 = 7.496 \cdot 10^{29},$$
$$d_2 = 9.668 \cdot 10^{34}.$$

The *lead compensator* with a proportional gain $k_p$ can be presented as follows:

$$K(s) = k_p(4s + 2)/(s + 2) \tag{41}$$

Substituting (40), (41) into (39) and assuming $H(s) = 1$, yields the following close-loop system characteristic polynomial (29), where:

$$a_{11} = d_{10},\ a_{10} = d_9 + 2d_{10},\ a_9 = d_8 + 2d_9,$$
$$a_8 = d_7 + 2d_8,\ a_7 = d_6 + 12d_7,\ a_6 = d_5 + 2d_6,$$
$$a_5 = d_4 + 2d_5 + 4k_p n_4,\ a_4 = d_3 + 2d_4 + 2k_p(2n_3 + n_4),$$
$$a_3 = d_2 + 2d_3 + 2k_p(2n_2 + n_3),$$
$$a_2 = 2d_2 + 2k_p(2n_1 + n_2),\ a_1 = 2k_p(2n_0 + n_1),$$
$$a_0 = 2k_p n_0.$$

For the eleventh order characteristic polynomial (29), two stability boundary polynomials can be presented as (32) and (33). By substituting all the coefficients into (32) and (33) and dividing (32) by (33), proportional gain $k_p$ can be excluded from the resulting single algebraic 6$^{th}$ order stability boundary equation with variable *k* as follows:

$$p_6 k^6 + p_5 k^5 + p_4 k^4 + p_3 k^3 + p_2 k^2 + p_1 k + p_0, \tag{42}$$

where:

$$p_6 = -dd_0 nn_3 + dd_1 nn_2 - dd_2 nn_1 + dd_3 nn_0,$$
$$p_5 = dd_0 nn_5 - dd_1 nn_4 + dd_2 nn_3 - dd_3 nn_2 + dd_4 nn_1 - dd_5 nn_{0,}$$
$$p_4 = -dd_2 nn_5 + dd_3 nn_4 - dd_4 nn_3 + dd_5 nn_2 - dd_6 nn_1 + dd_7 nn_0,$$
$$p_3 = dd_4 nn_5 - dd_5 nn_4 + dd_6 nn_3 - dd_7 nn_2 + dd_8 nn_1 - dd_9 nn_{0,}$$
$$p_2 = -dd_6 nn_5 + dd_7 nn_4 - dd_8 nn_3 + dd_9 nn_2 - dd_{10} nn_1 + dd_{11} nn_0,$$
$$p_1 = dd_8 nn_5 - dd_9 nn_4 + dd_{10} nn_3 - dd_{11} nn_2,$$
$$p_0 = -dd_{10} nn_5 + dd_{11},$$
$$dd_{11} = d_{10},\ dd_{10} = d_9 + 2d_{10},\ dd_9 = d_8 + 2d_9,$$
$$dd_8 = d_7 + 2d_8,\ dd_7 = d_6 + 2d_7,\ dd_6 = d_5 + 2d_6,$$
$$dd_5 = d_4 + 2d_5,\ dd_4 = d_3 + 2d_4,\ dd_3 = d_2 + 2d_3,$$
$$dd_2 = d_1 + 2d_2,\ dd_1 = d_0 + 2d_1,\ dd_0 = 2d_0,$$
$$nn_5 = 2n_4, nn_4 = 2n_3 + n_4, nn_3 = 2n_2 + n_3,$$
$$nn_2 = 2n_1 + n_2, nn_1 = 2n_0 + n_1, nn_0 = n_0.$$

Solution of equation (42) yields four real and two complex *k* roots. In accordance to Rule 10, only real roots could be considered for the marginal stability of the closed-loop system. Four real roots are $0.4912*10^{-6}$, $0.0139*10^{-6}$, $0.0077*10^{-6}$, $0.0006*10^{-6}$.

Value of $k_p$at the state of marginal stability can be calculated from (32) and presented as follows:

$$k_p = \text{C/D, where} \tag{43}$$
$$C = dd_{11} - dd_9 k + dd_7 k^2 - dd_5 k^3 + dd_3 k^4 - dd_1 k^5,$$
$$D = nn_5 k^3 - nn_3 k^4 + nn_1 k^5.$$

Substituting four real roots of (42) into (43) yield three positive and one negative values of $k_p$. Negative value leads to instability of the system because the coefficient $a_0$ of the system is directly proportional $k_p$, i.e. $a_0 = 2k_p n_0$, and cannot be negative. As a result, the minimum stability limit for the $k_p$ is zero, i.e. $k_{min} = 0$. The remaining three calculated positive value for $k_p$ are 0.0079, 0.2119, 0.1726. Solving for the roots of characteristic polynomial (29) for these three values of $k_p$ yields a pair of roots located on the imaginary axis of *s*-plane $\pm j0.1427 * 10^4, \pm j0.8488 * 10^4, \pm j1.1411 * 10^4$, respectively. The analysis of all solutions shows that only one gain value $k_{pmax}$ =0.0079 corresponds to the marginal stability condition of the closed-loop system where all the roots located at the left half of *s*-plane. Three pairs of roots located on imaginary axis of *s*-plane $[\pm j0.1427, \pm j0.8488, \pm j1.1411] * 10^4$ can be verified by plotting root locus graphs and it is shown in Fig. 8.

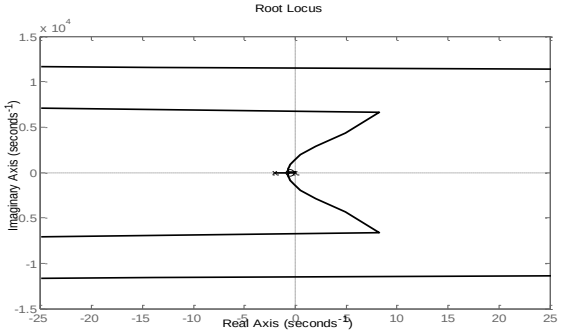


*Figure 8. System with absolute stability*

*b. Case of multiple gain controller design*

The advantage of applying expressions (2) and (3) for stability analysis of higher-order closed-loop dynamic systems can be demonstrated for the case of applying *multiple gain* controllers to the system. The criteria (2) and (3) was tested on the example of model of two-inertia system with PD controller. The plant model of such two-inertia system can be expressed as follows [20]:

$$G(s) = n_0/(\, d_4 s^4 + d_3 s^3 + d_2 s^2 + d_1 s + d_0), \text{ where:} \quad (44)$$
$$n_0 = 0.0625,\ d_4 = 1,\ d_3 = 2,\ d_2 = 1.5,\ d_1 = 0.5,$$
$$d_0 = 0.0625.$$

Substituting (44), $K(s) = k_p + s k_d$ into (39) and assuming $H(s) = 1$, yields the following fourth-order characteristic polynomial of the close-loop system:

$$d_4 s^4 + d_3 s^3 + d_2 s^2 + (d_1 + n_0 k_d)s + \left(d_0 + n_0 k_p\right) = 0 \quad (45)$$

The two stability boundary polynomials (3) for the characteristic polynomial (45) can be presented as follows:

$$d_4 = k d_2 - k^2\left(d_0 + n_0 k_p\right), \quad (46)$$
$$d_3 = k(d_1 + n_0 k_d). \quad (47)$$

By dividing (46) by (47), the following expression for $k_d$ can be derived:

$$k_d = [d_2 d_3 - d_3\left(d_0 - n_0 k_p\right)k - d_1 d_4]/n_0 d_4 \quad (48)$$

Substituting (48) into (47) yields the following quadratic equation:

$$\left(d_0 d_3 + d_3 n_0 k_p\right)k^2 - d_2 d_3 k + d_3 d_4 = 0. \quad (49)$$

Solution of (49) can be presented as follows:

$$k = [d_2 \pm \sqrt{d_2^2 - 4d_4(d_0 + n_0 k_p)}]/2(d_0 + n_0 k_p) \tag{50}$$

The stability boundary is achieved when the expression under square root is equal zero and solution of (50) yields a single positive answer for $k$ (Rule 10). As a result, at the stability boundary condition for the system the expression for maximum limit of $k_p$ can be derived from (50) as follows:

$$k_p^{max} = (d_2^2 - 4d_0 d_4)/(4d_4 n_0) \tag{51}$$

The minimum limit of $k_p$ can be obtained from the condition that for a stable system all the coefficients of characteristic polynomial (45) must be positive. Therefore, the coefficient $d_0 + n_0 k_p$ must have a positive value and the minimum value for $k_p$ can be calculated as follows:

$$k_p^{min} = -d_0/n_0 \tag{52}$$

In order to provide an absolute stability of the closed-loop system, the following condition for $k_p$ must be provided:

$$k_p^{min} < k_p < k_p^{max} \tag{53}$$

For any value of $k_p$ within the limits (53), two values for $ss$ are be calculated from (50) and subsequently two corresponding limit values for $k_d$ can be calculated from (48). An additional condition for the system stability is that the minimum limit for $k_d$ must be more than one calculated from the corresponding coefficient of the system characteristic polynomial, i.e.

$$k_d^{min} > -d_1/n_0. \tag{54}$$

Using all the stability conditions (54), (53), (52), (51), (50), and (48), the following graph of function $k_d = f(k_p)$ for the boundary values can be obtained, as shown in Fig. 9. For all the boundary values of the system gains, the solution of the characteristic polynomial (45) yields one pair of conjugate roots at the imaginary axis of s-plane, i.e. the system is at the condition of marginal stability.

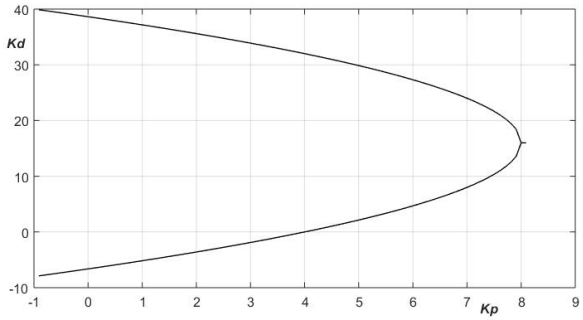


*Figure 9. Stability boundary curves for $k_d = f(k_p)$*

Fig. 9 shows the region of absolute stability of the system that lies in between upper and lower lines of the graph. The highest range of stability is at $k_p^{min} = -1$, where -8 < $k_d$ < 40. At $k_p^{max} = 8$, the stability region is reduced to a single value $k_d$ =16.

In case of applying PID controller $K(s) = k_p + sk_d + k_i/s$ to the model of two-inertia system [19], the following fifth order characteristic equation can be obtained:

$$d_4 s^5 + d_3 s^4 + d_2 s^3 + (d_1 + n_0 k_d) s^2 + \left(d_0 + n_0 k_p\right) s + n_0 k_i = 0 \quad (55)$$

Two stability boundary polynomials (2) for the characteristic polynomial (55) can be presented as follows:

$$d_4 = k d_2 - k^2 \left(d_0 + n_0 k_p\right), \quad (56)$$
$$d_3 = k(d_1 + n_0 k_d) - k^2 n_0 k_i \quad (57)$$

By dividing (56) by (67), the following formula for $k_p$ can be obtained:

$$k_p = (d_2 d_3 - d_1 d_4 - n_0 d_4 k_d)/(n_0 d_3 k) - \\ -(d_0 d_3 - n_0 d_4 k_i)/(n_0 d_3) \quad (58)$$

Substituting (58) into (56) yields the following quadratic equation:

$$(n_0 k_i) k^2 - (d_1 + n_0 k_d) k + d_3 = 0 \quad (59)$$

Solution of (59) can be presented as follows:

$$k = [d_1 + n_0 k_d \pm \sqrt{(d_1 + n_0 k_d)^2 - 4 d_3 n_0 k_i}]/(2 n_0 k_i) \quad (60)$$

The stability boundary is achieved when the expression of square root in (60) is equal zero and solution of equation (60) yields a single positive answer for $k$ (Rule 10). This condition yields the following boundary equation for $k_d$:

$$(n_0^2) k_d^2 + (2 n_0 d_1) k_d + d_1^2 - 4 n_0 d_3 k_i = 0 \quad (61)$$

The solution of (61) yields the boundary equation for $k_d$ as follows:

$$k_d = -d_1 \pm 2\sqrt{d_3 n_0 k_i} \quad (62)$$

A stability boundary is achieved when the expression of square root in (62) is equal to zero, i.e. when $k_i$=0. Therefore, for an absolute stability of the closed-loop system, the following condition must be satisfied:

$$k_i > 0 \quad (63)$$

For any value $k_i > 0$, formula (62) yields two limiting values for $k_d$. The additional condition for the system stability is that the minimum limit for $k_d$ must be more than one calculated from the corresponding coefficient of the system characteristic polynomial, i.e.

$$k_d^{min} > -d_1/n_0. \quad (64)$$

By substituting the two limiting values of $k_d$ into (60) and subsequently into (58), the remaining two limiting values for $k_p$ can be obtained. An additional condition for the system stability is that the minimum limit for $k_p$ must be more than one calculated from the corresponding coefficient of the system characteristic polynomial, i.e.

$$k_p^{min} > -d_0/n_0. \quad (65)$$

Using all the stability conditions (65), (64), (63), (62), (60), and (58), the following 3D graph of function $k_p = f(k_d, k_i)$ for the boundary lines of $k_p, k_d$ gains versus few values of $k_i$ is shown in Fig. 10. The absolute stability of the system is confined within the space outlined by the limiting values of three gains.

Fig.11 shows only 2D view of the lines shown in Fig. 10. The maximum values for $k_p, k_d$, $k_i$ gains are defined by the terminal condition when $k_p^{min} = k_p^{max}$ for raising in steps values of $k_i$ (63) and is calculated on MATLAB software. Increasing $k_i$ reduces that stability range of the system, i.e. stability ranges for other two gains. For all the boundary values of the system gains the solution of the characteristic polynomial (55) yields one pair of conjugate roots at the imaginary axis of s-plane, i.e. the system is at the condition of marginal stability. An exception is for the points where $k_p^{min} = k_p^{max}$. Fig. 12 shows a 2D graph of $k_p = f(k_d)$ for a single value $k_i$=0.

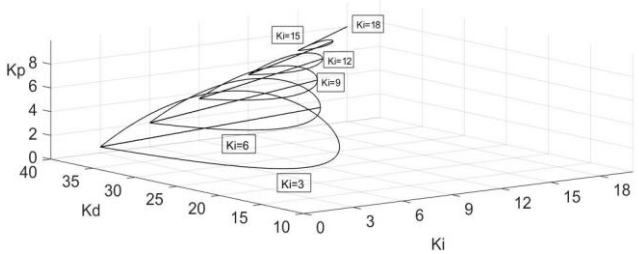


*Figure 10. 3D Stability boundary curves for $k_p = f(k_d, k_i)$*

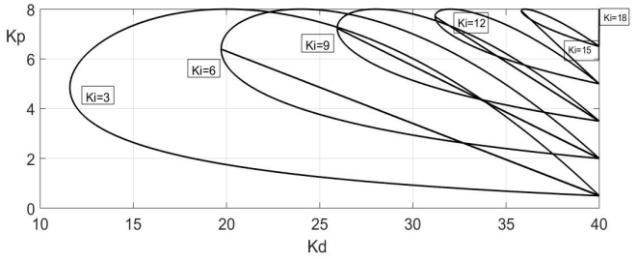


*Figure 11. 2D Stability boundary curves for $k_p = f(k_d, k_i)$*

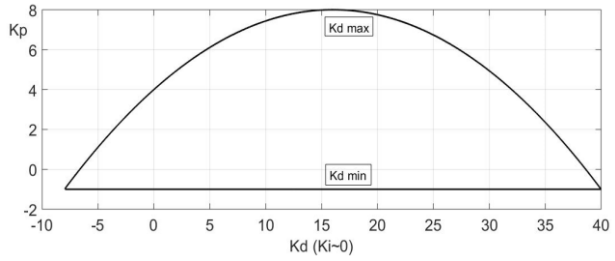


*Figure 12. 2D Stability boundary curves for $k_p = f(k_d)$, $k_i$=0*

If $k_i$=0, then $k_d^{min} = -8 < k_d < 40$ and $k_p^{min} = -1 < k_p < 8$ (Fig.11). At the left intersection of lines ($k_d^{min} = -8$ and $k_p^{min} = -1$), the roots of the closed-loop system are: -1.0000 + 0.7071i;

-1.0000 - 0.7071i; 0.0000 + 0.0000i; -0.0000 - 0.0000i; -0.0000 - 0.0000i. At the right intersection of lines ($k_d^{max} = 40$ and $k_p^{min} = -1$), the roots of the closed − loop system are: -2 + 0.0000i; -0.0000 + 1.2246i; -0.0000 - 1.2246i; -0.0000 + 0.0000i; -0.0000 + 0.0000i. When $k_i$ reaches its maximum value ($k_i^{max}$ =18), the plots on Fig. 9 and Fig. 10 are converged to a single point and other gains reach their single maximum values, i.e. $k_p^{max} = 8$, $k_d^{max} = 40$. The roots of the system characteristic polynomial at this point are -2.0000 + 0.0000i; -0.0000 + 0.8660i; -0.0000 - 0.8660i; 0.0000 + 0.8660i; 0.0000 - 0.8660i, i.e., the system has double conjugate roots on imaginary axis of s-plane.

**Conclusions.** The paper presents an effective and simple tool for analytical solution of stability problem of higher-order linear time-invariant dynamic systems. It has a major advantage compared to Routh–Hurwitz technique. The proposed universal stability criteria (2) or (3) establish

unique relations between the stability boundary values of the system characteristic polynomial coefficients and the newly introduced additional parameter *k*. It is a new approach and there are no similarities found to these criteria in the literature. The newly-developed method is a universal one and can be applied to any higher-order dynamic system. The authors of this paper have discovered and established a set of general expressions (2) or (3) that can be applied for derivation of necessary stability criteria for any order linear time-invariant dynamic system. The single analytical expressions of the non-zero coefficients of the system characteristic polynomial at its stability boundary conditions have been derived in section III for the systems with orders from 3 to 6 and successfully tested by using MATLAB software for numerous examples. The method has also been extended to prove numerically the stability boundaries problem solution for any system with order higher than six in section IV for a randomly selected example of eleventh-order system. The stability range of values for one of the coefficients of the characteristic equation for each of the dynamic system with orders from three to six has been derived analytically. The numerical example of eleventh order system is presented in the paper to prove validity of *fundamental law of marginal or boundary stability* for systems with orders higher than six. As a unique achievement, the marginal stability conditions for dynamic systems with *possible zero coefficients* and with multiple roots on the $j\omega$-axis of the *s*-plane have also been discussed in details. These results are new and have not been published currently in the literature and were obtained for special cases of marginal stability when the same exactly set of zero coefficients the system can be either in the state of *marginal stability* or *marginal instability*, i.e. the system exhibits a *dual behaviour*. Section V is dedicated to use of criteria (2) and (3) to provide marginal and absolute stability for the closed-loop control systems with proportional, derivative and integral gains. The paper discusses in detail the derivation of equations for precise stability boundary values of $k_p, k_d, k_i$ gains based on the two-polynomial criteria (2) and (3). The obtained results of analytical calculation of precision stability boundary values for a multiple-gain higher-order closed-loop system do not have analogy currently in the control theory. The results obtained in this paper prove that the developed system stability criteria or algorithm for stability analysis of a higher-order linear dynamic system is a step forward in analysing stability conditions of complex dynamic systems and deriving precise analytical expressions for multiple gains of closed-loop control systems. This method is successfully tested on the *model of hard disk drive* with single-gain lead compensator [19] and on the *model of two-inertia system* with multiple gain controller design [20].

## REFERENCES

[1]. N. S. Nise. *Transient response stability*. Control Syst. Eng., 5th Int. Student ed. Singapore: Wiley, 2008, ch. 6, sec. 2–4, pp. 291–306.
[2]. R. C. Dorf and R. H. Bishop. *The stability of linear feedback systems.* Modern Control Systems, 12th ed. Prentice–Hall, 2011, ch. 6, sec. 2, pp. 391–398.
[3]. M. Gopal. *Concept of stability and the Ruth Stability Criterion.* Control Systems, Principles and Design, 2nd ed. McGraw Hill,2003, ch.5, sec. 4, pp. 314-326.
[4]. B. Kuo and M. F. Golnaraghi. *Stability of linear control systems.* Automatic Control Systems, 7th ed. Englewood Cliffs, NJ: Prentice-Hall, 1995, ch. 6, sec. 5, pp. 334–343.
[5]. M. Ho, A. Datta, and S. P. Bhattacharyya. *An elementary derivation of the Routh-Hurwitz criterion*. IEEE Trans. Autom. Control, vol. 43, no. 3, pp. 405–409, Mar. 1998.
[6]. M. M. Fahmy and J. O'Reilly. *A note on the Routh-Hurwitz test*. IEEE Trans. Autom. Control, vol. AC-27, no. 2, pp. 483–485, Apr.1982.
[7]. K. S. Yeung. *Routh-Hurwitz test under vanishing leading array elements*. IEEE Trans. Autom. Control, vol. AC-28, no. 1, pp. 104–106, Jan. 1983.
[8]. K. Khatwani. *On Routh-Hurwitz criterion.* IEEE Transactions on Automatic Control, vol. 26, no. 2, pp. 583-584, Apr 1981.

[9]. S. Pillai. *The ε method of the Routh-Hurwitz criterion. IEEE Transactions on Automatic Control*, vol. 26, no. 2, pp. 584-584, Apr 1981.

[10]. S. S. Chen and J. S. H. Tsai. *On the singular cases of the complex Routh algorithm for stability tests*. IMA J. Math. Contr. Inform., vol. 10, pp. 71–82, 1993.

[11]. R. N. Clark. *The Routh-Hurwitz stability criterion, revisited. IEEE Control Systems*, vol. 12, no. 3, pp. 119-120, Jun 1992.

[12]. M. A. Choghadi and H. A. Talebi. *The Routh-Hurwitz Stability Criterion, Revisited: The Case of Multiple Poles on Imaginary Axis.* IEEE Transactions on Automatic Control, Vol. 58, No. 7, July 2013.

[13]. B.B. Alagoz, *On the Harmonic Oscillation of High-order Linear Time Invariant Systems.* Computer Science, Discrete Mathematics, arXiv: 1403. 2170, pp.1-12, 2014.

[14]. N. Tan, "*Computation of Stabilizing PI and PID controllers for processes with time delay*", ISA Transactions, 44, pp 213-223, 2005.

[15]. T. V. Moghaddam T.V. and Abbasi Y. *Tuning a Fractional Order PD and PID Controller with Lead Compensator for Integrating Time Delay Systems.* Journal of Electrical and Control Engineering, vol. 2, pp 34-41, 2012.

[16]. J. Chen, P. Fu. *Stability Analysis of Polynomially Dependent Systems by Eigenvalue Perturbation.* IEEE Transactions on Automatic Control, vol. 62, issue 11, pp. 5915-5922, 2017.

[17]. L. Wang, B. K. P. Horn, G. Strang. *Eigenvalue and Eigenvector Analysis of Stability for a Line of Traffic.* Studies in Applied Mathematics Journal, vol. 138, issue 1, pp. 103-132, 2017.

[18]. N. Mir-Nasiri, M. H. Ali. *A New Algorithm to Control Dynamic Stability of Higher-Order Systems.* Proceedings of IEEE International Conference on Control Systems, Computing and Engineering, 23-25 November, Penang, Malaysia, 2018.

[19]. A. Nath, S. Kaitwanidvilai. *High performance HDD servo system using GA based fixed structure robust loop Shaping control*. Proceedings of IEEE International Conference on Robotics and Biomimetics (ROBIO), 19-23 December, Guilin, China, pp. 1854-1859, 2009.

[20]. G. Zhang, J. Furusho. *Speed Control of Two-Inertia System by PI/PID Control*. IEEE Transactions on Industrial Electronics, vol. 47, issue 3, pp. 603-609, 2000.

**Received:** 15.02.2022

**Accepted:** 14.05.2022

MACHINE SCIENCE

ISSN: 2227-6912
E-ISSN: 2790-0479

2022, Volume 11, № 1. Pages 41 – 46

# RADIALLY EXPANDABLE RING-LIKE STRUCTURE WITH ANTIPARALLELOGRAM LOOPS

**Şebnem GÜR[1*], Koray KORKMAZ[2], Gökhan KİPER[3]**

[1,2,3]Department of Architecture, Izmir Institute of Technology, Izmir, Türkiye

*E-mail:* sebnemgur@iyte.edu.tr[1*], koraykorkmaz@iyte.edu.tr[2*], gokhankiper@iyte.edu.tr[3]

**Abstract:** As they constitute a substantial percent of deployable structures, scissor mechanisms are widely studied. This being so, new approaches to the design of scissor mechanisms still emerge. Usually design methods consider the scissor elements as modules. Alternatively, it is possible to consider the loops as modules. In this paper, loop assembly method is used such that antiparallelogram loops are placed along a circle, to construct a deployable structure. The research shows that it is possible to construct radially deployable structures with identical antiparallelogram loops with this method. Then kinematic and geometrical properties of the construction are analyzed. It is found out that the links of such a structure turn out to be similar generalised angulated elements. Furthermore, similar loops are used for the construction and deployable rings are obtained.

**Keywords:** *deployable ring-like structure, antiparallelogram loop, loop assembly method, radial expansion, angulated scissor element*

**Introduction.** Deployable structures are mechanisms that can go under transformation in order to achieve a compact (stowed) and an open (deployed) configuration [1]. This change in size offers a great advantage in packing and also in mobility, therefore making them suitable for many applications varying from retractable roofs [2-4] to space antennas [5-7].

One of the most important units of deployable mechanisms are scissor-like elements (SLEs). SLE is composed of two straight bars connected with a revolute joint, which is perpendicular to the common plane of the bars, called pantographic elements [8]. In 1960's Pinero published the first academic studies on deployable structures made of SLEs [9]. Later on the foldability conditions of SLEs were defined by Felix Escrig [10, 11]. Kinematics of deployable structures continued to be a research area for many others [12-14].

Angulated elements were first introduced by Hoberman [15, 16]. This new type of SLEs were able to subtend a constant angle. We observe the same property in Servadio's foldable polyhedra [17]. Hoberman's latter work, the Iris Dome [16], is nothing but a circular application of the angulated unit subtending constant angle between the unit lines, therefore capable of radial deployment.

Angulated units were further explored by You and Pellegrino [18] after the invention of Hoberman. They derived the geometric conditions of radial deployment and came up with two types of generalized angulated elements (GAEs): equilateral (type I) and similar (type II) GAEs. After You and Pellegrino, further research was conducted on the kinematics and mobility analysis of angulated elements [19, 20]. Kiper et al. [21] showed that the motion of the angulated elements in a radially expanding structure is the Cardan Motion.

Instead of using the angulated elements as modules for deployable structure design, Hoberman uses rhombus loops as modules [22]. This loop assembly method first places identical rhombus loops along a curve and then the link lengths are determined. Liao and Li [23] and Kiper and Söylemez [24] have found similar results independently from Hoberman.

**Loop Assembly Method.** In the literature there are three types of scissor units: transitional, polar and angulated units. When the scissor hinge is in the middle of straight bars, the result is a translational scissor. Maden et al. [25] have examined the possible arrangements of different types

of scissor units and provided formulations for their analysis and design. When several translational scissor units are assembled together in a row, the loops formed are rhombus loops (Fig. 1a). When the scissor hinge is not placed in the middle, polar units with kite loops are formed (Fig. 1b).

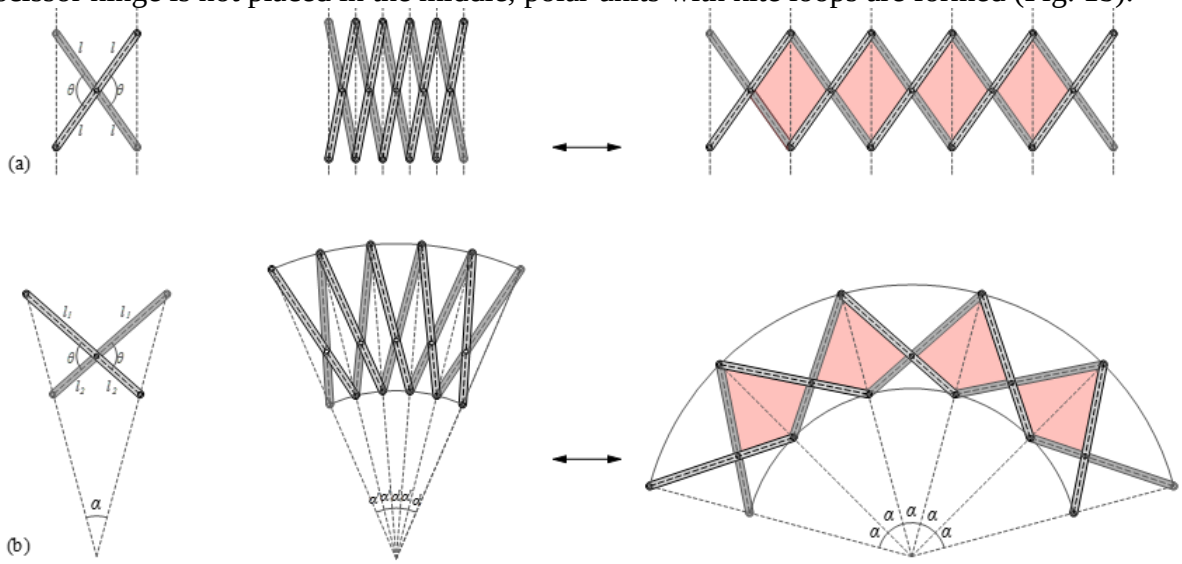


*Figure 1. – a) Rhombus loops formed with translational scissor units*
*b) Kite loops formed with polar scissor units [26]*

Hoberman devised a methodology using the loops to find the form of the links. By aligning rhombus loops on a curve, he derives angulated elements (Fig. 2). He also found out that it was possible to achieve deployable structures using different scales of the same rhombus along a given curve. In this study we use another type of loop, antiparallelogram loop, to compose single degree of freedom (DoF) radially expanding deployable structures.

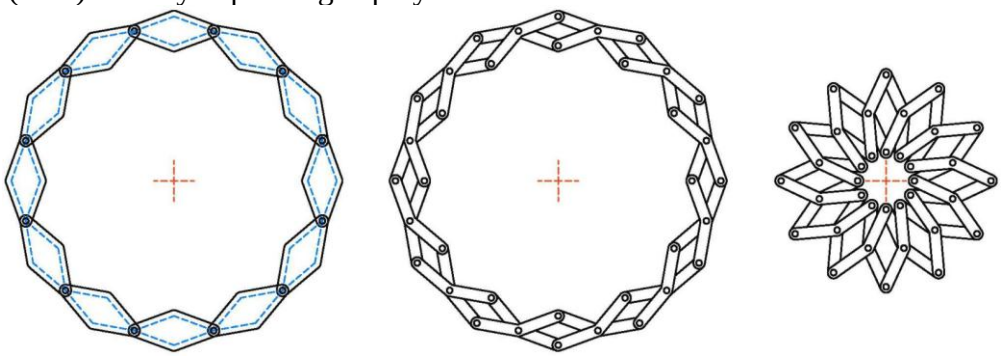

*Figure 2. – Assembly of rhombi loops on a circle [22]*

An antiparalellogram is also called a crossed parallelogram or a contraparallelogram. It is made up of two equal short and two equal long sides, in which long sides cross each other. During the motion the crossing point moves on the long edges and always stays on the mirror symmetry axis of the loop (Fig. 3).

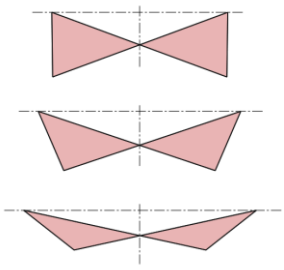

*Figure 3. – Motion of antiparallelogram loop*

In our study, we align antiparallelogram loops along a circle, similar to Hoberman's method. There are several variations of arrays in order to connect the loops at joints. Placing the loops in alternating order on the circle (sort of glide reflection along the circle) yielded a radially deployable structure (Fig. 4).

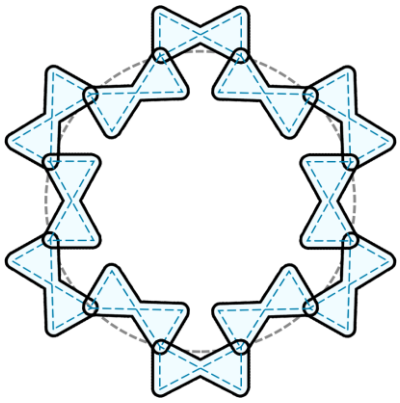

*Figure 4. – Antiparallel loops along a circle*

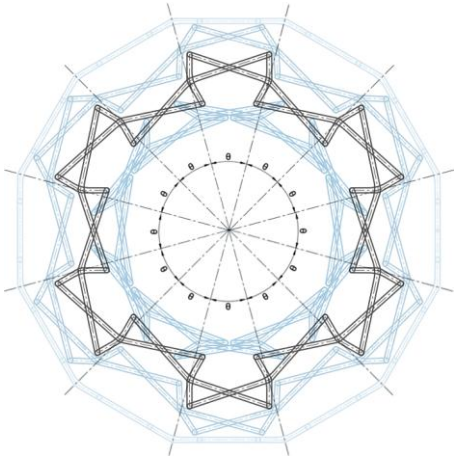

*Figure 5. – Deployable antiparallelogram ring mechanism*

In Fig. 5 it is seen that there is only one joint on each radial axis from the center, unlike the angulated scissor ring-like structures developed by Hoberman. Therefore it is not possible to locate the center with a single loop, but two loops are necessary so that the positions of three joints defines a circle. The relation between the subtended angle θ and kink angles α + β of the links can be observed with a geometrical analysis (Fig. 6). Also, due to alternating order of the loops, there are always even number of loops in the assembly.

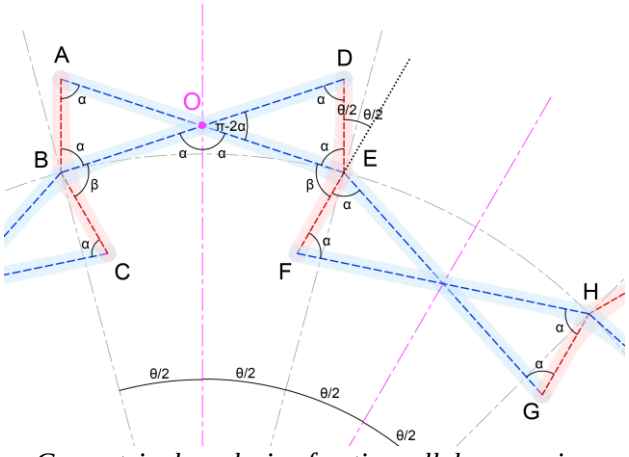


*Figure 6. – Geometrical analysis of antiparallelogram ring mechanism*

Initially AB arm of link ABC and DE arm of link DEF are parallel to each other. Let ∠EAB = α. Since |AB| = |DE| and |AE| = |BD|, all inner angles of ABDE antiparallelogram are equal to α. Let ∠AEF = β. It is seen from Fig. 6 that ∠DEF = ∠AEG = α + β, i.e. the kink angles of both types of angulated elements, DEF and AEG, are equal to each other. ∠BOE = 2α, being an outer angle of triangle OAB. A line through the intersection point O and parallel to AB and DE divides ∠BOE and also the subtended angle θ into two. The loop has mirror symmetry about this line. Such lines will be called unit lines. Since DE is parallel to the unit line through O, the angle between the radial axis through E and DE is equal to θ/2. Similarly one can conclude that the angle between EF and the radial axis through E is equal to θ/2. So, θ/2 + α + β + θ/2 = π, that is, the kink angles are α+β=π–θ.

Since identical loops are used to construct the mechanism, the two type of angulated links DEF and AEG have link lengths |DE| = |EF| and |AE| = |EG|. Also the kink angles of both type of angulated elements are equal. Therefore, the angulated elements are similar (type II) GAEs (Fig. 7). When the desired number of loops and the circle radius at the initial configuration is specified, one of the side lengths can be chosen freely and the other side length is dependent.

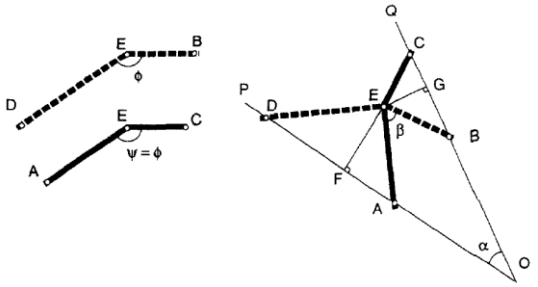


*Figure 7. – Similar (type II) GAEs - |AE|/|DE| = |EC|/|EB| and ψ=φ*

Next, we construct a ring with similar loops, instead of identical loops. For this construction, a random sequence of three different angles, θ, ψ and δ, are used to divide the circle into sections. When the mechanism is drawn in Solidworks® it is seen that this construction also yields a deployable ring structure (Fig. 8).

Geometric principles of the mechanism can be found similar to the construction with identical loops (Fig. 9). The short edges of each loop are parallel to the unit lines passing through the center of the circle and crossing point of the loop. The unit lines bisect the corresponding subtended angles θ, ψ and δ. Again, similar GAEs are used with identical kink angles. This time, the kink angles are determined by two adjacent subtended angle values. For example, ∠FED = ∠AEI = $\alpha + \beta_2 = \pi - (\theta/2 + \psi/2)$. For the example in Fig. 8, there are 6 different pairs of angulated elements (Fig. 8b). Within each pair, two angulated links have the same kink angle and proportional arm lengths, i.e. they construct a similar GAE.

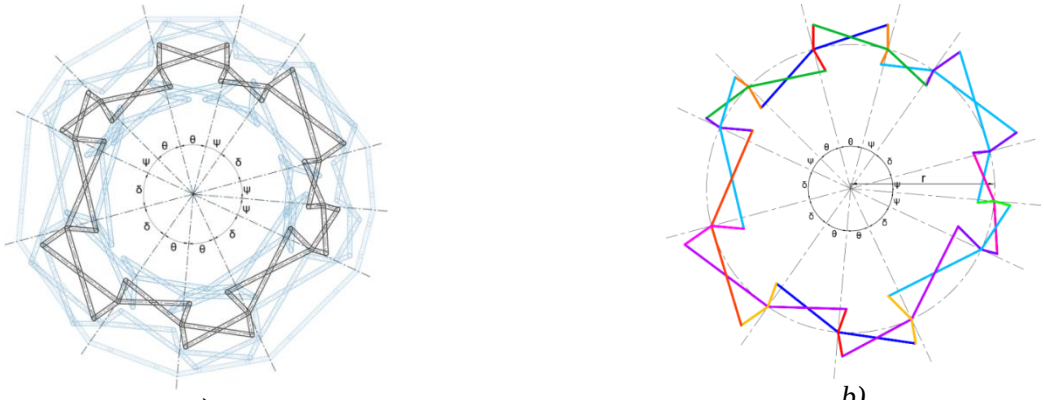

*a)* *b)*

*Figure 8. a) Deployable antiparallelogram ring mechanism with similar loops;*
*b) Link typology of the mechanism*

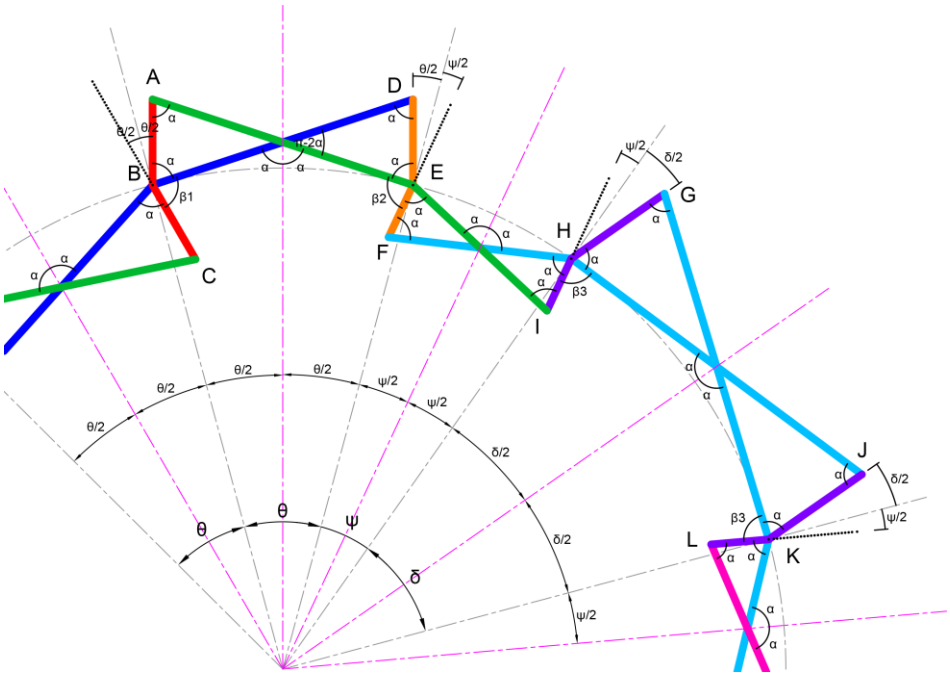


*Figure 9. – Geometrical analysis of antiparallelogram ring mechanism with similar loops*

**Conclusions.** Our study showed that it is possible to achieve deployable rings using antiparallelogram loops in alternating order on a circle using loop assembly method. The links resulted from the assembly are Type I GAE's with identical kink angles. Furthermore, the kink angles can be represented in terms of the subtended angles. It is seen that only one of the side lengths is independent when the number of loops and circle radius are given for the initial configuration. Unit lines of the loops do not pass through joints, but they are the symmetry axes of the loops.

In the second stage of the study, we used similar loops to construct and that also yielded a deployable mechanism, again resulting with Type I GAE's. In this construction the subtended angles varied. Once again, the kink angles can be represented in terms of the subtended angles.

**Acknowledgment**. This project has received funding from the European Union's Horizon 2020 research and innovation program under the Marie Skłodowska-Curie grant agreement No 689983.

## REFERENCES

[1]. C.H. Hernandez Merchan, C.H., *Deployable Structures*. 1987, Massachusetts Institute of Technology.
[2]. Mao, D. and Y.Z. Luo, *Analysis and design of a type of retractable roof structure.* Advances in Structural Engineering, 2008. 11(4): p. 343-354.
[3]. Jiang, Y.B. and X.R. Wang, *Movable Roof Design and Analysis of Retractable Roof Structures.* Civil Engineering in China - Current Practice and Research Report, 2010: p. 357-361.
[4]. Cai, J.G., et al., *Geometry and Mechanical Behaviour of Radially Retractable Roof Structures During the Movement Process.* International Journal of Steel Structures, 2016. 16(3): p. 755-764.
[5]. G. Kiper & E. Soylemez, *Deployable Space Structures.* Rast 2009: Proceedings of the 4th International Conference on Recent Advances in Space Technologies, 2009: p. 131-138.
[6]. Wang, Y., et al., *Design and Deployment Analysis of Modular Deployable Structure for Large Antennas.* Journal of Spacecraft and Rockets, 2015. 52(4): p. 1101-1111.
[7]. Qi, X.Z., et al., *A large ring deployable mechanism for space satellite antenna.* Aerospace Science and Technology, 2016. 58: p. 498-510.
[8]. Gantes, C.J., *Deployable structures: analysis and design*. 2001: Wit Press.

[9]. Pinero, E., *Project for a mobile theatre.* Architectural Design, 1961. 12(1): p. 154-155.
[10]. Escrig, F. *Expandable space frame structures*. in *Proceedings of the 3rd International Conference on Space Structures, ed: Nooshin, H., University of Surrey, Guildford, UK, Elsevier Applied Science Publishers, London*. 1984.
[11]. Escrig, F., *Expandable space structures.* International Journal of Space Structures, 1985. 1(2): p. 79-91.
[12]. Langbecker, T., *Kinematic Analysis of Deployable Scissor Structure s.* International Journal of Space Structures, 1999. 14(1): p. 1-15.
[13]. Nagaraj, B.P., R. Pandiyan, and A. Ghosal, *Kinematics of pantograph masts.* Mechanism and Machine Theory, 2009. 44(4): p. 822-834.
[14]. Zhao, J.S., F.L. Chu, and Z.J. Feng, *The mechanism theory and application of deployable structures based on SLE.* Mechanism and Machine Theory, 2009. 44(2): p. 324-335.
[15]. Hoberman, C., *Reversibly expandable doubly-curved truss structure*. 1990, Google Patents.
[16]. Hoberman, C., *Radial expansion/retraction truss structures*. 1991, Google Patents.
[17]. Servadio, I., *Deployable regular and semi-regular polyhedral structures using Hoberman's technique.* Bulletin of the International Association for Shell and Spatial Structures, 1995. 36(2): p. 91-97.
[18]. You, Z. and S. Pellegrino, *Foldable bar structures.* International Journal of Solids and Structures, 1997. 34(15): p. 1825-1847.
[19]. Patel, J. and G.K. Ananthasuresh, *A kinematic theory for radially foldable planar linkages.* International Journal of Solids and Structures, 2007. 44(18-19): p. 6279-6298.
[20]. Cai, J.G., X.W. Deng, and J. Feng, *Mobility analysis of planar radially foldable bar structures.* Proceedings of the Institution of Mechanical Engineers Part G-Journal of Aerospace Engineering, 2015. 229(4): p. 694-702.
[21]. G. Kiper, E. Söylemez & A.U.Ö. Kişisel, *A family of deployable polygons and polyhedra*, Mechanism and Machine Theory 43(5), 627-640, 2008
[22]. C. Hoberman, *Mechanical invention through computation - mechanism basics,* MIT Class 6.S080 online course material, http://courses.csail.mit.edu/6.S080/lectures/02_all.pdf, 2013.
[23]. Q. Liao & D. Li, *Mechanisms for scaling planar graph,* Chinese Journal of Mechanical Engineering 41, 140-143, 2005.
[24]. G. Kiper & E. Söylemez, *Irregular polygonal and polyhedral linkages comprising scissor and angulated elements,* In: Proc. 1st IFToMM Asian Conference on Mechanism and Machine Science (CD), Taipei, 455-459, 2010.
[25]. F. Maden, K. Korkmaz & Y. Akgün, *A review of planar scissor structural mechanisms: geometric principles and design methods,* Architectural Science Review 54, 246-257, 2011.
[26]. YAR, M., et al., *A Novel Planar Scissor Structure Transforming Between Concave And Convex Configurations.* International Journal of Computational Methods and Experimental Measurements, 2017. 5(4): p. 442-450.

**Received:** 11.01.2022
**Accepted:** 25.05.2022

MACHINE SCIENCE

ISSN: 2227-6912
E-ISSN: 2790-0479

2022, Volume 11, № 1. Pages 47 – 58

# THE EFFECT OF THE ROTATION DIRECTION OF CRANK ON THE KINEMATIC CHARACTERISTICS AND EXTREME FORCES OF THE RODS SUSPENSION POINT

**Anar HAJIYEV**

Department of "Mechatronic and machine design", Azerbaijan Technical University, Baku, Azerbaijan

*E-mail: anar_hajiyev_1991@mail.ru*

**Abstract:** In article carried out a kinematic study of a new constructive solution of pumping unit, which used in oilfield and the influence of the direction of rotation of the crank on the kinematic characteristics of the rod suspension point and extreme forces in both axial and deaxial-converting mechanisms was evaluated. Studies have shown that, according to the elementary theory, changing of direction of rotation of the crank does not affect the load on the rods suspension point, but according to the refined theory, the direction of rotation of the crank has a significant effect on the operation of the pumping unit. Because in this case, the laws of motion of the rods suspension point is sharply change. In addition, it was found that the fundamental difference between the axial and deaxial-converting mechanisms is due to the change in average speed during the up and down stroke movement of the rods suspensions point. It has been found that on pumping units with positive deaxial-converting mechanisms when the crank rotates clockwise, the rods suspension point moves upstroke faster than when it moves down, or vice versa, when the the crank rotates counterclockwise, the time at which the rods suspension point moves up is later than when it moves down. On pumping units with negative deaxial transforming mechanisms when the crank rotates clockwise, upstroke time of rods suspension point is less than it is downstroke time. And on pumping units with negative deaxial transforming mechanisms when the crank rotates clockwise, the upstroke time of the rods suspension point is longer than when it moves down and vice versa, when the crank rotates counterclockwise, the upstroke time of the rods suspension point is less than when it moves down.

***Key words:*** *pumping unit, axial, deaxial, rods, block, crank*

**Introduction.** One of the most important places in the economic development of the Republic of Azerbaijan takes the extraction and transportation of oil to world markets. It is no coincidence that in the former Soviet Union, the research institutes of Azerbaijan were the leaders in the design and production of pumping units used in oil extraction. The mechanical transmissions of the sucker-rod pumps designed by these research institutes, as well as the pumping units and reducers used in these mechanical transmissions were considered as standards. Therefore, in the modern stages of oil science, the creation of a new design of pumping units with a more advanced transmission mechanism, which saves electricity, reduces overall dimensions, increases longevity and efficiency, is relevant and have great practical importance for the mechanical transmission of pumping units.

It is known that the most common equipment used in mechanized oil production is a sucker-rod well pumping unit. These equipment consist of an individual well pump, which is lowered into the well with rods to the under dynamic level of the liquid, a pumping unit, its transmission and converting mechanisms. The plunger of downhole pump is actuated by the pumping unit. During the upstroke and downstroke movement of the plunger, the operation of the downhole pumps is observed by changing the direction of movement of the rod column [1-5].

Given the large number of these pumping units in operation, one of the urgent issues is to improve them and create new designs with a more perfect design. For this purpose at the Department of "Mechatronics and Machine Design" of Azerbaijan Technical University, was developed an original constructive solution of mechanical drive of the pumping unit, which provides both stable operation and energy saving, as well as a reduction in overall dimensions and an increase in reliability. The originality of the new equipment was confirmed by the patent of the

Intellectual Property Agency of the Republic of Azerbaijan (patent № İ 2021 0113) and the patent of the Eurasian Patent Organization (patent № 039650) [6,7].

At Figure 1 shown the overview of the new constructive solution of the sucker-rod pumping unit. The new constructive solution of the sucker-rod pumping unit consist from frame (1), three-phase short-circuited asynchronous motor (2), V-belt drive (3), rigidly connected two-flow three-stage reducer (4), on the drive shaft of which on one side mounted double-shaped brake (5) and on the other side V-belt pulley (6), and on the driven shaft of its installed two cranks (7); guide blocks (8, 9), ropes (10) connected to the rods suspension point.

The converting mechanism, which consists of two slider-crank linkage (12), converts the rotational motion of the crank into the upstroke and downstroke movement of the rod suspension point. The mechanical transmission has counterweights whose weight can be adjusted (14), located on a movable cross beam (13), which is connected with hinge joint to the connecting-rod.

The guide blocks are surrounded by a flexible rope, one end of which is connected to the movable beam, and the other end is connected to the rods suspension point. In addition, the mechanical drive has a guide system consisting of two vertically located cylindrical tubes (15) and the movable beam. The mechanical transmission has articulated front (18) and rear (19) arms, which can be adjusted by using (16,17) screw tensioners, a fixed cross beam (20) rigidly connected to the guide tubes. The screw tensioner (21) is connected to the frame of the construction, as well as to the joints with the front and rear arms.

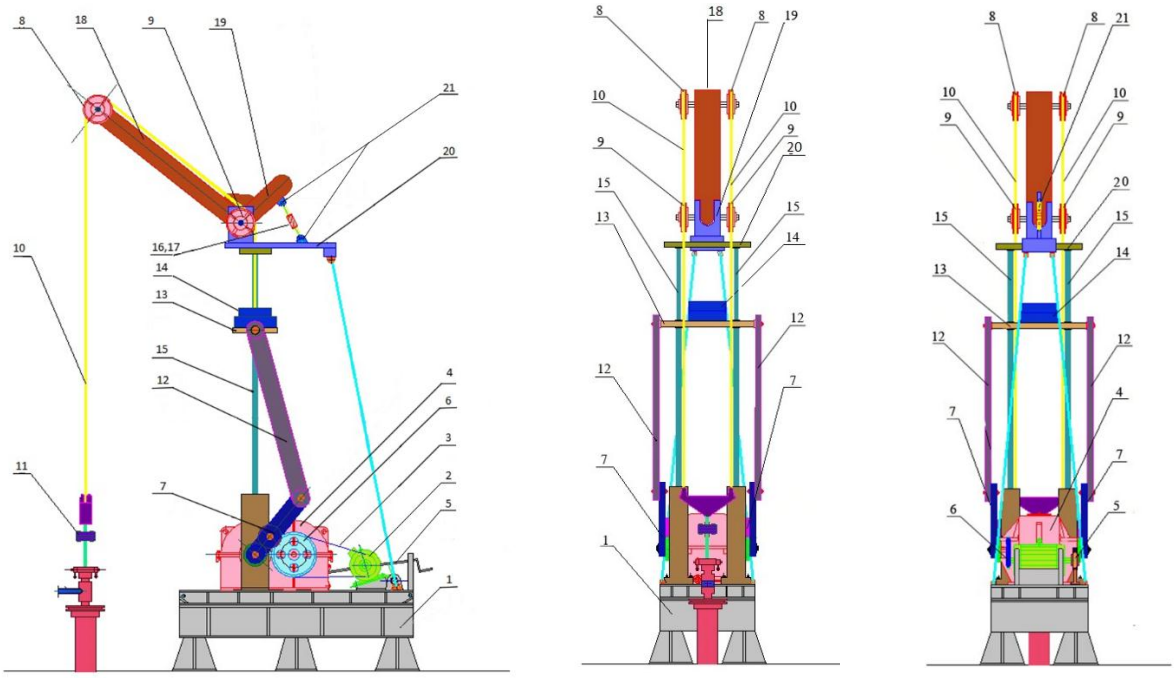


*Figure 1. New constructive solution of beamless pumping unit consisting of an slider-crank mechanism and a rope-block system:*
*a - side view; b - front view; c - rear view*

The converting mechanism is used on the pumping unit to ensure the upstroke and downstroke movement of the rods column. Currently, the four-link hinged slider-crank linkage mechanism is used in the converting mechanisms of the pinches. It is known that the purpose of kinematic analysis of each hinged mechanism is to determine the displacement, velocity and acceleration of its corresponding points.

**Formulation and solution of the problem.** The kinematic characteristics of the rods suspension point, i.e. the stroke of the rods suspension point, its speed, and the acceleration change

during a complete cycle of the pumping unit crank. Therefore, the laws of motion of the rods suspension point depend on the kinematic scheme of the adopted transforming mechanism. Depending on the type of transforming mechanism, the mechanical transmissions of the sucker-rod pumps can be divided into two types, namely, beam and beamless pumping units. In the first case, the upstroke and downstroke movement of the rods column is achieved by using the slider-crank mechanism with beam. In the slider-crank mechanism of a beam pumping unit, the lengths of the links may be constant or vary in length during one cycle of the pumping units transmission. In beamless pumping units, the upstroke and downstroke movement of the rods column is achieved by a flexible element (rope or chain) applied to the transforming mechanism.

The location of the crank on the transforming mechanism of the pumping unit is very important (Figure 2). This location significantly affects the operating parameters of the downhole pump.

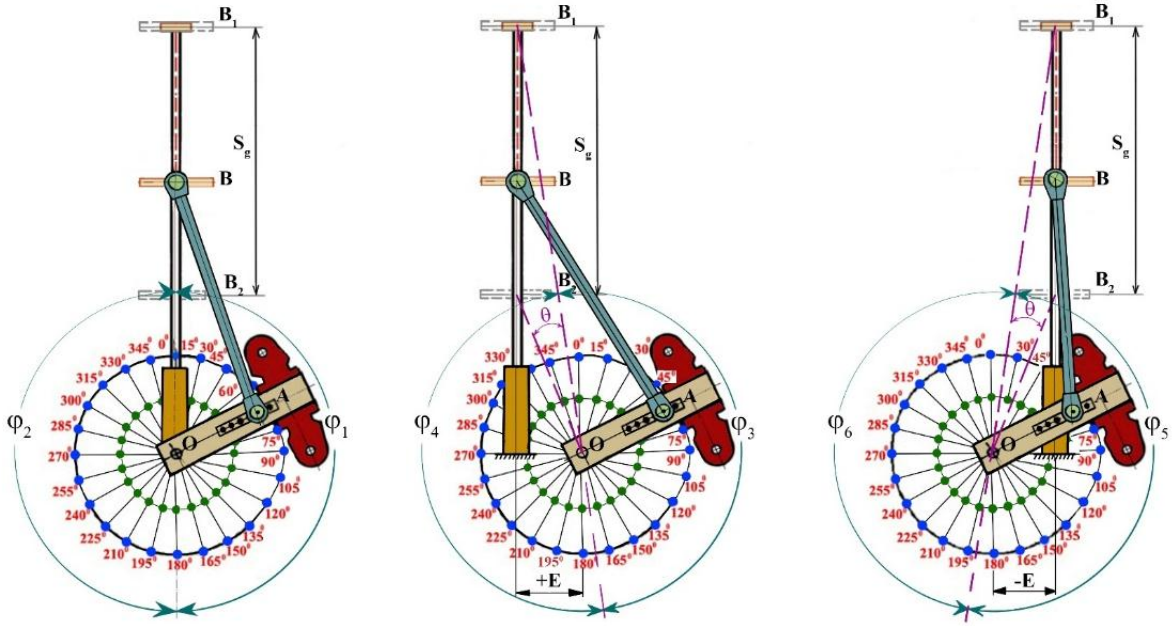


*a)* *b)* *c)*

*Figure 2. Scheme of the transforming mechanism of the pumping unit for three different positions of the crank*

In the transforming mechanism of the proposed innovative construction, the location point of the crank can be in three different variants.

If the center of the elbow is located on the straight line $B_1$-$B_2$, then such a mechanism is called a centrally symmetric axial mechanism. If the center of the crank is located to the right or left of the straight line $B_1$-$B_2$, then this mechanism is called an asymmetric mixed (daxial) mechanism.

Deaxial slider-crank mechanism itself can be positive ($O_1A_1BCD$) and negative ($O_2A_2BCD$) deaxial. The main difference between the slider-crank mechanisms is the change in the average speed during the up and down stroke movement of the rods suspension point.

Indeed, if the mechanism is axial (OABCD), during the displacement of the horse head from the lower edge position (B2) to the upper edge position (B1), the crank will rotate by an angle $\varphi_1$ in the direction of the clockwise movement (oil well head is on the left side). If vice versa, i.e., will rotate by an angle $\varphi_2$ during the horse head displacement from the upper edge position ($B_1$) to the lower edge position ($B_2$). In this case, since the mechanism is an axial mechanism, $\varphi_1 = \varphi_2 = 180^0$. Therefore, regardless of the direction of rotation of the crank, the time for both up and down stroke movement of the rods suspension point is the same (photo 2, a).

If the mechanism is positive deaxial ($O_1A_1BDC$), then during of the upstroke movement of the rods suspension point, the crank will rotate in the direction of clockwise movement (oil well

head is on the left side) by an angle $\varphi_3$, and during its downstroke movement by an angle $\varphi_4$. As can be seen from Figure 2, b, the angle $\varphi_3$ is smaller than the angle $\varphi_4$, so the time for the up stroke movement of the rods suspension point is faster than the time for it to down stroke movement or vice versa, and when the crank rotates in the opposite direction of clockwise movement the rods suspension point moves up stroke movement time is later than the time of its downstroke movement.

If the mechanism is negative deaxial ($O_2A_2BCD$), then during of the up stroke movement of the rods suspension point, the crank will rotate in the direction of clockwise movement (oil well head is on the left side) by an angle $\varphi_5$, and during down stroke movement by an angle of $\varphi_6$. As can be seen from Figure 2, c, the angle $\varphi_5$ is greater than the angle $\varphi_6$, so the time when the rods suspension point of the moves up is later than the time when it moves down, or vice versa, when the crank rotates in the opposite direction of the clockwise movement, the upstroke movement time of the rods suspension point is faster than the time it moves down.

In mining practice, the direction of rotation of the crank is usually assumed to be clockwise in both axial and deaxial pumping units. Such a choice of the direction of rotation of the crank has a great importance. Because even in axial (symmetrical) pumping units, the laws of movement of the rods suspension point are unsymmetrical.

According to the existing research methods, three main theories are applied, i.e. elementary, refined and exact theory, based on the degree of simplification and accepted assumptions when studying the laws of movement of the suspension point.

It is always possible to accurately determine the displacement of the rods suspension point, its speed and acceleration. In this case, the studied transforming mechanism is considered as a closed geometric figure in all cases. Such a figure has enough dimensions to find its angles and sides. However, it should be noted that even for simple mechanisms, the equations obtained by the exact method are so complex that their practical use for engineering calculations causes great difficulties. Therefore, elementary and refined theories are used more often when conducting kinematic research of transforming mechanisms in oil field practice (table 1) [8-15].

*Table 1. Formulas to finding of kinematic characteristics of sucker-rod pumps with axial and deaxial mechanisms*

| For axial mechanisms | | |
|---|---|---|
| Kinematic characteristics | Elementary method | Refined method |
| movement | $S_B = r(1 - cos\varphi)$ | $S_B = r\left(1 - cos\varphi + \frac{1}{2}\cdot\lambda^2 sin^2\varphi\right)$ |
| speed | $V_B = \frac{ds}{dt} = \omega\cdot r\cdot sin\varphi$ | $V_B = \frac{ds}{dt} = \omega\cdot r\cdot\left(sin\varphi + \frac{\lambda}{2}sin2\varphi\right)$ |
| acceleration | $a_B = \frac{dV_B}{dt} = \omega^2\cdot r\cdot cos\varphi$ | $a_B = \omega^2\cdot r\cdot\left(cos\varphi + \frac{\lambda}{2}cos2\varphi\right)$ |
| For deaxial mechanisms | | |
| Kinematic characteristics | Elementary method | Refined method |
| movement | $S_B = r\left[\sqrt{\left(\frac{1}{\lambda}+1\right)^2 - \varepsilon^2} - \frac{1}{\lambda} - cos\varphi\right]$ | $S_B = r\left[1 - cos\varphi + \frac{\lambda}{4}(1 - cos2\varphi) + \varepsilon\lambda sin\varphi - \frac{\varepsilon^2\lambda^2}{2(\lambda+1)} + \frac{\lambda\varepsilon^2}{2}\right]$ |
| speed | $V_B = \frac{ds}{dt} = \omega\cdot r\cdot sin\varphi$ | $V_B = \omega\cdot r\cdot\left[sin\varphi + \frac{\lambda}{2}sin2\varphi + \varepsilon\lambda cos\varphi\right]$ |
| acceleration | $a_B = \frac{dV_B}{dt} = \omega^2\cdot r\cdot cos\varphi$ | $a_B = r\omega^2\cdot[cos\varphi + \lambda cos2\varphi - \varepsilon\lambda sin\varphi]$ |

In order to evaluate the influence of the direction of rotation of the crank on the extreme forces at the rods suspension point, the kinematic characteristics of axial pumping unit model of СК-6-2,1-2500 and the deaxial pumping unit model of СКД6-2,5-2800 ($r = 1000\,mm, l = 2500\,mm$, E=1500 mm) for different values of the relative length factor ($\lambda$) and relative eccentricity ($\varepsilon$) respectively, the displacement of the rods suspension point, its speed and acceleration were determined based on both elementary and refined theories [16-20].

*Table 2. Results of calculations for constructing graphs of functions $S = f(\varphi), v = f(\varphi)$ and $a = f(\varphi)$.*

| Angel φ, degree | Elementary method | | | Refined method | | |
|---|---|---|---|---|---|---|
| | *S*, m | *v*, m/sec | *a*, m/sec$^2$ | *S*, m | *v*, m/sec | *a*, m/sec$^2$ |
| 0 | 0 | 0 | 175 | 0 | 0 | 245 |
| 15 | 34, | 108 | 169 | 47 | 150 | 230 |
| 30 | 134 | 209 | 152 | 184 | 282 | 187 |
| 45 | 293 | 296 | 124 | 393 | 380 | 124 |
| 60 | 500 | 362 | 88 | 650 | 435 | 53 |
| 75 | 741 | 404 | 45 | 928 | 446 | -15 |
| 90 | 1000 | 419 | 0 | 1200 | 419 | -70 |
| 105 | 1259 | 404 | -45 | 1445 | 363 | -106 |
| 120 | 1500 | 36 | -88 | 1650 | 290 | -123 |
| 135 | 1707 | 296 | -124 | 1807 | 212 | -124 |
| 150 | 1866 | 209 | -152 | 1916 | 137 | -117 |
| 165 | 1966 | 108 | -169 | 1979 | 67 | -109 |
| 180 | 2000 | 0 | -175 | 2000 | 0 | -105 |
| 195 | 1966 | -108 | -169 | 1979 | -67 | -109 |
| 210 | 1866 | -209 | -152 | 1916 | -137 | -117 |
| 225 | 1707 | -296 | -124 | 1807 | -212 | -124 |
| 240 | 1500 | -362 | -88 | 1650 | -290 | -123 |
| 255 | 1259 | -404 | -45 | 1445 | -363 | -106 |
| 270 | 1000 | -419 | 0 | 1200 | -419 | -70 |
| 285 | 741 | -404 | 45 | 928 | -446 | -15 |
| 300 | 500 | -362 | 88 | 650 | -435 | 53 |
| 315 | 293 | -296 | 124 | 393 | -380 | 124 |
| 330 | 134 | -209 | 152 | 184 | -282 | 187 |
| 345 | 34 | -108 | 169 | 47 | -150 | 230 |
| 360 | 0 | 0 | 175 | 0 | 0 | 245 |

Table 2 shows the results of calculations for constructing graphs of functions $S = f(\varphi), v = f(\varphi)$ and $a = f(\varphi)$. The speed and acceleration of the rods suspension point was performed for the case of the number of swings $n = 5\,min^{-1}$. Showing speed and acceleration on the graphs in this form shows more clearly the influence of the direction of rotation of the crank on the loading of the rods suspension point.

As can be seen from Graph 1, changing the direction of rotation of the crank does not affect the loading of the rod suspension point. Because the change of speed depending on the displacement of the rods suspension point occurs on a circle, and the change of acceleration occurs according to the straight line law.

As can be seen from the Graph 2, in reality, the direction of rotation of the crank has a significant influence on the working mode of the pumping unit. As can be seen from the graphs, the regularities of movement of the rods suspension point on these pumping unit are also drastically different from each other.

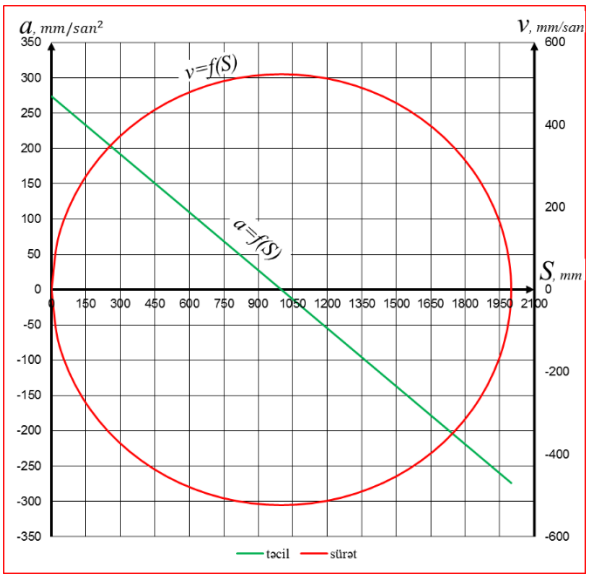


*Graph 1. Graphs of the dependence of the speed and acceleration of the axial transforming mechanism on the displacement of the rods suspension point according to the elementary theory*

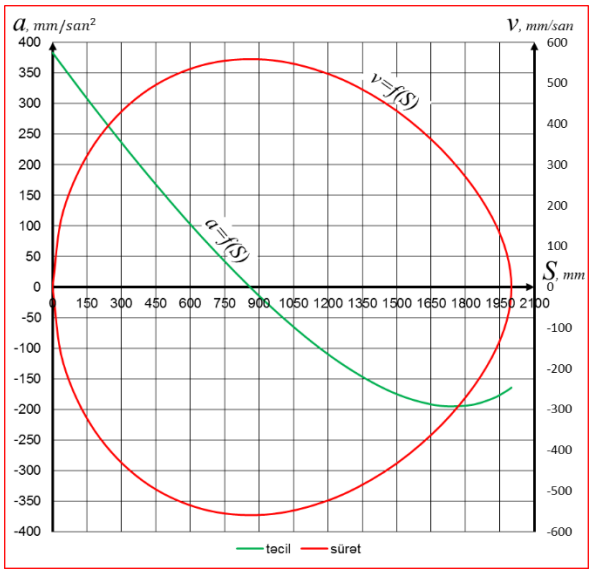


*Graph 2. Graphs of the dependence of the speed and acceleration of the axial transforming mechanism on the displacement of the rods suspension point according to the refined theory*

Indeed, during the clockwise rotation of the crank while the rods suspension point is moving upwards (oil well head is on the left side), its velocity corresponds to the $OAO_1$ curve, and the acceleration to the $CBC_1$ curve. During counterclockwise rotation of the crank (oil well head is on the left side), the speed of the rod suspension point corresponds to the curve $OA_1O_1$, and the curve $CBC_1$ corresponds to its acceleration. Let's assume that the combined deformation of the pipes lowered into the well and the rods column of the pumping unit being studied is $\lambda^* = 380\,mm$. Then, during the clockwise rotation of the crank, the displacement of the rod suspension point will correspond to the speed value of $380\,mm/sec$, and the acceleration value to $260\,mm/sec^2$. When the crank rotates in the counter-clockwise direction, the value of the speed will be $340\,mm/sec$, and the acceleration will be $365\,mm/sec^2$.

A comparison of these cases shows that it is more convenient to take the direction of rotation of the crank in the direction of clockwise rotation for pumping unit with an axial converter mechanism. Because in this case, the absolute values of the speed and acceleration decrease at the moment of recovery of the deformations of the pipes and rods during the upward movement. Reducing the absolute values of the speed and momentum at the time of recovery of the deformations of the pipes and rods leads to a reduction of the dynamic forces acting on the sucker-rod pumping unit [21-26].

According to the formulas proposed in table 1, the displacement of the rods suspension point, its speed and acceleration according to the kinematic characteristics of the deaxial pumping unit model of СКД6-2,5-2800 were calculated based on both elementary and refined theories, and the calculation results are shown in table 4.

Calculations were performed for both negative and positive deaxial converter mechanisms. In order to more conveniently analyze the studied kinematic schemes, they are conditionally divided into 4 schemes (table 3):

Scheme 1 – this scheme is a negative deaxial kinematic scheme, the direction of rotation of the crank is clockwise;

Scheme 2 – this scheme is a negative deaxial kinematic scheme, the direction of rotation of the crank is counter-clockwise;

Scheme 3 – this scheme is a positive deaxial kinematic scheme, the direction of rotation of the crank is clockwise;

Scheme 4 – this scheme is a positive deaxial kinematic scheme, the direction of rotation of the crank is counterclockwise.

*Table 3. diferent variants of schemes by type of converting mechanism*

| Variants | Type of converting mechanism | *r*, mm | λ | ε |
|---|---|---|---|---|
| | Axial | 1000 | 0,4 | - |
| 1,2 | Negative deaxial | 1000 | 0,4 | +1,5 |
| 3,4 | Positive deaxial | 1000 | 0,4 | -1,5 |

On the basis of the conducted studies, it was determined that during the rotation of the crank in the direction of clockwise motion, the largest value of the displacement of the rods suspension point during the upstroke movement in the pumping unit with positive deaxial converter mechanism is less time compared to the axial converter mechanism, and in the case of the negative deaxial converter mechanism more time is achieved (table 4).

During clockwise rotation of the crank, increasing the positive deaxial distance in the positive direction, its maximum value increases during upward movement of the rods suspension point, and decreases during downward movement. When the deaxial distance is increased in the negative direction, the maximum speed of the rod suspension point decreases during the upward movement, and increases during the downward movement.

*Table 4. Results of calculations of kinematic characteristics of sucker-rod pumps by elementary and refined methods*

| Angle, φ | Elementary method | | | | | | Refined method | | | | | |
|---|---|---|---|---|---|---|---|---|---|---|---|---|
| | Positive deaxial | | | Negative deaxial | | | Positive deaxial | | | Negative deaxial | | |
| | *S*, m | *v*, m/sec | *a*, m/sec$^2$ | *S*, m | *v*, m/sec | *a*, m/sec$^2$ | *S*, m | *v*, m/sec | *a*, m/sec$^2$ | *S*, m | *v*, m/sec | *a*, m/sec$^2$ |
| 0 | -337 | 0 | 274 | -337 | 0 | 274 | 321 | 314 | 383 | 321 | -314 | 383 |
| 15 | -303 | 135 | 264 | -303 | 135 | 264 | 524 | 491 | 317 | 213 | -115 | 402 |
| 30 | -203 | 261 | 237 | -203 | 261 | 237 | 805 | 624 | 210 | 205 | 80 | 374 |
| 45 | -44 | 370 | 193 | -44 | 370 | 193 | 1138 | 697 | 77 | 290 | 253 | 310 |
| 60 | 162 | 453 | 137 | 16 | 453 | 137 | 1491 | 701 | -60 | 451 | 3867 | 224 |
| 75 | 403 | 505 | 71 | 403 | 505 | 71 | 1828 | 639 | -182 | 670 | 476 | 135 |
| 90 | 662 | 523 | 0 | 662 | 523 | 0 | 2121 | 523 | -274 | 921 | 523 | 55 |
| 105 | 921 | 505 | -71 | 921 | 505 | -71 | 2346 | 372 | -324 | 1187 | 534 | -7 |
| 120 | 1162 | 453 | -137 | 1162 | 453 | -137 | 2491 | 205 | -334 | 1451 | 519 | -49 |
| 135 | 1369 | 370 | -194 | 1369 | 370 | -194 | 2553 | 43 | -310 | 1704 | 487 | -77 |
| 150 | 1528 | 261 | -237 | 1528 | 261 | -237 | 2537 | -101 | -264 | 1937 | 443 | -100 |
| 165 | 1628 | 135 | -264 | 1628 | 135 | -264 | 2456 | -220 | -212 | 2145 | 386 | -127 |
| 180 | 1662 | 0 | -274 | 1662 | 0 | -274 | 2321 | -314 | -164 | 2321 | 314 | -164 |
| 195 | 1628 | -135 | -264 | 1628 | -135 | -264 | 2145 | -386 | -127 | 2456 | 220 | -212 |
| 210 | 1528 | -261 | -237 | 1528 | -261 | -237 | 1937 | -443 | -100 | 2537 | 101 | -264 |
| 225 | 1369 | -370 | -194 | 1369 | -370 | -194 | 1704 | -487 | -77 | 2553 | -43 | -310 |
| 240 | 1162 | -453 | -137 | 1162 | -453 | -137 | 1451 | -519 | -49 | 2491 | -205 | -334 |
| 255 | 921 | -505 | -71 | 921 | -505 | -71 | 1187 | -534 | -7 | 2346 | -372 | -324 |
| 270 | 662 | -523 | 0 | 662 | -523 | 0 | 921 | -523 | 55 | 2121 | -523 | -274 |
| 285 | 403 | -505 | 71 | 403 | -505 | 71 | 670 | -476 | 135 | 1828 | -639 | -182 |
| 300 | 162 | -453 | 137 | 162 | -453 | 137 | 451 | -387 | 224 | 1491 | -701 | -60 |
| 315 | -44 | -370 | 194 | -44 | -370 | 194 | 290 | -253 | 310 | 1138 | -697 | 77 |
| 330 | -203 | -261 | 237 | -203 | -261 | 237 | 205 | -80 | 374 | 805 | -624 | 210 |
| 345 | -303 | -135 | 264 | -303 | -135 | 264 | 213 | 115 | 402 | 524 | -491 | 317 |
| 360 | -337 | 0 | 274 | -337 | 0 | 274 | 321 | 314 | 383 | 321 | -314 | 383 |

As a result of the comparative analysis carried out in this way, we determine that the reduction of the time for the upward movement of the rods suspension point o can be achieved by two methods. For this purpose, it is recommended to use either sucker-rod pumping units with a positive deaxial transformin mechanism when the crank rotates in the clockwise direction, or with a negative deaxial translation mechanism when the crank rotates in the opposite direction of the clockwise direction of movement (table 5).

*Table 5. The result of the comparative analysis*

| Variant of the scheme | Deaxial character | The direction of rotation of the crank | speed, m/sec | acceleration, m/sec$^2$ | The travel time of the rods suspension point | |
|---|---|---|---|---|---|---|
| | | | | | Upstroke, sec | Downstroke, sec |
| 1 | Negative | Clockwise movement | 0,325 | 0,199 | 7,85 | 5,54 |
| 2 | Negative | Counter-clockwise movement | 0,461 | 0,247 | 5,54 | 7,85 |
| 3 | Positive | Clockwise movement | 0,461 | 0,247 | 5,54 | 7,85 |
| 4 | Positive | Counter-clockwise movement | 0,325 | 0,199 | 7,85 | 5,54 |

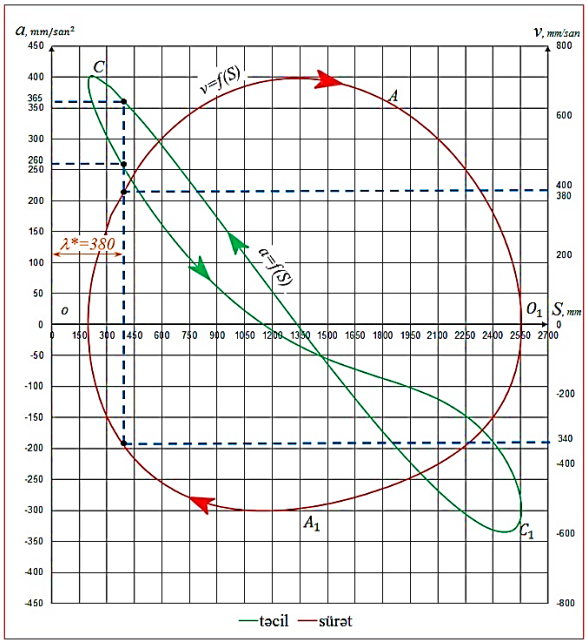


*Graph 3. Graphs of the dependence of the speed and acceleration of the rods suspension point from its movement on a positive deaxial pumping unit (according to the refined theory)*

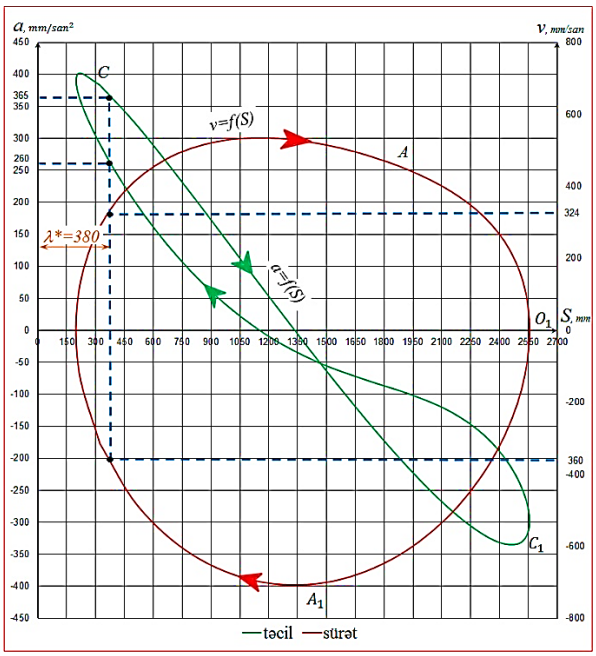


*Graph 4. Graphs of the dependence of the speed and acceleration of the rods suspension point from its movement on a negative deaxial pumping unit (according to the refined theory)*

Based on the conducted research, it was determined that increasing the average speed of the rods suspension point during the upstroke movement reduces the time of its upstroke movement. On the other hand, reducing the time of upstroke movement of the plunger pump also reduces the absolute cost of backflow of the pumped liquid between the plunger and the cylinder, which leads to an increase in its productivity. Therefore, in order to determine the degree of influence of the axial on the efficiency of the pumping unit, it is of great importance to quantify the effect of the size of the axial of the crankcase on the upstroke movement time of the rod suspension point (table 5).

If the crank rotates with a constant angular velocity, then the ratio of the angles of rotation will be as follows:

$$\frac{\varphi_1}{\varphi_2} = \frac{t_1}{t_2}$$

where $t_1$ and $t_2$ - are the times of up and down stroke of the rods suspension point, respectively.

Since the times $t_1$ and $t_2$ are known in the application, depending on the movement taken by the rods suspension point, the speeds during its upstroke and downstroke movement are known, then

$$\frac{v_1}{v_2} = \frac{t_2}{t_1} = \frac{\varphi_2}{\varphi_1} = K_0$$

burada $K_0$ – is the coefficient of change of the average speed of the rods suspension point. The value of this coefficient is usually determined depending on the change of the deaxial angle during the up and down movement of the suspension point of the bar:

$$K_0 = \frac{180^0 + \theta}{180^0 - \theta}$$

If the times of upstroke and downstroke movement of the rods suspension point are equal $\theta = 0$. That is, in this case, since the transforming mechanism is axial, $\varphi_1 = \varphi_2$.

And for deaxial mechanisms

$$\theta = arcsin\frac{E}{l+r} - arcsin\frac{E}{l-r} = arcsin\frac{\varepsilon\lambda}{(1+\lambda)} - arcsin\frac{\varepsilon\lambda}{(1-\lambda)} = arcsin\frac{-2\varepsilon\lambda^2}{(1-\lambda^2)}$$

This formula of the coefficient of variation of the average speed allows to determine the dependence $K_0 = f(E)$. Table 5 shows the initial data for establishing the proposed dependency at different line light of the movement for the known length of the connecting rod ($l = 2800\ mm$) for deaxial pumping unit model of СКД6-2,5-2800.

Based on the results of the calculation, the table shows how much time it takes for the rods suspension point to move up and to down by moving the reducer to the right or to the left from the position that ensures the symmetry of the crank-slide mechanism at different values of $\lambda$ and $\varepsilon$ in the specific upstroke movement of the rod suspension point on this pumping unit allows us to determine what is different (table 6).

*Table 6. The time of movement up and down of rods suspension depending on different values of λ and ε*

| relative eccentricity ε | Coefficient of variation of the average speed of the pumping unit | | | |
|---|---|---|---|---|
| | λ=0.1 | λ=0.2 | λ=0.3 | λ=0.4 |
| -2 | 1,02606 | 1,112603 | 1,297437 | 1,761422 |
| -1,75 | 1,02277 | 1,097725 | 1,253553 | 1,605115 |
| -1,5 | 1,01948 | 1,083101 | 1,212113 | 1,480191 |
| -1,25 | 1,01621 | 1,068718 | 1,172798 | 1,375248 |
| -1 | 1,01295 | 1,054562 | 1,135339 | 1,284158 |
| -0,75 | 1,00969 | 1,040623 | 1,09951 | 1,203203 |
| -0,5 | 1,00645 | 1,02689 | 1,065119 | 1,129933 |
| 0 | 1 | 1 | 1 | 1 |
| 0,5 | 0,99359 | 0,973814 | 0,938862 | 0,885008 |
| 0,75 | 0,9904 | 0,960962 | 0,909496 | 0,831115 |
| 1 | 0,98722 | 0,948261 | 0,880795 | 0,77872 |
| 1,25 | 0,98405 | 0,935701 | 0,852662 | 0,727141 |
| 1,5 | 0,98089 | 0,923275 | 0,825005 | 0,675588 |
| 1,75 | 0,97774 | 0,910975 | 0,797733 | 0,623008 |
| 2 | 0,9746 | 0,898794 | 0,77075 | 0,567723 |

For clarity, let's quantify how much the absolute value of leaks decreases when the time of the rod suspension point moves up, depending on the parameters adopted according to the specific well conditions. For this, let's assume that the number of oscillations of the rods suspension point of the pumping unit per minute is $n = 5\,min^{-1}$. Then, the total time for upstroke and downstroke movement of the rods suspension point (in one complete cycle of the crank) will be 13,39 seconds. For axial mechanisms, this time will be evenly distributed, that is, it will take 6,695 seconds to move both up and down. If we take the relative length coefficient as $\lambda = 0{,}4$ and the deaxial angle $\theta = 25^0$, then $K_0 = 1{,}322$ will correspond to this angle and $\frac{t_H}{t} = 1{,}322$. This time ratio can be provided in two ways:

1) In the tranforming mechanism of the pumping unit, assuming the case of rotation of the crank in the counter-clockwise direction, taking the relative deaxiality $\varepsilon = -1{,}107$;

2) In the tranforming mechanism of the pumping unit, taking the relative deaxiality $\varepsilon = +1{,}107$ and assuming the case of rotation of the crank in the clockwise direction.

**Results and conclusions.** The kinematic study of the new constructive solution of pumping unit was carried out, and the effect of the direction of rotation of the crank on the kinematic characteristics of the rods suspension point and extreme forces in the axial and deaxial converter mechanisms was evaluated. Studies have shown that, according to the elementary theory, changing of direction of rotation of the crank does not affect the load on the rods suspension point, but according to the refined theory, the direction of rotation of the crank has a significant effect on the operation of the pumping unit, because in this case, the laws of motion of the rods suspension point is sharply change.

According to the kinematic characteristics of the pumping unit model of СКД6-2,5-280, was calculated and numerically determined the average speed change during the upward and downward movement of the bar suspension point of the new beamless pumping unit with axial and deaxial transforming mechanism. It has been found that on pumping units with positive deaxial transforming mechanisms when the crank rotates clockwise, the rods suspension point moves upstroke faster than when it moves down, or vice versa, when the crank rotates counterclockwise, is later than when it moves down. On pumping units with negative deaxial transforming mechanisms with negative deaxial-converting mechanisms when the crank rotates clockwise, upstroke time of rods suspension point is less than it is downstroke time. However, on pumping units with negative deaxial transforming mechanisms when the crank rotates clockwise, the upstroke time of the rods suspension point is longer than it is downstroke time and vice versa, when the crank rotates counterclockwise, the upstroke time is less than when it moves down. Based on the comparative analysis, in order to reduce the losses caused by leaks in the liquid lifted by the plunger and to increase the actual productivity, it is possible to reduce the time of the suspension point of the pumping unit to move up in two ways. For this purpose, it is recommended to use either sucker-rod pumping units with a positive deaxial transforming mechanism when the crank rotates in the clockwise direction, or with a negative deaxial translation mechanism when the crank rotates in the opposite direction of the clockwise direction of movement.

## REFERENCES

[1]. Takacs G.: *Sucker-Rod Pumping Handbook*. Elsevier Science, 2015. 598 p.

[2]. Gray F. *Petroleum Production in Nontechnical Language, 2nd edition* / F. Gray -Oklahoma, Tulsa: Penn Well Publishing Company, - 1995, - 297 p.

[3]. Abdukhan, Zh. M. *Pumping unit for oil production with increased current* / Zh. M. Abdukhan, B. T. Murtazina // Bulletin of the Kazakh Academy of Transport and Communications. M. Tynyshpaeva.– 2018. – No 1(104). – P. 48-52. – EDN XPSPDV.

[4]. Zakharov, B. S. *Special types of sucker-rod pumps* / B. S. Zakharov // Chemical and Petroleum Engineering. – 2008. – Vol. 44. – No 3-4. – P. 217-223. – DOI 10.1007/s10556-008-9039-1. – EDN LKYWAR.
[5]. The ROTAFLEX Rod pump reliability for deep, high volume of trouble some wells // World oil, - 1990. Vol.210, №5, - p.68.
[6]. Abdullaev A.I. Nadjafov A.I., Ahmedov B.B., Chalabi I.G., Abdullaev A.A., Hajiyev A.B. *Mechanical drive of sucker-rod pumps.* Eurasian invention patent № 039650. EAPO 2022.02.21. https://www.eapo.org/ru/patents/reestr/patent.php?id=39650
[7]. Abdullaev A.I. Nadjafov A.I., Ahmedov B.B., Chalabi I.G., Abdullaev A.A., Hajiyev A.B. *Mechanical drive of sucker-rod pumps.* Patent of Intellectual Property Agency of the Republic of Azerbaijan № İ 2021 0113, a2019 0162, 2021.
[8]. Hajiyev, A. *About new constructive solution of sucker-rod oil pumping unit* / A. Hajiyev // Topical issues of rational use of natural resources : Scientific conference abstracts, St Petersburg, 17–19 june 2020. – St Petersburg: St. Petersburg Mining University, 2020. – P. 29-30. – EDN KETGHE.
[9]. Ahmedov, B. *Estimation of the equality of the beamless sucker-rod oil pumping unit by the value of the consumption current* / B. Ahmedov, A. Hajiyev, V. Mustafayev // Nafta-Gaz. – 2021. – Vol. 2021. – No 9. – P. 571-578. – DOI 10.18668/NG.2021.09.01. – EDN IORTLY.
[10]. Ahmedov, B., Hajiyev A. *Assessment of dynamic forces in new construction design for beamless sucker-rod pumping units* / B. Ahmedov, A. Hajiyev // Nafta-Gaz. – 2020. – Vol. 2020. – No 5. – P. 299-310. – DOI 10.18668/NG.2020.05.03. – EDN VFIPWH.
[11]. Ahmadov B.B., Hajiyev A.B., *Evaluation of elastic deformations in the elements of newly developed design solution for sucker-rod pumping unit*/ Ahmadov B.B., Hajiyev A.B // Azerbaijan Oil Industry Journal. – 2019. – № 2. – C. 33-37. – EDN TMKPJW.
[12]. I. Khalilov, B. Ahmedov, A. Hajiyev Study of the efficiency factor of sliding bearings of the new constructive solution of multistage reducer / I. Khalilov, B. Ahmedov, A. Hajiyev // Machine Science. – 2021. – Vol. 10. – No 1. – P. 33-42. – EDN HXMOFU.
[13]. Ahmedov, B. *Assessment of dynamic efforts taking into account of inertial and vibrating loads in deaxial pumping units* / B. Ahmedov // Journal of Petroleum Exploration and Production Technology. – 2020. – Vol. 10. – No 4. – P. 1401-1409. – DOI 10.1007/s13202-020-00836-1. – EDN VOPEJX.
[14]. Najafov A.M. The exploratiry designing of mechanical drive of succer-rod pumps. Saarbrücken/Germany, "Palmarium Academic Publishing", 2013, p-149.
[15]. B.Ahmedov, A.Najafov, A.Abdullayev, I.Chalabi, F.Veliev. Calculation of toothed gear mechanisms in machines and assemblies considering the effect of lubricants // - Kharkov Ukraine: Eastern European Journal Enterprise Technologies, - 2018. 5/7 ( 95 ), - p. 43-54.
[16]. Khalilov, I. A. Influence of the gap in clutches on the dynamic properties of drives / I. A. Khalilov // Russian Engineering Research. – 2010. – Vol. 30. – No 3. – P. 206-212. – DOI 10.3103/S1068798X10030032. – EDN XKJUPH.
[17]. Khalilov, I. A. Temperature variation of elastic elements in clutches on damping / I. A. Khalilov // Russian Engineering Research. – 2012. – Vol. 32. – No 4. – P. 322-325. – DOI 10.3103/S1068798X12040120. – EDN XKLLUT.
[18]. Khalilov I.A. Analysis of dynamic performances of machine actuators taking into consideration damper and structure features of couplers / Khalilov I.A.// Vestnik Mashinostroeniya. – 2013. – № 4. – P. 22-25. – EDN RCJHTZ.
[19]. Khalilov I.A. Method of lever mechanism synthesis, assuring specified motion law / Khalilov I.A., Kerimov S. Kh., Rzaeva G.M.// Vestnik Mashinostroeniya. – 2017. – № 3. – P. 3-5. – EDN YUPOWJ.
[20]. Khalilov, I. A. The Importance of Considering The Temperature Factors While Choosing The Elastic Couplings / I. A. Khalilov // IFAC-PapersOnLine, Baku, 13–15 сентября 2018 года. – Baku, Azerbaijan: Elsevier B.V., 2018. – P. 816-820. – DOI 10.1016/j.ifacol.2018.11.188. – EDN WTVKDW.
[21]. Ahmedov B., Najafov, A., Abdullaev, A. *Balancing of cyclically changing load with newly designed mechanical drive for sucker-rod pumps.* Oil GAS European Magazine, 45. Edition. Issue 4/2019. p. 112-115. (DOI 10.19225/1912xx)

[22]. Romero O. J., Almeida P. Numerical simulation of the sucker-rod pumping system // Ingeniería e Investigación, - 2014. vol.34, №3, - p. 4-11.
[23]. Steliga, I. An experimental and theoretical method of calculating the damping ratio of the sucker rod column oscillation / I. Steliga, J. Grydzhuk, A. Dzhus // Eastern European Journal Enterprise Technologies. – 2016. – V. 2. – № 7(80). – P. 20-25. – DOI 10.15587/1729-4061.2016.66193. – EDN VTQTEF.
[24]. Ahmedov B.B, Najafov A.M, Abdullayev A.I. Determination of the kinematic parameters of the new constructive solution of the beamless sucker-rod pump // - Trabzon Turkey: Journal of Structural Enginering & Applied Mechanics – 2018. Volume 1 Issue 3, - p. 128-135.
[25]. *A comprehensive review of sucker rod pumps' components, diagnostics, mathematical models, and common failures and mitigations* / S. Fakher, A. Khlaifat, M. E. Hossain, H. Nameer // Journal of Petroleum Exploration and Production Technology. – 2021. – Vol. 11. – No 10. – P. 3815-3839. – DOI 10.1007/s13202-021-01270-7. – EDN AFIZFR.
[26]. *Energy-efficient oil extraction by sucker rod borehole pumps in low-yield fields* / V. E. Brunman, A. S. Vataev, A. N. Volkov [et al.] // Russian Engineering Research. – 2017. – Vol. 37. – No 5. – P. 378-382. – DOI 10.3103/S1068798X17050082. – EDN XNMJDG.

**Received:** 29.03.2022
**Accepted:** 12.05.2022

MACHINE SCIENCE

ISSN: 2227-6912
E-ISSN: 2790-0479

2022, Volume 11, № 1. Pages 59 – 63

# DYNAMICS OF THE CAM MECHANISM AT DELAYS AND LIMITED POWER-SUPPLY

**Alishir ALIFOV**

Mechanical Engineering Research Institute of the Russian Academy of Sciences, Moscow, Russia

E-mail: a.alifov@yandex.ru

**Abstract:** The dynamics of a cam mechanism with delays in elasticity and friction is considered, the operation of which is supported by an energy source of limited power. The interaction between the cam mechanism and the energy source is described by nonlinear equations. To solve these equations, the method of direct linearization is used and the equations of non-stationary and stationary motions are derived. Relationships are obtained for calculating the stationary values of the amplitude and phase of oscillations, the speed of the energy source. A number of calculations have been performed in order to obtain information on the effect of delays on the dynamics of the cam mechanism.

**Keywords:** *cam, dynamics, oscillations, delay, elasticity, friction, energy source, limited excitation*.

**Introduction**. The determination of the parameters of the cam mechanism, taking into account its dynamics, is of great importance in the design. The functioning of the cam mechanism is supported by an energy source (engine), as a result of which their dynamics are also interconnected. Undesirable oscillatory processes that may occur during the operation of the cam mechanism also depend on the properties of the energy source that supports its operation. In this context, the well-known direction of the theory of oscillations comes to the fore, in which the interaction of an oscillatory system and an energy source is considered [1-2, etc.].

As is known [3-13 etc.], the characteristic of internal friction in materials, the imperfection of their elastic properties, etc. lead to a delay (hysteresis). It takes place in a number of devices (mills, vibrating machines, automatic control systems, conveyors, belt feeders, ball mills, flotation machines, drying drums, etc.) and technological processes. The delay leads to a deterioration in the dynamics and stability (up to loss) of the system. In this paper, the influence of delays in elasticity and friction on the dynamics of the cam mechanism is considered. It consists of an introduction, equations and their solutions, calculation results, conclusion.

**Model and equations.** In [14], the dynamics of the cam mechanism is considered on the basis of the model shown in Fig.1, where a round disk with an eccentricity $\varepsilon$ acts as a cam. The disk is driven by an engine having a torque characteristic $M(\dot{\varphi})$, where $\dot{\varphi}$ is the speed of rotation. In the friction force arising in contact $F = f_1 N$ ($N = const$ is normal pressure force), the friction coefficient $f_1$ has a nonlinear characteristic

$$f_1(\dot{x}) = \sum_n b_n \dot{x}^n, \qquad b_n = const, \qquad n = 0, 1, 2, 3, 4, \ldots \tag{1}$$

where $\dot{x}$ is speed of the pusher contact point.

Function (1) based on the direct linearization method [15, 16] is presented as

$$f_{1*}(\dot{x}) = B + k\dot{x} \tag{2}$$

$$B = \sum_n b_n S_n \upsilon^n, \qquad n = 0, 2, 4, \ldots \ (n \text{ is even number})$$
$$k = \sum_n b_n \bar{S}_n \upsilon^{n-1}, \qquad n = 1, 3, 5, \ldots \ (n \text{ is odd number})$$

where $B$ and $k$ are the linearization coefficients, $\upsilon = \max|\dot{x}|$, $S_n = (2r+1)/(2r+n+1)$, $\bar{S}_n = (2r+3)/(2r+n+2)$, $r$ is *linearization accuracy parameter*, which is not limited, but it is enough to choose in the interval (0.2).

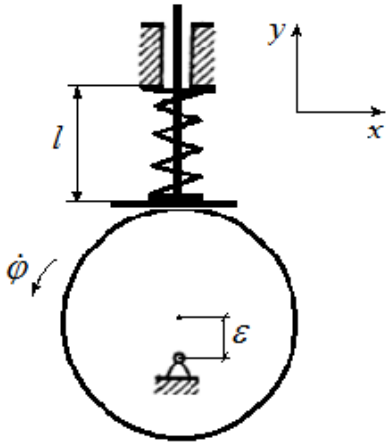


*Figure1. System model*

The motions of the system under the condition of continuous contact between the disk and the pusher are described [14] by the equations

$$m\ddot{x} + c(\varphi)x = F(\varphi, \dot{\varphi}, \dot{x})$$
$$I\ddot{\varphi} = M(\dot{\varphi}) - r(\varphi)F(\varphi, \dot{\varphi}, \dot{x}) \qquad (3)$$

where $F(\varphi, \dot{\varphi}, \dot{x}) = (B + k\dot{x})\left[N_0 - y_0(c_y - m_T\dot{\varphi}^2)\cos\varphi + y_0 k_н \dot{\varphi}\sin\varphi\right]$

$$c(\varphi) \approx c_0(1 - \lambda\cos\varphi), \quad r(\varphi) \approx r_0 - \mu + \varepsilon\cos\varphi + \mu\cos 2\varphi, \quad \mu = \varepsilon^2/4r_0, \quad N_0 = B_y + c_y y_0.$$

In (3), the first equation describes the movement of the pusher, the second - the disk or energy source. Here $m$ is the mass of the pusher brought to the point of contact, $I$ is the moment of inertia of the disk, taking into account the mass of the rotating parts of the energy source, $r(\varphi)$ is the radius of the contact point of the disk and the pusher, $B_y$ and $c_y$ are the linearization coefficients of the nonlinear elastic force of the spring $f_2(y) = \sum_i c_i y^i$, $c_i = const$, $i = 0, 1, 2, 3$, $c_0$, $\lambda$, $r_0$, $\varepsilon$, $y_0$, $m_T$, $k_н$ are constant values.

In the presence of delays in friction $\dot{x}_\eta$ and elasticity $x_\tau$, the first equation (3) takes the form

$$m\ddot{x} + k_\eta \dot{x}_\eta + c_\tau x_\tau + c_0(1 - \lambda\cos\varphi)x = F(\varphi, \dot{\varphi}, \dot{x}) \qquad (4)$$

where $k_\eta = const$, $c_\tau = const$, $\dot{x}_\eta = \dot{x}(t-\eta)$, $x_\tau = x(t-\tau)$, $\eta = const$ and $\tau = const$ are delays.

**Equation solutions.** The action of the force $c(\varphi)x$ can lead to parametric oscillations. They are strongly manifested in the regions of parametric resonances, among which the most significant is the region of the main parametric resonance, where the ratio of the natural frequency to the frequency of the parametric excitation is about 1/2. Since the parametric excitation frequency is formed by the variable $\varphi$, which can be represented [17] as $\varphi = \Omega t + \hat{\varepsilon}_{oscil}$, where $\hat{\varepsilon}_{oscil}$ are the small oscillation components that are not taken into account, then in the region of the main parametric resonance $\Omega \approx 2\omega$, $\omega^2 = c_0/m$ is the natural frequency.

According to the method of change of variables with averaging [15], solutions (4), taking into account the delays $\dot{x}_\eta = -\upsilon \sin(\psi - p\eta)$, $x_\tau = a\cos(\psi - p\tau)$, have the form

$$x = a\cos\psi, \qquad \dot{x} = -\upsilon\sin\psi, \qquad \psi = pt + \xi \tag{5}$$

which, taking into account $p = \Omega/2$, give the following relations for determining the amplitude, phase of oscillations and speed of the energy source:

$$\frac{da}{dt} = \frac{a}{4m}(\delta\sin 2\xi + kG\cos 2\xi + L\Omega^{-1})$$

$$\frac{d\xi}{dt} = \frac{1}{4m}(\delta\cos 2\xi - kG\sin 2\xi + A\Omega^{-1}) \tag{6}$$

$$\frac{d\Omega}{dt} = \frac{1}{I}\left[M(\Omega) - B(R_0N_0 - 0.5\varepsilon G)\right]$$

where $\upsilon = ap = a\Omega/2$, $\delta = ky_0k_и\Omega - 2\lambda c_0\Omega^{-1}$, $G = y_0(c_y - m_r\Omega^2)$, $R_0 = r_0 - \mu$,

$$L = 2\Omega(N_0k - k_\eta\cos p\eta) + 4c_\tau\sin p\tau, \quad A = m(4\omega^2 - \Omega^2) + 2(k_\eta\Omega\sin p\eta + 2c_\tau\cos p\tau).$$

From (6) for $\dot{a} = 0$, $\dot{\xi} = 0$, $\dot{\Omega} = 0$ we obtain the equations for stationary motions

$$A^2 + L^2 = \Omega^2(k^2G^2 + \delta^2)$$

$$tg2\xi = -(AkG - L\delta)/(LkG + A\delta) \tag{7}$$

$$M(\Omega) - S(\Omega) = 0$$

where $S(\Omega) = B(R_0N_0 - 0.5\varepsilon G)$.

The $S(\Omega)$ expression determines the load on the energy source and the intersection points of the $M(\Omega)$ and $S(\Omega)$ curves give the stationary values of the speed $\Omega$.

**Calculations**. Calculations were carried out to obtain information about the effect of lag on the dynamics of the cam system. The main design parameters are as follows: $\lambda$=0.02, $N_0 = 0.5$, $\omega = 1\text{c}^{-1}$, $c_0 = 1\ \text{kgf}\cdot\text{cm}^{-1}$, $c_\tau = 0.05\ \text{kgf}\cdot\text{cm}^{-1}$, $k_\eta = 0.02\ \text{kgf}\cdot\text{c}\cdot\text{cm}^{-1}$. The linearization coefficients used $S_2 = 3/5$, $\overline{S}_3 = 3/4$, and for delays $p\eta$ and $p\tau$ values from the interval (0,2π).

Since the frequency difference is small in the resonance region, the approximate $\Omega \approx 2\omega$ was also used.

For calculations, the friction coefficient is chosen in the form

$$f_1(\dot{x}) = 0.303 + 0.0624\dot{x} + 0.648\dot{x}^2 - 0.18\dot{x}^3$$

which is a special case of the characteristic that is widespread [1-2,18-19, etc.] in practice $T(U) = q(1 - \alpha_1 U + \alpha_3 U^3)$ where $U = V - \dot{x}$, $q$, $V$, $\alpha_1$, $\alpha_3$ are constants and $V = 1.2\,\text{cm}\cdot\text{c}^{-1}$.

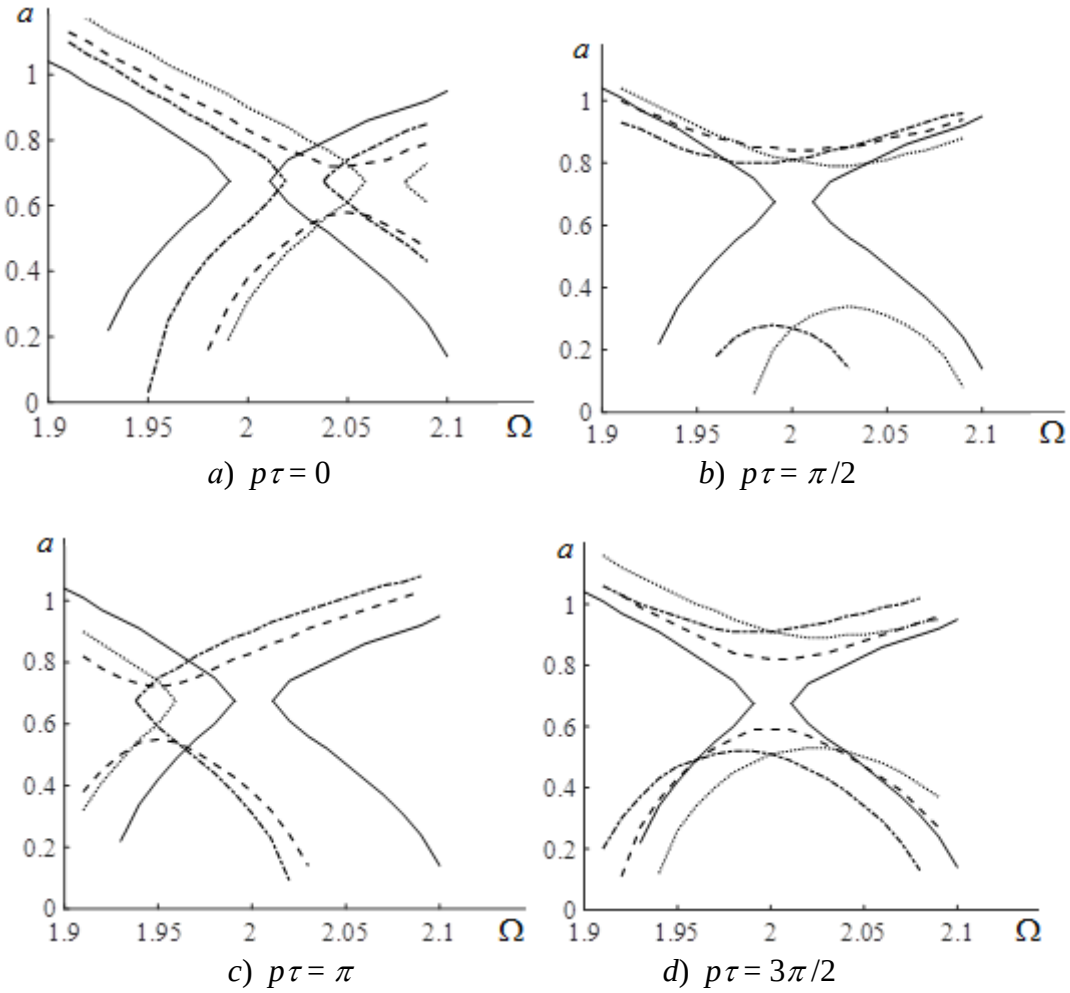


*a*) $p\tau = 0$ *b*) $p\tau = \pi/2$

*c*) $p\tau = \pi$ *d*) $p\tau = 3\pi/2$

*Figure 2. Amplitude-frequency curves:*
*solid curves – $c_\tau$ =0, $k_\eta$ =0, double dotted – $p\eta = \pi/2$,*
*dashed – $p\eta = \pi$, dash-dotted – $p\eta = 3\pi/2$.*

Fig.2 shows the amplitude-frequency curves $a(\Omega)$ for different delays. Solid curves correspond to the absence of $c_\tau = 0$ and $k_\eta = 0$ delays, double dotted curves, $p\eta = \pi/2$, dashed curves, $p\eta = \pi$ and dash-dotted curves, $p\eta = 3\pi/2$. As can be seen from the figures, delays have a qualitative and quantitative effect on the amplitude-frequency curves, shift them in the frequency domain.

**Conclusion**. As follows from the above results, the combined action of various combinations of elasticity delay and damping can strongly influence the dynamics of the cam mechanism. Depending on various combinations of delay values, the oscillation amplitude undergoes qualitative and quantitative changes, the resonance zone can shift in frequency.

## REFERENCES

[1]. Kononenko, V.O. *Vibrating Systems with Limited Power-Supply*. Iliffe Books, London (1969).
[2]. Alifov, A.A., Frolov, K.V. *Interaction of Nonlinear Oscillatory Systems with Energy Sources*. Hemisphere Publishing Corporation, New York, Washington, Philadelphia, London (1990).
[3]. Encyclopedia of mechanical engineering. – URL: https://mash-xxl.info/info/174754/.
[4]. N.A.Babakov, A.A.Voronov, A.A.Voronova and others. *Theory of automatic control: Textbook for universities on spec. "Automation and telemechanics"*. Part I. Theory of linear automatic control systems. Higher school, Moscow, Russia, (1986) (in Russian).
[5]. Applied mechanics. Textbook for universities // ed. V.M.Osetsky. 2nd ed., revised and additional. Engineering. Mashinostroyeniye, Moscow (1977) (in Russian).
[6]. Tretyakova, T.V., Vildeman, V.E. *Spatial-temporal inhomogeneity of the processes of inelastic deformation of metals*. Fizmatlit, Moscow (2016) (in Russian).
[7]. Garkina, I.A., Danilov, A.M., Nashivochnikov, V.V. *Simulation of dynamic systems with the delayed*. Modern Problems of Science and Education. No.1-1, 285 (2015) (in Russian).
[8]. Rubanik, V.P. *Oscillations of Quasilinear Systems with Time Lag*. Nauka, Moscow (1969) (in Russian).
[9]. Tsykunov, A.M. *Robust stabilization system for an object with state delay*. Bulletin of the Astrakhan State Technical University. Series: management, computer technology and informatics. No.1, 65-73 (2013) (in Russian).
[10]. Zhirnov, B.M. *On self-oscillations of a mechanical system with two degrees of freedom in the presence of delay*. Journal of Applied Mechanics. Vol.9. No.10, 83-87 (1973) (in Russian).
[11]. Abdiev, F.K. *Delayed Self-Oscillations of a System with an Imperfect Energy Source*. Izv. Academy of Sciences of the Azerbaijan SSR. Series of physical, technical and mathematical Sciences, No.4, 134-139 (1983).
[12]. Daza, A., Wagemakers, A., Sanju´an, M.A.F. *Wada property in systems with delay*. Commun. Nonlinear. Sci. Numer. Simul. 43, 220-226 (2017).
[13]. Akhmetsafina, R.Z., Akhmetsafin, R.D. *Inverse Z-transform in the identification of discrete systems with delay*. Instrumentation. Vol.57. No.5, 15-25 (2014) (in Russian).
[14]. Alifov, A.A. *On oscillations in cam mechanisms, taking into account the properties of the energy source*. Problems of mechanical engineering and automation. No.1, 87-91 (2018) (in Russian).
[15]. Alifov, A.A. *Methods of Direct Linearization for Calculation of Nonlinear Systems*. RCD, Moscow (2015) (in Russian).
[16]. Alifov, A.A. *Method of the Direct Linearization of Mixed Nonlinearities*. Journal of Machinery Manufacture and Reliability, Vol.46. No.2, 128-131 (2017). DOI: 10.3103/S1052618817020029.
[17]. Alifov, A.A. *On the calculation of oscillatory systems with limited excitation by the methods of direct linearization*. Engineering and Automation Problems, No.4, 92-97 (2017).
[18]. I.I.Blekhman. *Oscillations of nonlinear mechanical systems*. Vibrations in technology: directory. Vol.2. Engineering, Moscow (1979) (in Russian).
[19]. Bronovec, M. A., Zhuravljov, V.F. *On self-oscillations in systems for measuring friction forces*. Izv. Ros. Akad. Nauk, Mekh. Tv. Tela. No.3, 3-11 (2012) [Mech. Sol. (Engl. Transl.) 47 (3), 261-268 (2012)].

**Received:** 01.06.2022

**Accepted:** 25.06.2022

**MACHINE SCIENCE**

**ISSN: 2227-6912**
**E-ISSN: 2790-0479**

**web site: msj.aztu.edu.az; e-mail: msj@aztu.edu.az Tel: (+994 12) 538 94 12**

# SUBMISSION GUIDELINES

**General requirements.**
Article should not be earlier published in any edition, stated in the short form and edited. The scientific article maintenance should correspond to one of the following scientific directions: Designing of machines; Materials technology; Mechanics; Manufacturing engineering; Economy and management; Automatics and ICT; Technical information.

**The documents applied to article**.
The conclusion of the corresponding organization (chair, etc.); The expert opinion on expediency of the publication of the article; The covering letter; The Information on the authors ( name, patronymic, surname, the exact address, place of work and position, scientific degree, area of scientific activity, contact phones, e-mail address ,etc.).

**Preparation rules.**
*Format* - A4; *Margins from each party* - 20 mm; *Program* - Microsoft Office Word; *Font* - Times New Roman, a font size - 12, an interval - 1.
The scientific article can be written only in English language, and it is represented in duplicate.
*Article volume* - 5 … 8 pages.

**Sequence of compilation:**
1. Article name - on the center;
2. Names and surnames of the authors - on the center;
3. Full addresses of a place of work of authors - on the center;
4. Co-ordinates of authors: e-mail address, phone numbers.
5. The abstract: not less than two-three offers, and no more than 100 words. In the summary: article summary, problem statement, and the information on the received results should be reflected.
6. Keywords: often used 3 ÷ 5 terms under the article.
7. The basic text.
8. The references.

**The main text of article should be divided as follows:**
For example: "*Introduction*", "*Problem statement*", "*Decision or test methods*", "*Results of the decision or tests and their estimation*".
*In introduction*: the description of the problem statement, the work purpose and etc.;
*In the main part*: formation of problem statements; research and methods of the decision, their advantage and difference from existing methods; examples confirming efficiency of the offered method of the decision and the results received.
*In the conclusion*: evaluation of the results.
**Drawings**. *Formats* - DOC, JPEG, TIFF and PDF (600 dpi). *The size* – min. 5 × 5, max. 10 × 15. *Arrangement* - ("In the text", in the center). Images of drawings should be accurately visible, and all symbols well are read.
Drawings, paintings, schedules and algorithms should correspond to standard requirements.
**Tables** are located in the text and are numbered, and the name of each table should be specified in the right top corner.
**Formulas** should be written down in format *Equation* in the separate line. It is not recommended to use special symbols in the text written on the same line in format *Equation*. Formulas should be written down in certain sequence and are numbered on the right.
**The references** should correspond to the text and sequence of article. It is recommended to refer to sources published in last 10 years.
**The additional information**. Edition has the right to spend necessary updating and reductions. Authors bear a scientific article maintenance responsibility. To the publication those articles which have received a positive response are represented only. If article is not published, the edition decision is possible to data of authors, the manuscript and disks do not come back.

**MACHINE SCIENCE № 1, 2022**

***Editorial address:***
AZ1073, Azerbaijan, Baku, H.Javid av., 25.
Telephone: (+994 12) 538 94 12

E-mail: msj@aztu.edu.az
Web site: http://msj.aztu.edu.az/

Format: 60×84 1/8.
Number of copies printed: 100.

**Publisher: AzTU Publisher**